53rd Scientific Conference for Young Students of Physics and Natural Sciences

Open Readings 2010

Laisvieji skaitymai 2010

March 24-27, 2010, Vilnius, Lithuania

Programme and Abstracts

ISSN 2029-4425

Vilnius University is the oldest university in this part of Europe, and no doubt the best. This is proved through the ages and is proved each day, by excellent research produced in the laboratories of the university.

Among other faculties, the Faculty of Physics is the best, as it is shown by fifty two student conferences which where in the past. And now you have it: the proceedings of 53rd Scientific Conference for Young Students of Physics and Natural Sciences.

One of the goals of the conference programme was to highlight, young researchers in all fields of research performed in our university. Also worth to mark, that this conference is starting to go internationally, and I wish, that in few years it will be the main students conference of physics and natural sciences in the Baltic region at least.

The local organizing team and the conference coordination under the leadership of deans office and colleagues from the faculty managed the conference logistics professionally.

It is my pleasure to thank Department of Quantum Electronics, who took care of this conference for long years.

I wish to thank delegates, exhibitors, students and staff for making this conference rewarding experience.

For us these proceedings also represent, we hope, the start of a few solid academic careers, several lifelong friendships and a well-supported annual event that inspires young academics and provides an open forum for their work.

And if anyone ever asks you, tell them: students can do research.

Pro-rector for Research of Vilinus University

Prof. habil. dr. Juras Banys

Organized by

Vilnius University Faculty of Physics Students Scientific Association (VU FP SSA)

Vilnius University Faculty of Physics (VU FP)

Editors Committee:

prof. habil. dr. Valerijus Smilgevičius

doc. dr. Roaldas Gadonas

doc. dr. Alytis Gruodis

Organizing Committee:

Mindaugas Karaliūnas

Aistė Norkutė

Vytautas Butkus

Egidijus Songaila

Vytautas Aukštikalnis

Viltė Girdzijauskaitė

Giedrius Medzevičius

Bronius Razgus

Sponsored by:

UAB MGF „Šviesos konversija“

UAB „Fima“

UAB „Ekspla“

UAB „Altechna“

Technologijos.lt

Vtex

Vilnius University Faculty of Physics alumni Association

Programme

March 24, Wednesday

19:00 Welcome party in a pub „Šnekutis“

March 25, Thursday

9:00 Registration

10:00 Conference Opening:

10:00 Dean prof. V. Balevičius

10:10 Pro-Rector for International Affairs doc. dr. Rimantas Vaitkus

10:20 President of Students Science Association Aistė Norkutė

10:30 UAB „*Fima*” invited Mees Lodder „How to Make Money from Science: trends and challenges that are met by technologies today and how to cope with them“

11:30 Coffee break

12:00 Oral session I – Material science and technologies, theoretical physics

Chairman prof. S. Juršėnas

12:00 Tomas Serevičius „Luminescence Properties of MBE-grown ZnO and MgZnO Epitaxial Layers“

12:15 Justinas Tilindis „Plastic Deformation Efficiency Evaluation of Multilayer Bar Under Axial Load“

12:30 Antanas Stonkus „Charge Transfer in Pyridine-silver Complexes“

12:45 Simonas Krotkus „Peculiarities of Carrier Recombination in Highly-excited GaN“

13:00 Gediminas Krišanskas „Approximate description of decaying Quasi-stationary State“

13:15 Jevgenij Chmeliov „Modeling of Excitation Dynamics in Carbon Nanotubes“

13:30 Lunch break

14:30 Oral session II – Interdisciplinary

Chairman doc. dr. S. Bagdonas

14:30 Martynas Pelakauskas „Estcube-1 Satellite – Sailing on Solar Wind“

14:45 Piotr Klimczak „Fuel Cell Technology: Hopes, Challenges and Possible Applications“

15:00 Irma Vejelytė „Titanite U-Pb Dating of A Mylonite from The Druksiai-Polotsk Deformation Zone, The East European Craton“

15:15 Andrius Kleinauskas „The Research of Appropriation of Superparamagnetic Magnetite Nanoparticles for MR Imaging and Radiotherapy“

15:30 Vilmantas Gėgžna „Analysis of Fluorescence of Cervical Supernatant Excited with 355 nm Microlaser Comparing Normal, Cervicitis and CIN2+ Groups“

15:45 Aleksėjus Kononovičius „Stochastic Model of Return Matching to The Data of Financial Markets with Differing Liquidity“

16:00 Excursion to Molėtai Astronomical Observatory

March 26, Friday

10:00 Poster session

12:00 Invited Vygintas Jankus “Physics of Organic Materials and Light Emitting Diodes – Towards Flexible Displays and Lighting”

12:30 Invited Remigijus Vasiliauskas “Growth of Cubic Silicon Carbide”

13:00 Lunch break

14:00 UAB „*Altechna*” invited Cliff Jolliff “Precise positioning and applications to laser systems”

15:00 Oral session III - Lasers physics and technologies

Chairman prof. V. Sirutkaitis

15:00 Invited Mangirdas Malinauskas “Ultrafast laser 3D nanostructuring of photopolymers”

15:30 Skirmantas Ališauskas „Generation of powerful pulses by optical parametric amplification“

15:45 Tomas Tolenis „Complex study on advanced Nb_2O_5/SiO_2 and ZrO_2/SiO_2 mixture coatings with continuously tunable optical properties“

16:00 Donatas Majus „Three-Dimensional Mapping of Multiple Filament Arrays“

16:15 Conference photo

March 27, Saturday

12:00 Café Scientifique and Conference Closure

Oral session I

Material science and technologies, theoretical physics

OP1

LUMINESCENCE PROPERTIES OF MBE-GROWN ZnO AND MgZnO EPITAXIAL LAYERS

T. Serevičius, S. Miasojedovas, E. Kuokštis, S. Juršėnas

Institute of Applied Research, Vilnius University, Sauletekio Ave. 9-III, LT-10222 Vilnius, Lithuania
tomas.serevicius@ff.stud.vu.lt

ZnO based materials attracted recently much attention due to their unique optical properties, such as high exciton binding energy (e.g. in ZnO 60 meV [1]). High exciton binding energy leads to the existence of excitons even at room and higher temperatures. Such property of ZnO could be utilised for creation of UV laser involving excitons with very low operation threshold. High operation efficiency of such lasers can be reached by employing multiple quantum wells structures with MgZnO, as a barrier material.

Luminescence properties of ZnO and MgZnO MBE grown samples were explored in this work. Sample A is just a ZnO layer (thickness of 650 nm) grown on sapphire substrate, sample B is ZnO layer (thickness of 340 nm) grown on sapphire substrate with undoped GaN buffer layer and sample C is MgZnO layer (thickness of 320 nm) on the top of ZnO-u-GaN-sapphire system. Time-integrated and time- resolved luminescence spectra were studied at high and low excitation conditions. Low power light emitting diodes and semiconductor laser were used for low excitation regime. Luminescence signal was detected by CCD camera (*Hamatsu H6780*) and time correlated single photon counting system (*Picoquant Picoharp 300*). High excitation conditions were performed by utilising picosecond laser *Ekspla PL – 2140*. Time-resolved spectra were measured by applying optical Kerr gate technique.

UV luminescence band at 3.24 eV due to excitonic radiative recombination and defect states related green luminescence band are observed at 2.4 eV at low excitation regime. No luminescence signal was detected from MgZnO epilayer at low excitation regime (order of μW). Time-resolved luminescence demonstrated ~6 ns luminescence decay time from ZnO layer at near-band edge region which indicated high optical quality of MBE-grown sample.

Under high excitation, ZnO samples exhibit a single luminescence band of exitonic origin in spectral region of 3.25-3.27 eV (Fig. 1). Luminescence intensity linearly depends on excitation power density; the band maximum does not shift and broadens with increasing excitation. These feature can be attributed to inelastic exciton-exciton scattering (P_∞ band). After a particular excitation density (>0.3 mJ/cm^2, similar in both A and B samples), a new luminescence band at about 3.14 eV emerges. Emission intensity dependence on excitation density shows super-linear

behaviour, which is typical for stimulated emission, in particular involving inelastic exciton-exciton scattering process. With increase of excitation power density, stimulated emission band starts to redshift and broaden. This implies that a new recombination mechanism, namely, recombination of electron-hole plasma (EHP) rises up. Redshift of EHP band is accounted to the band gap renormalization effect [2]. The insulator-conductor transition in a dense exiton system is called the Mott transition and is typical for highly excited semiconductor materials [2]. The estimated critical Mott density in ZnO is of 10^{19} cm^{-3}. As both ZnO A and B samples exhibit similar luminescence properties, it can be suggested that buffer layer in ZnO B sample does not improve crystal quality of MBE grown ZnO epilayers.

Two dominating luminescence bands are observed in the luminescence spectra of MgZnO (sample C) (triangles in Fig. 1). The origin of the first luminescence band located at about 2.7 eV is related to intrinsic point defect states. In accordance with the increased bandgap of this ternary compound, it is blueshifted in respect of well known green luminescence of ZnO. The second luminescence band is peaked at about 3.95 eV and is caused by radiative transition at near band-edge of MgZnO. Linear luminescence intensity dependence on excitation power density reveals excitonic nature of MgZnO band. It should be noted, that intensity of MgZnO luminescence band is about 20 times lower than that of ZnO samples (sample A).

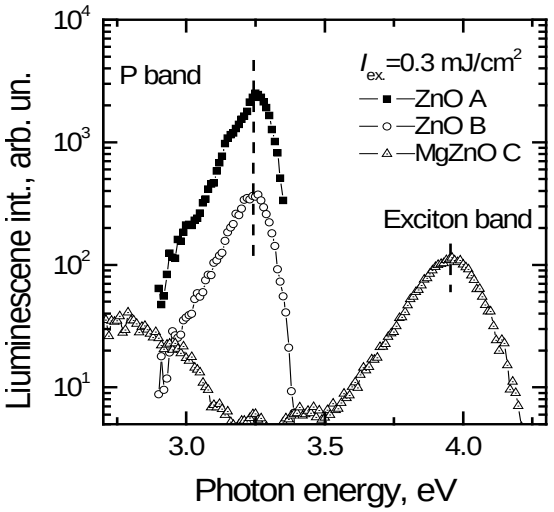

Fig 1. Luminescence spectra of ZnO and MgZnO samples at high excitation conditions (I_{ex}=2 mJ/cm^2) at room temperature.

Taking into account the peak position of the band edge emission one can roughly estimate the value of Mg concentration being 30%. This Mg concentration is close to the critical value when MgZnO lattice changes from wurtzite to cubic [1]. Therefore phase transition of in MgZnO system can cause poor optical quality of the epilayer and thus can rise further problems for creation of ZnO/MgZnO multiple-quantum-well based light emitting devices.

1. H. Morkoc, U. Ozgur, *Zinc Oxide* (Willey VCH, Weinheim, 2009).
2. C. F. Klingshirn, *Semiconductor Optics* (Springer, Berlin, 2007).
3. T. Serevičius, S. Miasojedovas, V. Gavryushin, S. Juršėnas, Phys. Stat. Sol. C, **6** (12), 2671 (2009).

OP2

PLASTIC DEFORMATION EFFICIENCY EVALUATION OF MULTILAYER BAR UNDER AXIAL LOAD

J. Tilindis[1], V. Kleiza[2]

[1] *Kaunas University of Technology, Faculty of Technology, Department of Mechanical technology, Daukanto 12, LT-35209 Panevežys, Lithuania*

jtjlt@yahoo.com

[2] *Kaunas University of Technology, Faculty of Technology, Department of Physical Sciences, Klaipedos 1, LT-35212 Panevežys, Lithuania*

Multilayer structural elements (MSE) are used in various mechanical structures because they enable to combine different materials, thus reaching the required mechanical properties. Most of the MSE calculation methods calculate the state of loaded MSE, only within elasticity limits. While in

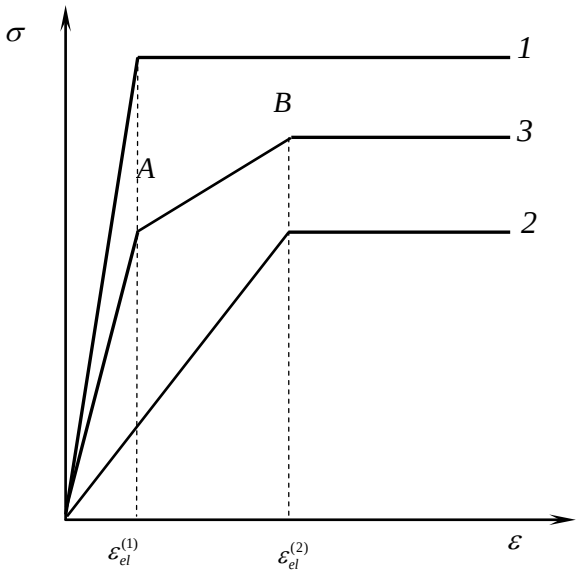

Fig.1. Schematized stress-strain diagrams of a stretchable two layer bar comopsed of ideally elasto-plastic materials. 1,2 are the stress-strain diagrams of materials that compose a bar, 3 is that of a multilayer bar.

some mechanical structures slight plastic deformation could be allowed, in the MSE this deformation could be permissible as well. When the load increases up to level that in one or even more MSE layers plastic deformations arise, the layers in the elasticity zone, take over a part of the bigger load. The ratio between the increased load with the limiting load, which is calculated in

deforming a body within the limits of elasticity, determines the plastic deformation effectiveness. In paper [2], this effectiveness was calculated by studying the two layer bar. The stress-strain diagrams of two layer bar composed of ideally elasto-plastic materials presented in Fig. 1.

It is known [1] that, in extended bars made of the same material, the limiting loads and the coefficient of plastic deformation in the case of elastic-plastic deformation depend on the fastening conditions of the bars, the structure of the bar system, and other factors. In [2], the effect of different factors on the strength and rigidity of multilayer bars under elastic deformation is investigated.

The authors have proposed here the method for calculating stretchable multilayer bar limiting loads, obtained under ideally elasto-plastic deformation, calculation method and analysis of effectiveness coefficient of the bar depending on materials, of which it is composed: elasticity module, stress that causes material plasticity, and on the variation of cross-section areas occupied by these materials.

Mathematical expressions have been proved by means of which it is very simple to calculate the values of the coefficient with arbitrary values of cross-section areas.

So final equation was determined:

$$m = \frac{N_{Kpl}}{N_{Kel}}, \tag{1}$$

where m – coefficient, N_{Kpl} – limiting plastic load, N_{Kel} – limiting elastic load. These variables depend on properties of each material composing bar: elasticity module E_i, stress σ_i, and cross-section A_i, and i – number of materials used in the bar [3].

1. J. Bareisis, D. Garuckas, *Mechanika*, Vol. **24** No. **4**, 23-30 (2000).
2. J. Bareišis, V. Kleiza, *Mechanics of Composite Materials*, Vol. **40** No. **2**, 135-144 (2004).
3. J. Bareišis, V. Kleiza, Multilayer Bars Evaluation, under elastic and elasto-plastic deformation, Proceedings of International Conference Mechanika-2001. Kaunas, 2001, p. 254-259.

OP3

CHARGE TRANSFER IN PYRIDINE-SILVER COMPLEXES

A. Stonkus[1], V. Arcišauskaitė[2], N. Galikova[1], M. Kelminskas[1], A. Gruodis[1]

[1] *Faculty of Physics, Vilnius University, Sauletekio 9, korp.3, Vilnius, Lithuania*

antanas.stonkus@ff.stud.vu.lt

[2] *Faculty of LIFE Sciences, University of Copenhagen, Thorvaldsensvej 40, Frederiksberg C, Denmark*

Interactions between light and molecules, adsorbed on the metal surface, are investigated widely in theoretical and experimental physics. In 1974 Fleischmann et al. experimentally observed an example of this interaction named surface-enhanced Raman scattering (SERS) [1]. Theoretical models that describe SERS can give results, comparable to vibrational experiments, but further improvement is necessary. Several hybrid theories have been introduced in this study. For example, a hybrid quantum mechanics / molecular mechanics methods are useful for modeling of charge transfer excitation energies in pyridine–silver complexes [2].

The object for our calculations is pyridine molecule (Pyr) near Ag_{20} cluster (Fig. 1). Pyridine molecule is one of the most often used objects in SERS experiments. Ag_{20} tetrahedral cluster is the face-centered cubic (FCC) lattice of silver atoms. This work is devoted to study electron transfer dynamics in Pyr..Ag_{20} cluster using Fermi golden rule equation:

$$W_{12} = \frac{2\pi}{\hbar}\left\langle \Psi_1 \left| \hat{H}_{12} \right| \Psi_2 \right\rangle^2 \rho(E_1 - E_2) \tag{1}$$

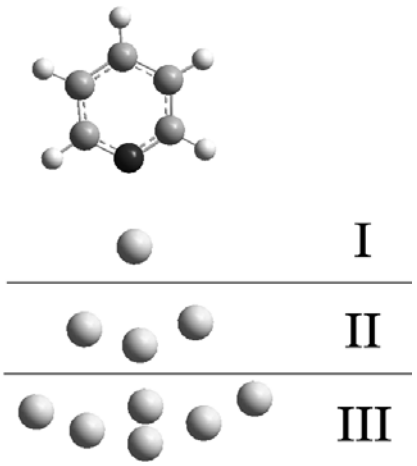

Fig. 1. Pyridine..Ag_{20} cluster. Three different layers under estimation

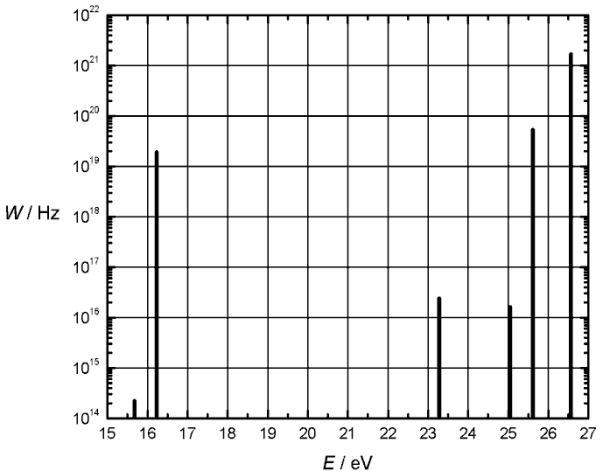

Fig. 2. Rate of electron transfer in Pyr..Ag_{20} cluster as function on one-particle state energy

The calculations were made using *GAUSSIAN03* [3] and *NUVOLA* [4] programs. Presented model allows to estimate electronic couplings between one-particle states: electronically excited states of Pyr and vacant (unoccupied) states of Ag_{20} cluster. Fig. 2 represents the rate of ET as function on state energy.

Fig. 3 and Fig. 4 show the two-dimensional maps of electronic charge redistribution which occurs after electron jumps: i) between Pyr atom number 6 (N) and Ag_{20} cluster atoms nr. 9 and nr.10; ii) between Pyr atoms nr. 2 (C) and nr. 3 (C) and Ag_{20} cluster atoms nr. 9 and nr.10; (both Fig. 3) iii) between Pyr atoms nr. 4 (C) and nr. 5 (C) and Ag_{20} cluster atom nr. 1 (Fig. 4). Both maps represents the charge transfer processes between third layer of Ag_{20} cluster and -CNC- chain of Pyridine when influence of the first and second layer of Ag_{20} cluster could be named as minimal. Presented results allow creating the model of charge transfer which allows to describe the role of the second and third layer of Ag_{20} cluster. Also orientational aspects of Ag_{20} cluster to Pyr molecule must be involved.

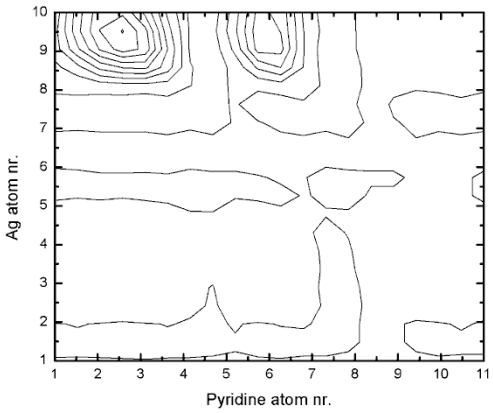

Fig. 3. Two-dimensional map of electronic charge redistribution

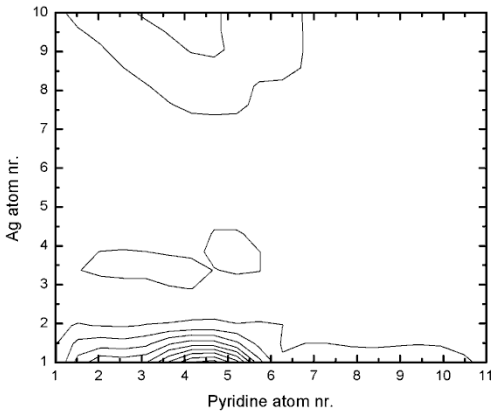

Fig. 4. Two-dimensional maps of electronic charge redistribution

1. M. Fleischmann, P.J. Hendra, A.J. McQuillan, Chemical Physics Letters 26 (1974) 163.
2. V. Arcišauskaitė , J. Kongsted, T. Hansen, K.V. Mikkelsen, Chemical Physics Letters **470** 285–288 (2009)
3. Gaussian 03, Revision D.01, M. J. Frisch, G. W. Trucks, et al, and J. A. Pople, Gaussian, Inc., Wallingford CT, (2004)
4. N. Galikova, A. Gruodis, Innovative infotechnologies for science, business and education, 2 (2008) 12.1.

OP4

PECULARITIES OF CARRIER RECOMBINATION IN HIGHLY-EXCITED GaN

S. Krotkus[1], S. Miasojedovas[1], and S. Juršėnas[1]

[1] *Institute of Applied Research, Vilnius University, Sauletekio Ave. 9-III, LT-10222 Vilnius, Lithuania*
skrotkus@gmail.com

Gallium nitride (GaN) is a wide-band gap semiconductor which is used in the high-frequency electronic and optoelectronic devices due to its superior characteristics (thermal conductivity, breakdown field, thermal/chemical stability, etc.) in the high power/temperature applications. In order to understand the processes in the semiconductor devices under high power/temperature regime one must be aware of the processes in semiconductor layer with high non-equilibrium carrier concentration ($>10^{18}$ cm^{-3}). One of the methods to reach such a high concentration and to characterize semiconductor material is its photoluminescence (PL) measurement under high intensity laser excitation. In this work we present results of PL measurements of GaN sample in 80-300 K temperature range under various layer excitations (0.05-3 mJ/cm^2). We show that broad luminescence band peaking at 3.38 eV and dominant at room temperature is due to spontaneous emission of electron-hole plasma (EHP, see Fig. 1), which is common in highly-excited GaN. In order to identify luminescence band with a peak at 3.3 eV at low temperatures time-resolved luminescence measurements were performed which showed that the latter band can be attributed to stimulated emission (SE).

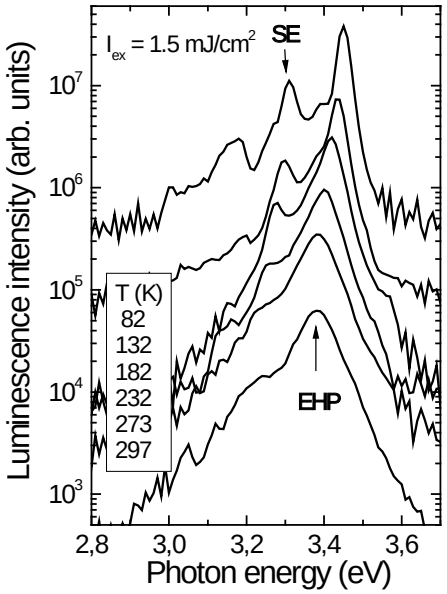

Fig. 1. Time -ntegrated luminescence spectra in 80-300 K temperature range under constant excitation (1.5 mJ/cm^2). SE and EHP stands for identified luminescence mechanisms: stimulated emission and spontaneous emission of electron-hole plasma, respectively.

Additionally, non-equilibrium carrier lifetimes were deduced from transient luminescence behavior (Fig. 2). Carrier lifetimes varied from 100 to 400 ps and decreased with increasing temperature (Fig. 2, inset), which is a consequence of a dominant non-radiative carrier recombination mechanism. Linear luminescence decay was observed in GaN layer contrary to speculations about Auger recombination, claimed by some authors to be the main cause of the efficiency droop in the InGaN-GaN based optoelectronic devices [1, 2]. On the other hand, non-linear decay at the early stage of carrier recombination is due to SE mechanism.

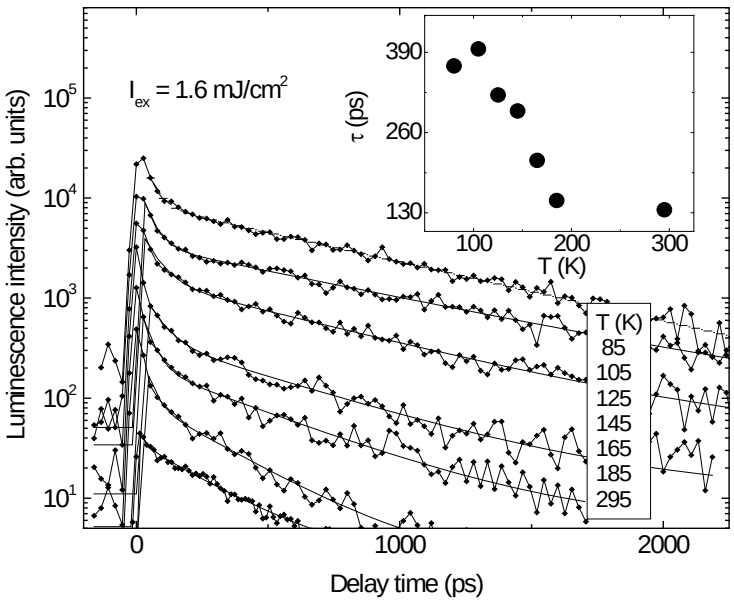

Fig. 2. Transient luminescence behavior in various temperatures under constant excitation (1.6 mJ/cm^2). Fitting of transient luminescence curves led to determination of carrier lifetime dependence on temperature (inset).

Furthermore, by fitting of the high energy side of EHP luminescence band enable us to evaluate carrier temperature and its time dependence by using luminescence spectra at various times after excitation. Estimated maximum plasma's overheat reached nearly 500 K at the first moments after excitation. It was showed that plasma's cooling rate has got fast and slow cooling components. The former is due to emission of LO phonons, which is common in nitrides, while in order to explain the latter other mechanisms of carrier scattering must be taken into account.

1. Y.C. Shen, G.O. Mueller, S. Watanabe, N.F. Gardner, A. Munkholm, and M.R. Krames, App. Phys. Lett. **91**, 141101 (2007).
2. M. Zhang, P. Bhattacharya, J. Singh, and J. Hinckley, App. Phys. Lett. **95**, 201108 (2009).

OP5

APPROXIMATE DESCRIPTION OF DECAYING QUASI-STATIONARY STATE

G. Kiršanskas[1], A. Matulis[2]

[1] *Department of Theoretical Physics, Vilnius University, Saulėtekio 9, LT-10222 Vilnius, Lithuania*

gediminas.kirsanskas@ff.stud.vu.lt

[2] *Semiconductor Physics Institute, A. Goštauto 11, LT-01108 Vilnius, Lithuania*

Progress in nanometer technology has triggered a broad activity in low dimensional quantum systems [1]. During the last five years the interest has shifted to graphene [2, 3], the single layer of graphite that is an ideal two-dimensional system. Charge carriers in graphene behave like “relativistic” massless particles, and due to so-called Klein effect [4] the control of their behavior by means of the electromagnetic fields is one of the most challenging tasks. This situation occurs because the quantum dots in graphene have no bound states, and the electrons escape from them sooner or later. Thus, the description of quasibound states becomes of importance. For this purpose various approximate methods are used, mostly considering some approximate stationary problem. One of them is so called the *complex energy technique* [5], which relates the imaginary part of energy eigenvalue with the inverse lifetime of quasibound state. The other way to determine the above lifetime is to extract it from the width of resonances in so called *local density of states* of artificially confined system [6, 7]. The quasi-classical approach [8] for the description of the quasibound states is also used.

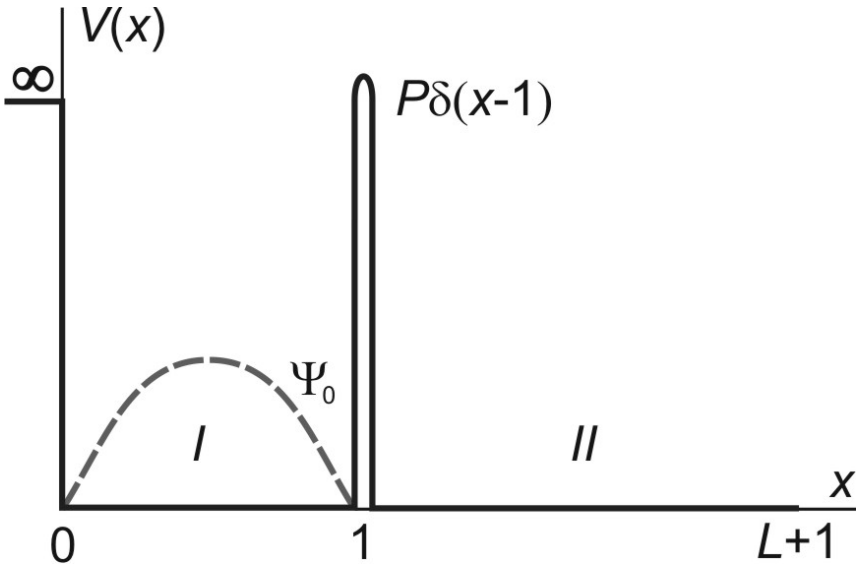

Fig. 1. Potential for Schrödinger equation.

The aim of this work is to evaluate the advantages and shortcomings of various approximate quasibound state description methods comparing the results with the exact solution for analytically solvable model of decaying quantum state, which is an example of most simple non-stationary problem. For this purpose we use the model of one-dimensional (1D) quantum system, described by Schrödinger equation

$$i\hbar \frac{\partial}{\partial t}\Psi(x,t) = \left\{ -\frac{\hbar^2}{2m}\frac{\partial^2}{\partial x^2} + V(x) \right\} \Psi(x,t), \qquad (1)$$

where the electron moves in the potential *V(x)* shown in Fig. 1, with repulsive δ-function that separates the quantum dot (region I) from the infinite half *x*-axis (region II) [9]. At initial time moment (t=0) electron is described by wavefunction Ψ_0, which corresponds to ground state of isolated quantum dot, i.e. $P = \infty$. This model has been examined by a number of people, in particular, by Petzold [10] and Winter [11], and more recently by Dijk [12] mostly in relation with the problem of radioactive decay of nucleus.

1. T. Chakraborty, Quantum dots (Elsevier, Amsterdam, 1999).
2. K. S. Novoselov, A. K. Geim, S. V. Morozov, D. Jiang, M. I. Katsnelson, I. V. Grigorieva, S. V. Dubonos, and A. A. Firsov, Nature (London) **438**, 197 (2005).
3. Y. Zang, Y. W. Tan, H. L. Stormer, and P. Kim, Nature (London) **438**, 201 (2005).
4. M. I. Katsnelson, K. S. Novoselov, and A. K. Geim, Nat. Phys. **2**, 620 (2006).
5. P. Hawageegana and V. Apalkov, Phys. Rev. B **77**, 245426 (2008).
6. A. Matulis and F. M. Peeters, Phys. Rev. **77**, 115423 (2008).
7. M. R. Masir, A. Matulis, and F. M. Peeters, Phys. Rev. **79**, 155451 (2009).
8. Hong-Yi Chen, V. Apalkov, and T. Chakraborty, Phys. Rev. Lett. **98**, 186803 (2007).
9. A. Matulis and G. Kiršanskas, Lith. J. Phys. **49**, 373 (2009).
10. J. Petzold, Z. Phys. **155**, 422 (1959).
11. R. G. Winter, Phys. Rev. **123**, 1503 (1961).
12. W. van Dijk, F. Kataoka, and Y. Nogami, J. Phys. A:Math. Gen. **32**, 6347 (1999).

OP6

MODELING OF EXCITON DYNAMICS IN CARBON NANOTUBES

J. Chmeliov[1], L. Valkūnas[1,2]

[1] *Department of Theoretical Physics, Faculty of Physics, Vilnius University, Sauletekio ave. 9-III, LT-10222 Vilnius, Lithuania*

Jevgenij.Chmeliov@ff.vu.lt

[2] *Institute of Physics, Savanoriu ave. 231, LT-02300 Vilnius, Lithuania*

Carbon nanotubes (CNTs) are large elongated carbon molecules which can be viewed as a strip cut from an infinite graphene sheet rolled up to form a tube. With a typical diameter of several nanometers but up to centimeters in length, they exhibit an unprecedented length/diameter aspect ratio exceeding 10^7 and thus are probably the best known example of the quasi-one-dimensional systems [1]. Possessing many amazing properties such as high mechanical strength, high thermal conductivity and tunable electrical properties, CNTs appear ideal for a wide range of current and future applications. On the other hand, many possible properties are still not explored, some of them still lack proper theoretical reasoning. Currently, there is considerable interest in understanding the optical spectra, ultrafast dynamics and related physical mechanisms due to their fundamental importance and direct relevance to many of the potential applications.

Experimental studies of the excitation dynamics in the single-walled carbon nanotubes employing ultrafast pump-probe and time-resolved fluorescence techniques with sub-100 fs time resolution reveal very fast decay kinetics on the time scale of a few hundreds of femtoseconds. As follows from the analysis of the decay behavior of the kinetics and the dependence of the corresponding amplitude on excitation intensity, it was concluded that during the initial part of the kinetics the exciton-exciton annihilation process dominates, while with time, when only one exciton per nanotube is left, the diffusion process becomes predominant [2].

While comparing the mentioned decay kinetics with the existing theoretical models [2], the full agreement is still not achievable. In order to solve this problem and describe the exciton dynamics in CNTs in a more detailed way, a new stochastic model is investigated in this work. In this model, describing the system containing multiple excitons, the only two lower excitonic energy levels (E_{11} and E_{22} respectively) are taken into account with the possible exciton generation/relaxation pathways represented by arrows in Fig. 1. The calculated excitation decay kinetics, obtained by solving the corresponding Master equations for the probabilities $P_{i,j}$, are in better agreement with experimental data for the initial times while there are still some deviations, probably due to the influences of the particular sample preparations and/or surroundings conditions.

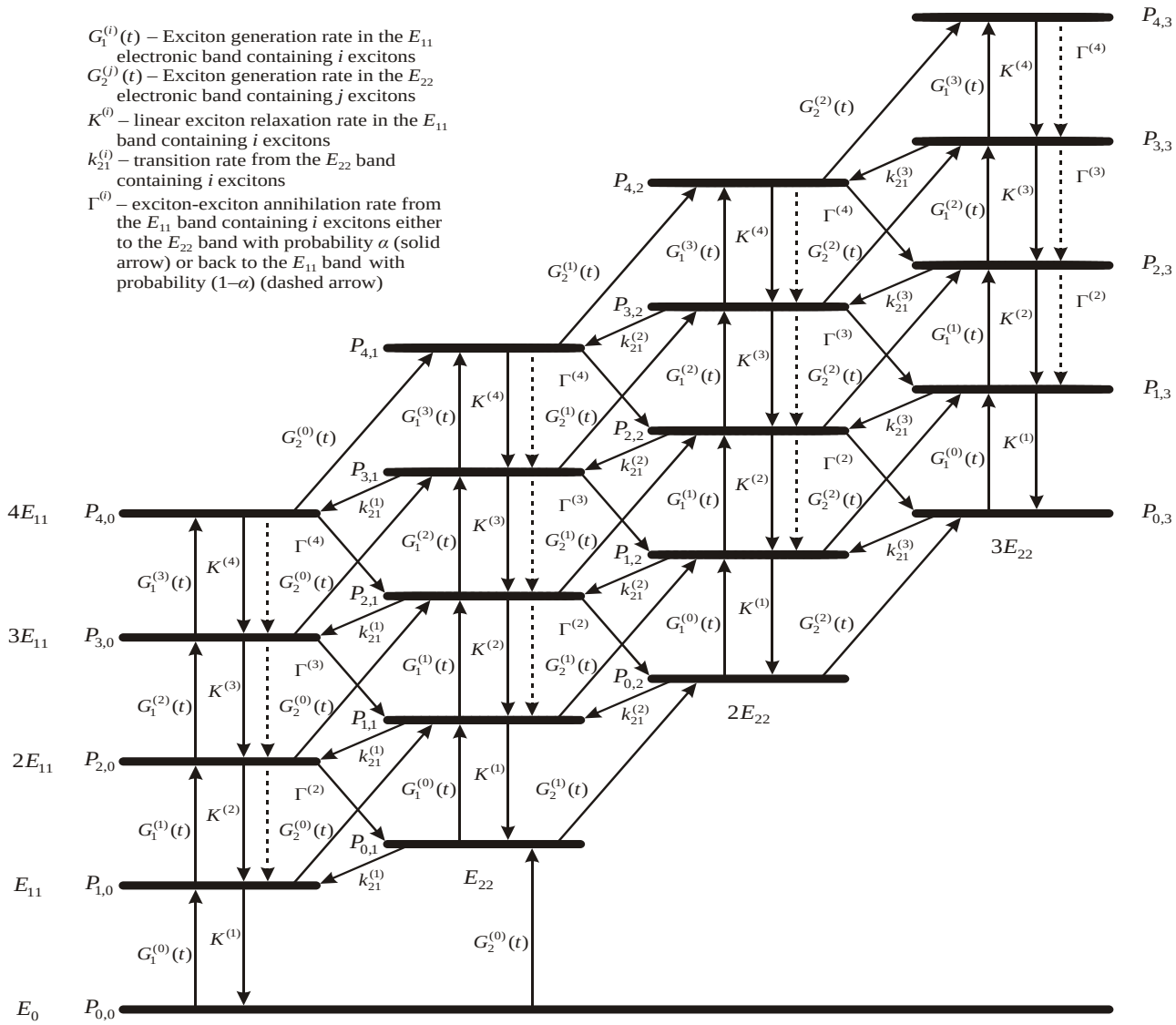

Fig. 1. The kinetic scheme for the system with multiple exciton population of both E_{11} and E_{22} exciton states. The lowest energy level E_0 (long bar in the bottom) indicates the ground state. The population of the E_{11} exciton band is reflected in the upward direction with the corresponding energies of E_{11}, $2\,E_{11}$, $3\,E_{11}$, … (shown up to $4\,E_{11}$), while the population of the E_{22} exciton band is indicated rightwards (with the corresponding energies of E_{22}, $2\,E_{22}$, … (shown up to $3\,E_{22}$)). In addition, the levels of the combined population corresponding to energies $E_{i,j} = i \cdot E_{11} + j \cdot E_{22}$ are also shown. The probabilities of the occupation of these energy levels are denoted as $P_{i,j}$, and the possible transition pathways between different states are indicated with arrows (for the labeling see the legend in the kinetic scheme). For clarity, the upper electronic band $E_{nn} \cong 2E_{11}$ involved in exciton-exciton annihilation is not shown since the excitons relax from this state almost instantaneously (comparing with other characteristic rates in this model) either to the E_{22} or back to the E_{11} band.

1. L. Valkunas, Y. Z. Ma, and G.R. Fleming, Physical Review B, **73**, 115432 (2006).

Jorio, G. Dresselhaus, and M.S. Dresselhaus (Eds.), *Carbon Nanotubes. Advanced Topics in the Synthesis, Structure, Properties and Applications* (Springer, Berlin, 2008).

ORAL SESSION II

Interdisciplinary

OP7

ESTCUBE-1 SATELLITE – SAILING ON SOLAR WIND

M. Pelakauskas, M. Noorma, K. Voormansik

[1] *University of Tartu, Faculty of Science and Technology Tähe 4, 51010, Tartu, Estonia*
martynas@ut.ee

ESTCube-1, the first Estonian student satellite (www.estcube.eu), is a student project which is aiming to create, build and launch a CubeSat specification satellite. The satellite's primary mission will be to test the concept of the electric solar sail (www.electric-sailing.com) in space for the first time. The novel electric propulsion technology based on the interaction of charged particles with a microscopic tether will be tested together with partners from the Finnish Metrological Institute (FMI), Jyväskylä University and Helsinki University (all from Finland), and the German Space Agency (DLR).

The launch of ESTCube-1 is scheduled in 2011. Currently the project is in the late stages of Phase B – first prototypes and work results of all the subsystems are nearing completion. The main subsystems of the satellite include the Electrical Power System (EPS), the Command and Data Handling System (CDHS), the Communications System (COM), the Attitude Determination and Control System (ADCS), the Payload (PL) and the Structure (STR).

If successful, the project will confirm the concept of the electric solar sail, thus taking the first step towards a new spacecraft propulsion technology.

OP8

FUEL CELL TECHNOLOGY: HOPES, CHALLENGES AND POSSIBLE APPLICATIONS

P. Klimczak

Technical University of Lodz

piotr.klimczak@onet.eu

Fuel cell is an electrochemical cell that converts a source fuel into an electrical current and water. This technology is the most promising idea for the future development of world energy systems due to its high efficiency and unique environmentally friendly features, since the only waste product is water vapor and hydrogen is one of the most common element on the earth [2,3].

Fuel cells are very useful as a power sources (Fig.1) and this technology is very likely to successfully replace a contemporary energy sources applied in different areas [5]. However, at the moment there are still some limitations in their applicability. Therefore, this technology is being intensively developed in EU countries, Japan and USA.

This paper gives a general outlook on the fuel cell construction, size and weight, its applications and efficiency. Additionally, the fundamental principles of fuel cell thermodynamics and fuel cell power plant engineering are summarized. Afterwards, the main obstacles in further development of that technology are presented, together with leading ideas of overcoming them. Finally, the hydrogen economy, storage and refueling options are discussed as an important problem associated with any real application of fuel cells in future [4].

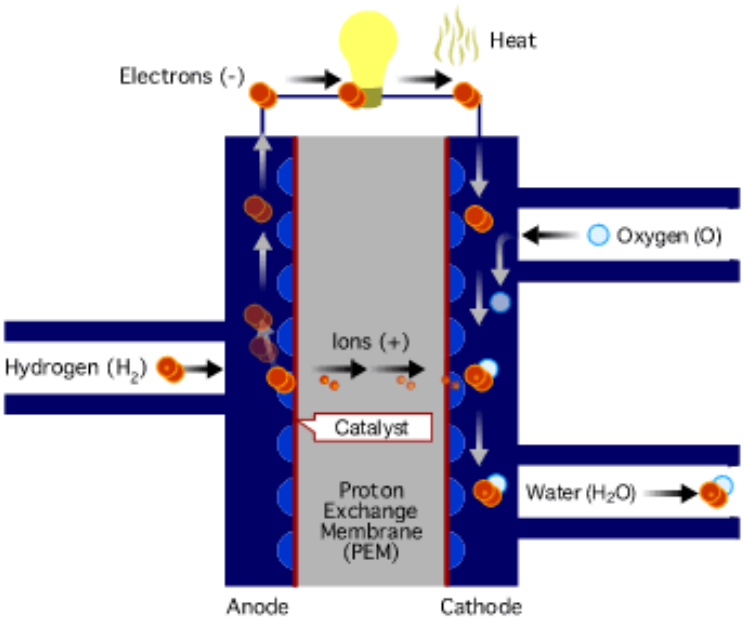

Fig. 1. A schematic construction of fuel cell [1].

1. Fuel Cell and Evaluation Center (FCTec) website: http://www.fctec.com/
2. J.H. Scott, Proceedings of the IEEE **10(94)**, 1815-1825 (2006).
3. B. Cook, Engineering Science and Education Journal **6(11)**, 205- 216 (2002).
4. P. Gilreath, B.N. Singh, P. Rastgoufard, Fuel cell technology: economic, social, and political aspects, 2003 Annual Technical Conference. New Orleans, Louisiana, 11 April, 2003, p. 29.
5. T. Jacobs, J. Beukes, Suitability of fuel cell technology for electricity utility standby power applications, INTELEC 2006: 28th Annual International Telecommunications Energy Conference. Providence, September 2006, p. 1.

OP9

TITANITE U-PB DATING OF A MYLONITE FROM THE DRUKSIAI-POLOTSK DEFORMATION ZONE, THE EAST EUROPEAN CRATON

Irma Vejelyte[1], Svetlana Bogdanova[2], Ekaterina Salnikova[3]

[1] *Department of Hydrogeology and Engineering Geology, Faculty of Natural Science, Vilnius University, Čiurlionio 21, LT-03113 Vilnius, Lithuania*

Irma.Vejelyte@gf.vu.lt

[2] *Lund University, Department of Earth and Ecosystem Sciences, SE-22362 Lund, Sweden*

[3] *Institute of Precambrian Geology and Geochronology, emb. Adm. Makarov 2, Sankt Petersburg, Russia*

The Lithuanian crust was formed between 1.9 and 1.8 Ga along with the amalgamation of the entire East European Craton and is subdivided into several tectonic domains, having different structural and geophysical patterns, crustal composition and evolution. The major are the West Lithuanian Granulite Domain and East Lithuanian Domain, which are adjoined along the Mid-Lithuanian Suture Zone, and partly the Belarus-Podlasie-Granulite Belt in SE Lithuania [1]. The Paleoproterozoic crust in Lithuania is completely overlain by the Phanerozoic sedimentary cover ranges from 200 m in the east to 2300 m in the west. Several E-W-striking, crustal-scale deformation zones (e.g. the Telsiai shear zone and the Druksiai-Polotsk deformation zone) cut sharply the mostly NS- and NW-trending Palaeoproterozoic structural pattern.

Titanite (CaTiSiO5) is one of accessory minerals in the crystalline rocks, which can be used for age determinations of metamorphic and deformational events. The ratio of U and Pb in titanite, balance of U in the lattice during crystal growth and slow diffusion of radiogenic Pb provide available conditions for geochronology of such geological processes.

In this study titanite from an augen mylonite of granitic composition have been taken from the Druksiai-Polotsk deformation zone (DPDZ). The 35–40 km wide DPDZ is well marked by gravity and magnetic linear anomalies, striking E-W. The crystalline rocks within the DPDZ are granulites, biotite granites and migmatites, consisting of amphibole-plagioclase paleosome and plagioclase-quartz-biotite±microcline±amphibole neosome. The macro- and microscopic structural studies show that the DPDZ rocks experienced multiple ductile and brittle deformations that involved a variety of textural and softening reaction processes. Due to ductile shearing gneisses, augen mylonite, mylonites and ultramylonites were produced in the DPDZ. The latest reactivation was due to brittle deformation forming breccia.

In thin sections, rounded porphyroclasts of plagioclase show some evidence of plastic deformation, whereas fracturing was resulted from brittle deformation. Recrystallized quartz grains

are irregular in shape with undulatory extinction, indicating dynamic recrystallization mainly by subgrain rotation to grain boundary migration recrystallization. Some quartz grains have a strain-free appearance, and boundaries are straight formed by static recrystallization. The borders of amphibole grains and intragranular cracks are filled with epidote and biotite. Biotite flakes are recrystalized to very fine-grained aggregates outlining the foliation which surrounds porphyroclasts.

Two fractions of brown to yellow titanite have been analysed. Both analyses show uranium contents from 86.3 to 87. 3 ppm and lead contents of 35.4 to 38.6 ppm. The titanite from this DPDZ mylonite has yielded a U–Pb concordant age of 1534±9 Ma. This light brown titanite follows the folation in the host rock and was obviously formed during retrogression from amphibolite- to epidote-amphibolite facies and coeval mylonitization. Thus, the obtained age is dating the deformation and formation of the DPSZ.

Shear zones of the same age are known in southern and central Sweden and in NE Poland. These E-W trending deformation zones accommodate both mafic and granitoid intrusions and are probably related to an extensional period in the Mesoproterozoic evolution in the western part of the East European Craton.

This is a contribution to the project “The Precambrian structure of Baltica as a control of its recent environment and evolution” of the Visby Programme supported by the Swedish Institute and the Lithuanian State Science and Studies Foundation.

1. G. Skridlaitė, G. Motuza, Tectonophysics, **339**, 113-133 (2001).

OP10

THE RESEARCH OF APPROPRIATION OF SUPERPARAMAGNETIC MAGNETITE NANOPARTICLES FOR MR IMAGING AND RADIOTHERAPY

A. Kleinauskas[1], S. Bagdonas[1], P. Juzenas[2]

[1] *Vilnius University Laser Research Centre, Sauletekio 9, Building 3, LT-10222 Vilnius, Lithuania*

Andriaus.Kleinausko@gmail.com

[2] *Department of Radiation biology, institute for cancer research, Norwegian Radium Hospital, Rikshospitalet University Hospital, Montebello 0310 Oslo, Norway*

The cancer is a plague of 21st century. There are a lot of treatment and therapy methods for this disease. But almost all of them have drawbacks. Photodynamic therapy is applied to treat only superficial tumors, radio- and chemotherapy negatively affect a whole organism. To reduce this effect and make radiotherapy more selective, various nanoformations, various nanoparticles, conjugates of nanoparticles and photosensitisers are studied intensively [1]. Especially promising are bimodal nanoformations that can be used not only for therapy, but also for diagnostics.

In this research we have investigated such bimodal nanoparticles - magnetite nanoparticles coated with organic polymer - alginate. Particles were monodisperse, about 207 nm in diameter, prepared by ultrasonication of ferrous and ferric salts solution [2]. Applicability of those particles in MRI was studied in three model systems: in phosphate buffered saline (PBS) at pH =7.4, in cell culture medium RPMI and in PBS with proteins at pH =4. Third model system is similar to internal environment of lysosome. For each MRI experiment two specimens were taken, one with small concentration of nanoparticles and other - without particles. MR images were taken 24 hours after preparing of solutions (Fig. 1). These images show that nanoparticles were superparamagnetic and applicable for MRI, moreover, it were stable and did not coagulate in low pH mediums after 24 hours.

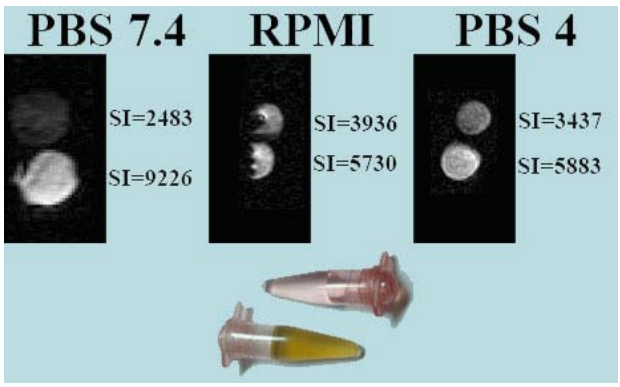

Fig. 1. MR images with values of signal intensity in three model systems. Two specimens are also shown.

Suitability for radiotherapy was studied in vitro in two prostate cancer cell lines – Du 145 and LNCaP. Pharmacokinetic research has shown that even high particle concentrations (1.5 mg/ml) are not toxic in dark conditions for both cell lines. Based on microscopy, cell survey of both cell lines was carried on for 24 hours and 0.2 mg/ml concentrations of particles were chosen for other experiments. Fluorescence microscopy with cell trackers established that nanoparticles accumulate in perinuclear region of cells and in lysosomes.

Cell viability after various exposures to X-ray irradiation, i.e. radio therapeutic effect was investigated after 72 hours under above- mentioned conditions of incubation. This experiment showed that applied nanoparticles had no significant radiotherapeutic effect. Cells treated with particles survived similarly like those without treatment (Fig. 2).

Theoretical calculations of a total cross section for the photoelectric effect and Compton scattering demonstrated that in wavelength diapason used for those experiments, a total cross section of magnetite is small and comparable with that of glycerol.

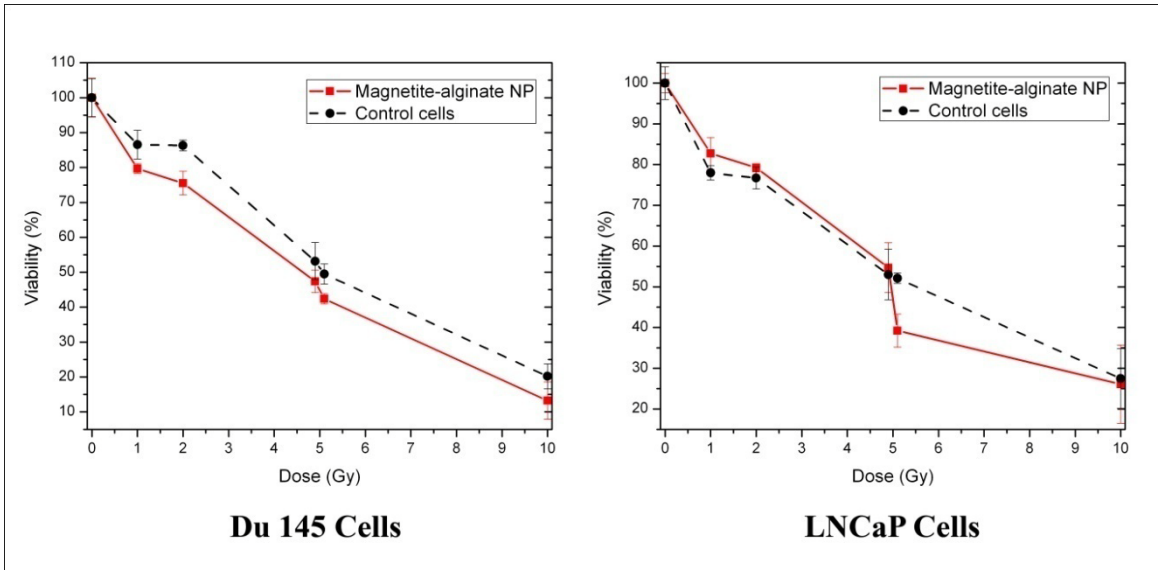

Fig. 1.Cell viability with and without treatment with nanoparticles and irradiation with X-Ray.

The lack of cytotoxic effect from magnetite nanoparticles in this research was probably determined by inappropriate microlocalization in cells and not optimal irradiation source. This does not mean that nanoparticles cannot by used in radiotherapy at all, it only shows that there are a lot of challenges to overcome in future studies.

1. P. Juzenas, W. Chen, Y-P. Sun et al., Adv Drug Deliv Rev. **60(15)**, 1600-1614 (2008).
2. K. Melcher, L.-M. Ng, E. Zhou et al., Photodynamic Therapy **7380** (2009).

OP11

ANALYSIS OF FLUORESCENCE OF CERVICAL SUPERNATANT EXCITED WITH 355nm MICROLASER COMPARING NORMAL, CERVICITIS AND CIN2+ GROUPS

V. Gėgžna[1,2], A. Vaitkuvienė[1], R. Kurtinaitienė[3]

[1]*Institute Applied Research, Vilnius University, Vilnius, Lithuania*

[2]*Faculty of Natural Sciences, Vilnius University, Vilnius, Lithuania*

Vilmantas.Gegzna@gf.stud.vu.lt

[3] *Santariškių Clinics, Vilnius University, Vilnius, Lithuania*

Cervical cancer is one of the most common forms of cancer in women. Success in diagnostics of this disease is due to the use of cytological smear analysis (the Pap test). However, the test gives significant portion of both false-positive and false-negative conclusions. In searching for alternative or supplementary test our group delved into analysis of fluorescence of cervical supernatant as method of cervical pre-cancer diagnosis. Previous investigations [1] [2] showed that it has potential to be suitable for medical purposes. Extremely promising was 355 nm excitation which enabled to achieve 90.9% sensitivity and 100% specificity distinguishing normal and pre-cancerous groups. Unfortunately there were only 11 normal vs. 7 pre-cancerous samples. The aim of this investigation was to analyze more samples and get more precise results. The license was given by Lithuanian Bioethics Committee.

355 nm microlaser was used to excite sediments of supernatant which were dried on quartz plates. 40 samples of normal, 28 of CIN2+ (precancerous state – cervical intraepithelial neoplasia of 2nd degree or higher and carcinoma *in-situ*) and 12 cases of cervicitis (80 samples overall) were analysed. Fluorescence spectra registered and approximated with a few Gaussian curves. The SPPs (SPP - ratio of component's area to the area under whole experimental curve) of Gaussian curves (the components) were compared among histological/cytological groups using Mann Whitney test. Further ROC (receiver operating characteristic) analysis was made for 13 cases, in which Mann Whitney test showed statistically significant differences between the SPPs. The method enabled us to separate normal group from others with accuracy of 70.0%, cervicitis with accuracy of 68.8% and CIN2+ with accuracy of 73.8%.

1. A. Vaitkuviene, V. Gegzna, S. Juodkazis, S. Jursenas, S. Miasojedovas, R. Kurtinaitiene, J. Rimiene, J. Vaitkus, Fluorescence spectrum and decay measurement for HSIL vs NORMAL cytology differentiation in liquid PAP smear supernatant. LASER FLORENCE 2008: Selected Presentations at the International Laser Medicine Congress Florence (Italy), 31 October–1 November, 2008. AIP Conference Proceedings Volume 1142, pp. 21-25.
2. A. Vaitkuviene, V. Gegzna, R. Kurtinaitiene, J. Rimiene, J. Vaitkus, 355 nm Microlaser for autofluorescence diagnosis in PAP spin, Lasers Med Sci (2009) 24 (Suppl 1):S32.

OP12

STOCHASTIC MODEL OF RETURN MATCHING TO THE DATA OF FINANCIAL MARKETS WITH DIFFERING LIQUIDITY

A. Kononovičius[1,2], V. Gontis[2]

[1] *Vilnius University, Faculty of Physics*

[2] *Institute of Theoretical Physics and Astronomy of Vilnius University*

aleksejus.kononovicius@gmail.com

Classical theories of economics were developed in the times then elaborate analysis of empirical data was impossible. Therefore classical economics are unable to give convincing explanation of interesting effects discovered, while analyzing high frequency (min^{-1} – h^{-1}) time series. One of those, in classical sense, anomalous, but universal, effects is power law statistical properties observed in various financial markets around the world [1]. Though in scientific literature one usually finds analysis of mature financial markets (such as New York Stock Exchange (further NYSE)), which exhibit high liquidity, while juvenile markets, which exhibit low liquidity, are neglected. Therefore it is of scientific interest to know how statistical properties scale as liquidity drops.

We analyzed tick by tick trades of 4 stocks traded on NASDAQ OMX Vilnius Stock Exchange (further VSE), low liquidity financial market, for 50 months since May 2005, empirical data was provided by VSE. We also extended our previous analysis [2] of NYSE empirical data – 24 stocks traded for 27 months since January 2007. By definition differing market liquidity causes evident difference in mean inter-trade times – *362 s* in VSE, *3.02 s* in NYSE. But scaling of statistical properties of absolute return, which we define as

$$r_{\Delta t}(t) = [\ln p(t) - \ln p(t - \Delta t)], \qquad (1)$$

where *p(t)* is price function of time and Δt is width of return time window (we use 60 s, 600 s and 1800 s values), seems less evident. We obtained perfect match of distributions by ignoring zero return values, probability of which dramatically rises if mean inter-trade times are not significantly smaller than return time window. While spectral density, obviously, can't be matched by using previous technique, though power spectra from both financial markets seem to overlap better with larger absolute return time windows. Obtained matches allows us to conclude that main reason for visible differences in statistical properties is differing financial market liquidity.

We proposed to model return as double stochastic process with long-range memory [2,3]. In order to improve control of model results, we rewrote main model stochastic differential equation as

$$\mathrm{d}x = \left[\eta - \frac{\lambda}{2} - \left(\frac{x}{x_{max}}\right)^2\right] \frac{(1+x^2)^{\eta-1}}{\left(1+\epsilon\sqrt{1+x^2}\right)^2} x\mathrm{d}t_s + \frac{(1+x^2)^{\frac{\eta}{2}}}{1+\epsilon\sqrt{1+x^2}}\mathrm{d}W_s, \quad (2)$$

where x is dimensionless return, t_s is dimensionless time and W_s is accordingly scaled Wiener process. As in [2, 3], we integrate solutions of Eq. (2) within dimensionless time intervals, corresponding to return calculation time window Δt, and modulate them with q-Gaussian [4] noise in order to obtain time series statistically comparable with empirical data. Using same model parameter set we obtained match between statistical properties exhibited by NYSE, VSE and our model in three different time scales (Δt values 60 s, 600 s and 1800 s).

1. R. Cont. *Long range dependance in financial markets.* (Springer, Berlin, 2008).
2. A. Kononovičius. *Modeling of return in financial markets*. Undergraduate thesis, VU, 2009.
3. V. Gontis, J. Ruseckas, A. Kononovičius. Physica A **389**, p. 100-106 (2010).
4. Cf. Gell-Mann, C. Tsallis. *Nonextensive Entropy - Interdisciplinary Applications*. (Oxford University Press, New York, 2004).

ORAL SESSION III

Lasers physics and technologies

OP13

GENERATION OF POWERFUL PULSES BY OPTICAL PARAMETRIC AMPLIFICATION

S. Ališauskas

Department of Quantum Electronics, Vilnius University, Sauletekio ave. 9, 10222 Vilnius, Lithuania

skirmantas.alisauskas@ff.vu.lt

Ultrafast optics is a rapidly evolving field of modern science. Furthermore, the high intensities that can be generated using femtosecond light pulses allow exploring new regimes of light-matter interaction. Considerable effort has been dedicated to the achievement of shorter light pulses, to improve temporal resolution for time-resolved spectroscopy applications; other efforts have been dedicated to expansion of wavelength tunability of the pulses for chemical and biological applications, since this would make it possible to excite in resonance different materials, and to probe optical transitions occurring at different frequencies.

There are two ways to generate powerful laser pulses: chirped pulses amplification in laser media and optical parametric amplification in nonlinear crystal. Several unique properties, like high gain per pass, broad amplification bandwidth and high contrast ratio give optical parametric amplifiers a favorable edge over conventional laser amplifiers based on media with population inversion.

This report will be devoted to the state-of-the-art of generation of powerful pulses by optical parametric amplification including latest results achieved in the laboratories of Department of Quantum Electronics at Vilnius University.

OP14

COMPLEX STUDY ON ADVANCED NB_2O_5/SIO_2 AND ZRO_2/SIO_2 MIXTURE COATINGS WITH CONTINUOUSLY TUNABLE OPTICAL PROPERTIES

T.Tolenis[1], A. Melninkaitis[2]

[1] *Institute of Physics, Savanoriu ave. 231 LT-02300, Vilnius, Lithuania*

Tomas.Tolenis@ff.stud.vu.lt

[2] *VU Laser Research Center, Sauletekio ave. 10, LT-10223 Vilnius, Lithuania*

Optical interference coatings are thin film layers, which are used in surfaces of laser systems in order to increase their reflection/transmission or spectral efficiency. Vast majority of the interference coatings are made of fixed high and low refractive indexes layers by using conventional so called thermal deposition techniques. Typically such coatings are produced by electron beam or resistance heating evaporation as well as thermal evaporation with ion assisted beams. However main problems in such traditional coatings are related to their low optical resistance (they cannot withstand a high intensity of laser light), layer inhomogeneity, defects and roughness of the surface. Advanced IBS (Ion beam sputtering) technology with high kinetic energy particles [1, 2] allows avoiding similar problems and results in superior optical quality of the coatings. Furthermore it allows also vaporizing optical coatings by mixing different materials at the same time. That property of the process opens up the possibility to continuously tune the refractive index inside the coating. The rage of refractive indices is varied between the low and high indices of materials used for the mixture. Continuous change in refractive index allows fabrication of more complex coatings, in example so called *Rugate Notch Filters* and *Chirped Mirrors*. However before the applications of these mixtures in practice, it is necessary to investigate their optical properties with respect to material ratio in the coating. To our knowledge there is a lack of publications dedicated to the Nb_2O_5/SiO_2 and ZrO_2/SiO_2 mixtures and their properties so the main goal of this study was complex characterization of such coatings. This study is governing the spectra-photometric reflectance/transmittance, total optical scattering, atomic force microscopy, X-ray diffraction and optical resistance measurements.

All the samples, in our experiments, were coated by IBS technology on fused silica (FS) substrates under the identical evaporation conditions. The optical thicknesses of all coatings were kept constant (6 QWOT – quarter wavelength of optical thickness). From spectrometric transmittance and reflectance measurements absorption *k* values were evaluated (Fig.1 and 2). At

the same time, the volumetric proportions of high and low index materials were evaluated by using

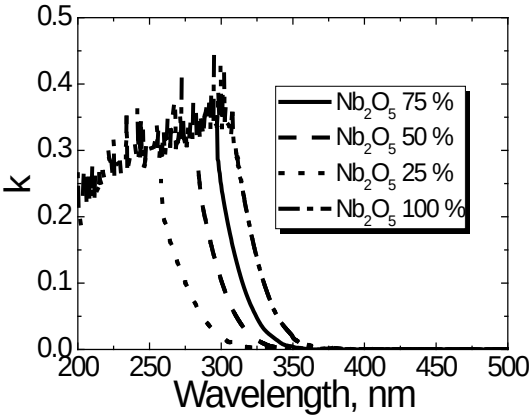

Fig.1. Absorption (*k*) spectra of Nb_2O_5/SiO_2.

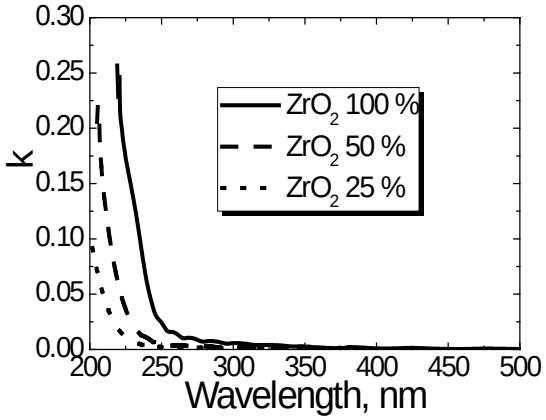

Fig.2. Absorption (*k*) spectra of ZrO_2/SiO_2.

the Bruggeman‘s approximation.

It was shown that increase of the high index material content in the coating results in the “red shift” of optical band-gap. This also influences the refractive index, optical scattering, roughens and optical resistance so called LIDT (Laser induced damage threshold) in femtosecond range (Fig. 3 and 4). All LIDT measurements were performed in 1-on-1 mode at 1030 nm wavelength.

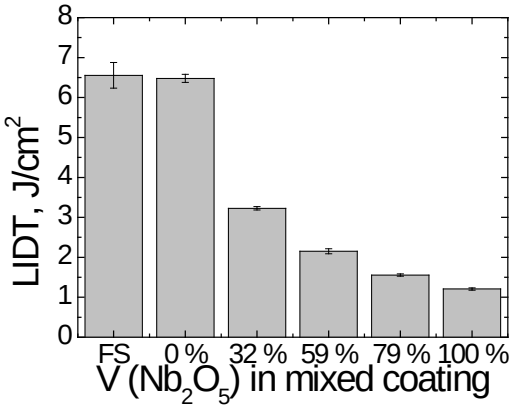

Fig.3. LIDT values in of Nb_2O_5/SiO_2.

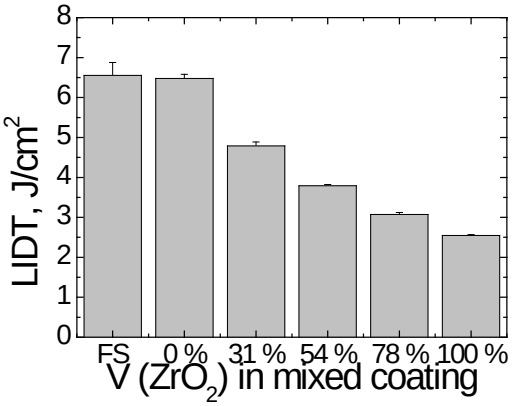

Fig.4. LIDT values of ZrO_2/SiO_2.

1. F. Stewart, S. Lu, M. Tehrani, C. Volk, *Ion beam sputtering for optical coatings*, (5500 Canoga Ave. MS 19 Woodland Hills, CA 91367).
2. N. Kaiser, H. K. Pulker, *Optical Interference Coatings*. Springer – Verlag Berlin (Heidelberg New York, 2003).

OP15

THREE-DIMENSIONAL MAPPING OF MULTIPLE FILAMENT ARRAYS

D. Majus, V. Jukna, G. Tamošauskas, G. Valiulis, A. Dubietis

Department of Quantum Electronics, Faculty of Physics,
Vilnius University, Saulėtekio avenue 9, Building 3, LT-10222 Vilnius, Lithuania
donatas.majus@ff.stud.vu.lt

The phenomenon of multiple filamentation of intense laser beams, whose power exceeds the critical power for self-focusing by many times, is gaining an increasing scientific and technological interest. A significant effort is directed to studies of the multiple filamentation in dense dispersive media, and particularly in transparent solids, foreseeing many technological challenges in parallel material processing, integrated optics, microfabrication and device applications. The most relevant examples outline excitation of coherent multichannel white light radiation, generation of parallel plasma channels, inscription of parallel optical waveguides in transparent media, phase-matched Raman frequency conversion with ultrashort light pulses, and excitation of the arrays of coherent lasing sources. A particularly interesting case of multiple filamentation refers to spontaneous break-up of intense elliptical laser beams, yielding highly reproducible periodic MF patterns, despite being initiated by random intensity modulation [1]. More precisely, the transition from random to deterministic beam break-up owes to multistep degenerate four-wave mixing, and the period of the MF array is controlled solely through the input beam intensity [2]. Despite the fact, that many tools for control and regularization of MF arrays have been elaborated recently, many aspects of their spatiotemporal dynamics in condensed media are still unrevealed. Therefore we study the spatiotemporal dynamics that emerges in the MF regime by self-focusing of femtosecond elliptical laser beams in fused silica by employing three-dimensional mapping technique [3] with high temporal (30 fs) and spatial (5 μm) resolution.

Experimental and numerical investigation revealed a number of interesting features. Although in any case the elliptical input-beams carrying femtosecond light pulses form regular and periodic MF patterns in the spatial domain (with time integration (Fig. 1 (c)) the spatiotemporal behaviour of the individual filaments exhibits surprising differences, depending on the input-beam ellipticity. In the case of moderate input-beam ellipticity, the individual filaments propagate in curved trajectories (Fig. 1 (a), (b)) arising from skewed (spatiotemporal) coherence. The spatiotemporal propagation dynamics is regularized by increasing the input-beam ellipticity, and in part due to permanent modifications of fused silica that occur under intense irradiation. Highly elliptical input-beams

break-up into regular spatiotemporal patterns (Fig. 1 (d)), which undergo strong reshaping that gives rise to occurrence of extremely short (<5 fs), localized peaks at the leading edge, propagating at superluminal velocity. They are followed by the sub-pulses centered on the input-pulse top, and trailed by subluminally propagating pulses with rather complex transverse intensity distribution. Each individual filament is a replica of its neighbour, just with different temporal position of the leading peak, indicating earlier or later pulse break-up event as a function of the local input-beam intensity.

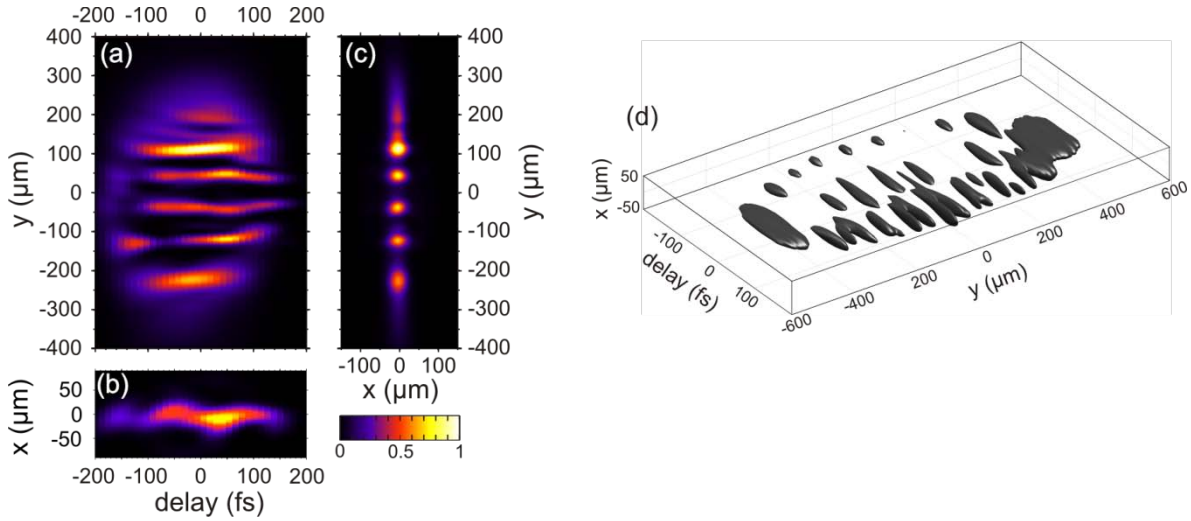

Fig. 1. Spatiotemporal intensity distribution in (a) t-y and in (b) t-x planes of 12 μJ input pulses; (c) Time integrated image; (d) Isointensity surface at 45% maximum intensity level of 58 μJ pulse after nonlinear propagation in 20-mm length fused silica slab.

1. Dubietis, G. Tamošauskas, G. Fibich, and B. Ilan, Opt. Lett. **29**, 1126 (2004).
2. D. Majus, V. Jukna, G. Valiulis, and A. Dubietis, Phys. Rev. A **79**, 033843 (2009).
3. M. A. C. Potenza, S. Minardi, J. Trull, G. Blasi, D. Salerno, A. Varanavicius, A. Piskarskas, and P. Di Trapani, Opt. Commun. **229**, 381 (2004).

Poster session

PP1

FLORESCENCE CONCENTRATION QUENCHING OF PERYLENEDIIMIDE DERIVATIVES

G. Armonaite, K. Kazlauskas , S. Jursenas

Institute of Applied Research, Vilnius University, Sauletekio Ave. 9-III, LT-10222 Vilnius, Lithuania

gintare.armonaite@ff.vu.stud.lt

Perylenediimides (PDIs) are widely investigated organic materials with important applications in optoelectronics. Although the key-application of PDIs so far is in laser dyes, such as famous perylene orange and red dyes, other potential applications of PDIs in organic field-effect transistors, photovoltaic cells, and light-emitting diodes are being explored. Chemical, thermal and photo stability accompanied by high luminescence efficiency and good solution processability, makes PDI derivatives outstanding organic compound in such optoelectronic applications as laser industry. For example, the imide nitrogen substituted PDI derivatives demonstrate excellent thermal and photostability, and show superior luminescence quantum yield (QY) (up to 100 %). However, in solid state (which is essential for solid state lasers) these compounds show drastically reduced emission efficiency. This luminescence quenching is mainly the result of the formation of close packed structure with enhanced excitation migration to quenching sites associated with molecular oxygen unintentionally introduced in the PDI films during their preparation in ambient conditions. To reduce concentration quenching it is essential to inhibit the formation of these aggregates. PDI derivatives substituted at the bay positions of the perylene core using C-O, C-C and C-N coupling are considered to be promising, owing to the fact that the steric hindrance and perylene core twisting induced by the bay substituents could prevent π□π stacking, and thus, reduce luminescence quenching.

Here we report, luminescence properties of five PDI derivatives with different electron accepting substituents at the bay positions of the perylene core. By estimating QY and luminescence decay time, the relation between the florescence concentration quenching and substitute at the bay position of the PDI derivatives was established.

PP2

THE INFLUENCE OF THE ELECTRIC FIELD ON THE EMISSIONS PROPERTIES OF THE Sc-Ba DISPENSED EMITTERS WITH THE W MATRIX

O.V. Verbytska, I.I. Bekh, V.V. Il'chenko and V. V. Shcherban

Taras Shevchenko Kiev University, Volodymyrska str. 64, 01033 Kiev, Ukraine

verbitskaja@gmail.com

The influence of the electric field on the emission properties of the Sc-Ba dispensed emitters with the W matrix is studied in a high vacuum. In this work is shown, that in contrast with previous results [1], the increasing of electric field intensity, applied to emitter with W matrix at constant temperature, don't cause to substantial alteration chemical composition of emission-active matter.

The researches were carried out in UHV chamber and the pressure of residual gases did not exceed $5 \cdot 10^{-9}$ torr. The measurement of the emission properties was made in a flat diode system at a pulse mode. Pulse duration of the anodic voltage is 7 μs. The amplitude of anodic voltage can change up to 600 V. The anode was the molybdenum plate (2x2x0.2 sm.), which was heating to the high temperature by the electron impact. The emitter-anode spacing interval *d* was equal to 1,2 mm, 1 mm, 0,8 mm and 0,6 mm and has been carefully controlled. Such set of distances allowed us to study influence of the electric field on the emissions properties of samples in the wide interval of field intensity.

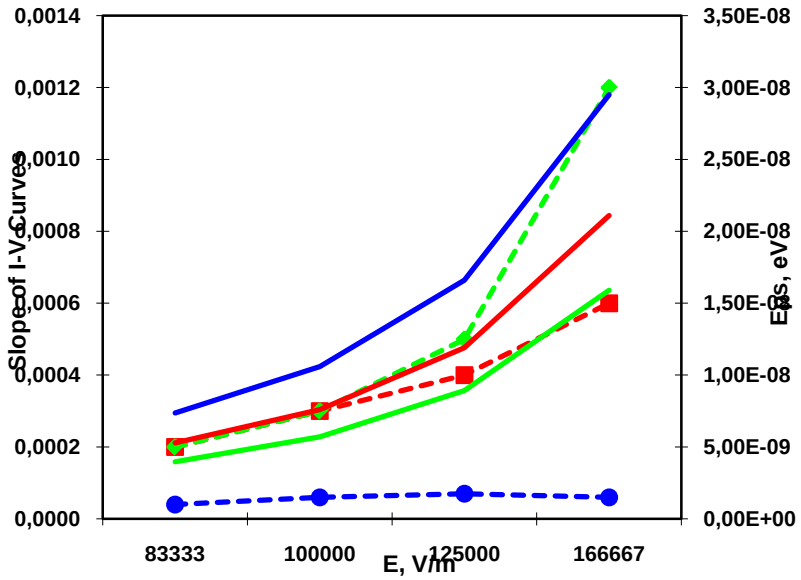

Fig. 1. Numerical calculations results and slope of voltage-current characteristics of emitters with W matrix (dashed lines) depends on the electric field intensity.

For detailed analysis of the influence of electric field on the emission properties of Sc-Ba dispensed emitters with the W matrix and for comparison with the previous results for the emitters with Re-W matrix [1], it was made numerical calculation of the energy of displacement position of the maximum of electrons concentration in the emitters depends on electric field intensity for the case of a triangular potential barrier with the absence of image forces. The comparative analysis between experimental results and obtained calculated dependencies was made. Results of such comparison are shown on figure.

Obtained results shows, that presence and absence of qualitative agreement between numerically calculated dependencies and experimental data can be presented as one more argument that processes of forming of emitter's work surface with different material of matrices are substantial different.

As one can see from figure, with the increase of the electric field intensity for the sample with W matrix at constant temperature clear tendency for growing of slope of its voltage-current characteristic is presents. The only exception is characteristic, measured at the 1100 K. Such temperature is not sufficient to optimize chemical composition and microstructure of the emitter's surface.

The increasing of the electric field intensity, applied to emitters with W matrix at constant temperature don't cause to substantial alteration chemical composition of emission-active matter. Thus in the case of emitters with the W matrix the main factor of field emission is geometrical dimensions of crystallites and geometrical coefficient of the field amplification.

1. I.I. Bekh, O.V. Verbytska, O.I. Getman, V.V. Il'chenko, A.E. Lushkin. // Bulletin of the University of Kiev, Series: Physics & Mathematics, – 2008, – V. 4, – P. 203 – 206.

PP3

XP AND IMPEDANCE SPECTROSCOPY OF $Li_{1,4}Ti_{1,9}P_3O_{12}$ SOLID ELECTROLYTE CERAMICS

J. Banytė, V. Venckutė

Faculty of Physics of Vilnius University, Sauletekio ave. 9-III, LT-10222 Vilnius, Lithuania

Juste_banyte@yahoo.com

The development of fast lithium conductors is attracting much of attention because of their applications in high-energy Li-ion batteries and electrochemical sensors [1, 2]. It is known that $LiTi_2P_3O_{12}$ compound with the NASICON-type structure is a pure ionic conductor and its bulk ionic conductivity at room temperature was found to be $\sigma_b = 2 \cdot 10^{-4}$ S/m [3]. High ionic conductivity of above mentioned NASICON- type structure solid electrolyte compounds stimulate further investigation of the materials. In the present work we report the technological conditions for the synthesis of $LiTi_2P_3O_{12}$ powder, sintering of the ceramics, the results of the investigations of X-ray diffraction (XRD) from the powder, X-ray photoelectron spectroscopy (XPS) and electrical properties of the ceramics in the frequency range from 10 to $3 \cdot 10^9$ Hz in the temperature range from 300 to 600 K. The solid electrolyte compound was synthesized by a solid state reaction. The results of XRD have shown that at room temperature investigated compounds belong to hexagonal symmetry (space group $R\bar{3}c$) with six formula units in the unit cell. Ti 2p, P 2p, O 1s and Li 1s core level XP spectra were fitted. It was ascertained that there are four different kinds of oxygen on the ceramic surface, including lattice oxygen, chemisorbed oxygen in the forms O^{2-}, O_2^- and oxygen in hydroxyl environment (O_H). The deconvolution of the P2p core level XPS can be associated with different amounts of P^{5+} and P^{3+} states in the investigated ceramics. Two dispersion regions were found in conductivity spectra for investigated samples. The high frequency part of the recorded spectra may be attributed to the relaxation processes in grains, while the lower frequency part corresponds to relaxation processes in grain-boundary. The processes are thermally activated and dispersion regions shift toward higher frequencies as temperature increases. A good agreement is found between the activation energy of the ionic migration process in the grain and the activation energy of the characteristic relaxation frequency. It is shown that the major role in the temperature dependence of bulk conductivity is played by the Li^+ ion mobility that increases as temperature increases.

1. V. Thangadurai, J. Schwenzel, and W. Weppner, Ionics **11**, 11 (2005).
2. F. Salam, P. Birke, and W. Weppner, Electrochem. Solid-State Lett. **2**, 201 (1999).
3. H. Aono, E. Sugimoto, Y. Sadaoka, N. Imanoka, and G. Adachi, J. Electrochem. Soc. **137**, 1023 (1990).

PP4

INVESTIGATION OF TlBr PHOTOELECTICAL PROPERTIES

A. Ziminskij[1], V. Kažukauskas[1], G. Davidyuk[2], V. Bozhko[2], G. Mirunchuk[2]

[1] *Institute of Applied Research, Vilnius University, Sauletekio Ave. 9-III, LT-10222 Vilnius, Lithuania*

andzej.ziminskij@stud.ff.vu.lt

[2] *Volyn National University, Lutsk, Ukraine*

Thallium bromide (TlBr) is an attractive and promising material for X- and □-ray spectroscopy because of its wide bandgap (2.68 eV), high density (7.56 g/cm^3) and high atomic numbers (Tl: 81 and Br: 35) [1]. Such properties ensure a high photon stopping efficiency. Though, presence of the ionic conductivity is still preventing it from the practical application.

We had investigated photoelectrical and current transient properties of TlBr from 100 K up to 300 K, where the effect of the ionic conductivity changes notably. From the photocurrent spectra defect- related transitions at 2,14 eV, 1,75 eV and 1,45 eV were identified, being dependent on sample excitation by light and voltage. The induced extrinsic photoconduction phenomenon was identified at the low temperatures.

Non-monotonous conductivity variation with temperature was identified, demonstrating mobility-related maximum that was superimposed on an intrinsic conductivity growth. After measuring the thermostimulated current several defect traps were identified the best pronounced of them having the thermal activation energy values of 0,08 – 0,095 eV, and 0,11 – 0,17 eV.

We had investigated degradation effects in TlBr crystal under prolonged bias voltage and current relaxation after different excitation by light.

1. K. Hitomi, M. Matsumoto, O. Muroi, T. Shoji, and Y. Hirarate, IEEE Trans. Nucl. Sci. **49** (5), pp. 2526-2529, 2002.

PP5

OPTICAL AND ELECTICAL CHARACTERISATION OF COMERCIAL LED LAMPS

A. Petrulis, P. Vitta

Institute of Applied Research, Vilnius University, Sauletekio Ave. 9-III, LT-10222 Vilnius, Lithuania

andrius.petrulis@gmail.com

Here it is represented an optical and electrical investigation of the LED lamps and statistical data handling. Optical parameters were measured using multi-channel spectrometer (Hamamatsu C7473) and integration sphere (Sphereoptics) where the light was collected and smoothed. The electrical characteristics of MR16 cap (12 V DC) lamps were measured by power source Keithley 2430. The experimental setup was calibrated by specified spectral distribution calibration lamp (Bentham CL2). Our research objects were LED lamps of red, yellow, green, blue and white light colors with three types of connection caps (GU10, MR16 and E27).

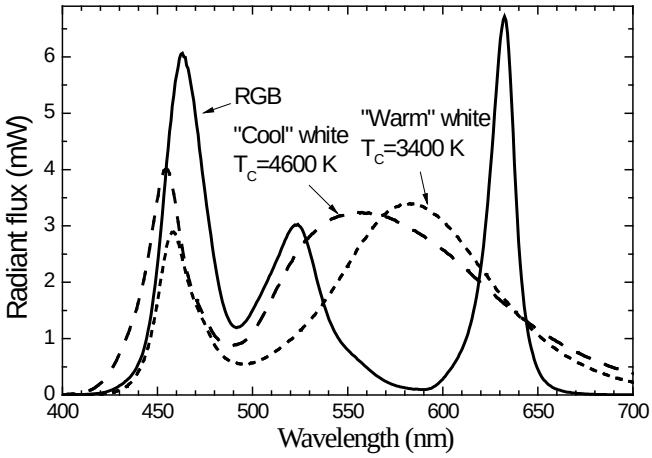

Fig.1. Spectral distribution of the white LED lamps

Wall-plug efficiency of the LED lamps is determined by four efficiency components: intrinsic LED characteristics, power supply electronics, optics and heat management. In this stage of research only the total optical flux and wall-plug efficiency of the lamps were measured without a consideration of separate components. Statistical analysis was based on measurement results form several units of the same type LED lamps. Standard deviation of optical and electrical parameters was calculated for representation of the trustiness and quality of production. It was shown that 3% of the production were damaged during the manufacturing process and are not suitable for exploitation. According to the results, we conclude that a manufacturer uses insufficient quality control procedures, which must be improved in order to prevent the reject and parameter scattering of the production.

The author acknowledges Students research award (project “Promotion of Students’ Scientific Activities”) from Lithuanian Science Council.

PP6

SIMULATIONS OF THE DEFECT DEPENDENT VARIATIONS OF ELETRICAL CHARACTERISTICS IN Si PIN DIODES

J. Kusakovskij, T. Čeponis, E. Gaubas

Institute of Applied Research, Vilnius University, Sauletekio Ave. 9-III, LT-10222 Vilnius, Lithuania

Jevgenij.Kusakovskij@tmi.vu.lt

The local modification of carrier lifetime in semiconductor devices by high energy particle irradiations is an effective technological tool for manipulation of diode recovery rate and operation frequencies. However, versatile models of evolution of the radiation induced point and extended defects are yet to be developed. In silicon based devices, digital simulations are implemented by considering an intricate system which includes carrier density and field equations solved together to described the majority of phenomena appeared within static and dynamic characteristics during device functioning. The Synopsys Technology Computer Aided Design (TCAD) simulation platform has been exploited in this work to design the irradiation regimes and to foresee variations of the static and dynamic electrical characteristics in power PIN rectifiers irradiated by 2-3 MeV protons varying energy and fluence of particles.

The simulations have been performed by involving various deep level sets ascribed to radiation defects. The digital calculation procedures have been controlled from PC console linked to a computer cluster installed at the Institute of Applied Research supported by Synopsys TCAD platform. Voltage-Current (I-V) and Voltage-Capacitance (C-V) characteristics have been simulated for three dimensional non-irradiated PIN rectifiers to test the software capabilities and to calibrate the fitting procedures applied for extraction of the essential parameters from the experimental characteristics. Two-dimensional approach for doping profiles was accepted in modelling to save computational resources and time consumption needed to solve the problems. This approach appeared rather efficient to get reliable results and to approximate sufficiently the main experimental characteristics. Three deep level system, known as the Hamburg model, and four deep level system as well as an improved by author of this work four level model, have been employed to simulate the I-V and C-V characteristics in protons irradiated PIN diodes containing a δ-shape layer of implanted protons. Trapped charge diagrams were calculated to visualize the deep levels. The DLTS spectra and the leakage current variations dependent on temperature indicated that a considerable amount of VOH complexes should be incorporated to get agreement between the simulated and measured characteristics. Peculiarities of simulation processes and of selecting parameters will be discussed.

PP7

STUDY OF CARRIER RECOMBINATION AND GENERATION CENTRES IN Si PIN DIODES IRRADIATED BY VARIED ENERGY OF PROTONS

A.Dzimidavičius, A.Uleckas, E.Gaubas

Institute of Applied Research, Vilnius University, Sauletekio Ave. 9-III, LT-10222 Vilnius, Lithuania
antanas.dzimidavicius@ff.stud.vu.lt

The trade-off between dynamic and steady-state characteristics of power rectifiers operational at rather high frequencies can be only reached by using radiation and doping technologies for enhancement of reverse recovery rate by introduction of fast recombination centres. Carrier recombination lifetime at high excitation level determines the recovery speed of the pin diode and softness of switchover. However, carrier generation lifetime is a limiting factor which governs leakage current. To reveal the possible ways for improvement of both parameters, i.e. to increase carrier generation lifetime and to reduce carrier recombination lifetime, the different profiles of radiation and doping induced deep centres of the enhanced density have been studied in this work.

Spectra of carrier generation centres have been examined by capacitance deep level transient spectroscopy (C-DLTS). A commercial DLS-82E spectrometer has been exploited to record the DLTS spectra. The vacancy associated complexes have been identified in the as-irradiated diodes. The dominant DLTS peak has been ascribed to VOH centre which density increases with 2-3 MeV protons fluence. To reduce leakage current of the irradiated diodes, the heat treatments have been applied in the temperature range of 80- 420^0 C. Evolution and transforms of carrier generation centres have been deduced from the changes of DLTS spectra after each heat treatment step. Scenarios of inter-defect reactions will be discussed.

Carrier recombination lifetime has been synchronously examined by measurements of photoconductivity decays probed by microwaves. To reveal the radiation induced distribution of recombination centres along the base of irradiated pin diodes, the cross-sectional scan regime on the boundary of the diode has been employed. The home-made instrument VUTEG-4 has been exploited for the investigations of carrier recombination lifetime.

Correlations of densities of the recombination and generation defects introduced by 2-3 protons beam are analysed. Corrections of the ratio between carrier recombination and generation centres made by heat treatments and promising ways to optimize this parameter will be discussed.

PP8

FIRST PRINCIPLES DENSITY FUNCTIONAL CALCULATIONS OF ELECTRONIC STRUCTURE AND OPTICAL PROPERTIES IN BiSBr AND BiSeBr CRYSTALS

R. Sereika, A. Budinavičius and S. Garunkštis

Department of Physics, Vilnius Pedagogical University, Studentu 39, LT-08106 Vilnius, Lithuania

sereika@vpu.lt

BiSBr and BiSeBr are semiconductors which belong to the group of V-VI-VII compounds. This type crystals own several interesting physical properties, such as high photoconductivity, ferroelectricity, electrooptical effect, electromechanical effect, piezoelectricity, and a large temperature dependence of the band gap [1-4].

The structure of these crystals in the paraelectric phase is orthorhombic, with D_{2h}^{16} space group containing four molecules per unit cell. The crystals consist of double chains of atoms. All atoms in these crystals lie on mirror planes normal to the ***c*** – axis. In the double chains a short and strong Bi-S or Bi-Se bonds take place. Weak Van der Waals type bonding links these double chains.

Electronic structure and optical properties of BiSBr and BiSeBr crystals were investigated by the full potential linearized augmented plane wave (FL-LAPW) method with density functional theory (DFT) using Wien2k [5] package. The lattice constants and positions of the atoms in the unit cell were taken from [3, 4]. The calculation was performed with $Rk_{max} = 7$ (R is the radius of the smallest muffin-tin sphere and k_{max} is the cut off the plane wave) for the convergence parameter for which the calculation stabilize and convergence in terms of the energy are achieved. The values of the muffin-tin radii $R^{MT} = 2.94$ for Bi, $R^{MT} = 1.90$ for S, $R^{MT} = 2.02$ for Se and $R^{MT} = 1.96$ for Br. A mesh of 14 x 29 x 11 k-points in the irreducible part of the Brillouin zone was used. The iteration halted when the difference in the eigen values was less than 0.0001 between steps of convergence criterion. The separation of valence and core states was chosen as -6 Ry.

The dielectric functions $\mathrm{Im}\,\varepsilon$, $\mathrm{Re}\,\varepsilon$ calculated with DFT in the wide range of the energy are shown in Fig. 1. Theoretical dependences were calculated in three directions xx (***a*** – axis), yy (***b*** – axis) and zz (***c*** – axis). As one can see anisotropy of $\mathrm{Im}\,\varepsilon$ and $\mathrm{Re}\,\varepsilon$ (xx and zz directions) is evident just in the lower energy range about 3 – 7 eV. This also occurs in the n(E), k(E) and R(E) spectra. Also it is seen that BiSeBr is marginally more anisotropic than BiSBr. The $\varepsilon_i(0)$ value ($\varepsilon_i(\omega)$ at $\omega = 0$), which is correlated with the refractive index n_i, $n = \sqrt{\varepsilon_i(0)}$ is higher in the zz – direction,

than in xx – direction. Small maxima of the imaginary and real part of dielectric functions in the range 0 – 2.5 eV correspond to the low – probable (indirect transition) between the top of valence band and the conducting states of the range 2 – 3 eV.

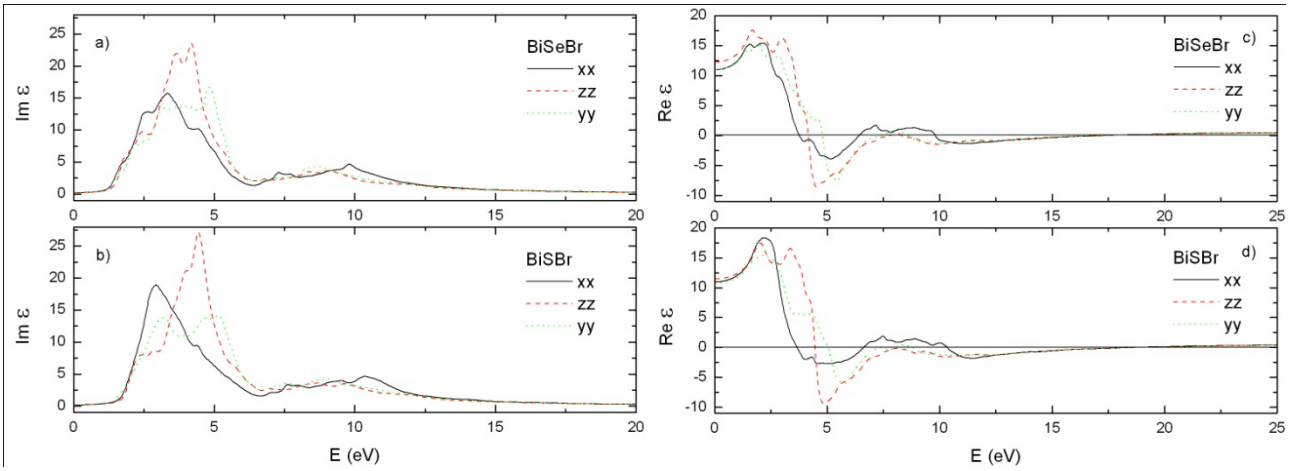

Fig. 1. Theoretical imaginary and real part of dielectric functions for BiSeBr and BiSBr crystals.

At intermediate energies (1 to 25 eV) the energy losses are due primary to a complicated mixture of single electron excitations and collective excitations (plazmons). Plasmon losses correspond to a collective oscillation of the valence electrons and their energy is related to the density of valence electrons. The energy that of the maximum peak of $\mathrm{Im}[-\varepsilon^{-1}(E)]$ is assigned to the energy of volume plasmon $\hbar\omega_p$. At this energy, the real part of the dielectric function $\mathrm{Re}\,\varepsilon$ coming from the high frequency side goes through zero. The maximum peak of $\mathrm{Im}[-\varepsilon^{-1}(E)]$ is located at energy of 20 eV for BiSBr and at energy of 18.8 eV for BiSeBr. Dielectric function $\mathrm{Re}\,\varepsilon$ changes sign (vanishes) at the same energy.

1. P.I. Rentzeperis, Prog. Cryst. Growth Charact. Mater. **21**, 113-138 (1991).
2. A. Audzijonis, G. Gaigalas et al, J. Elec. Spec. Relat. Phenom. **162**, 13-18 (2008).
3. E. Furman, O. Brafman, J. Makovsky, Phys. Rev. B **13**, 1703-1710 (1976).
4. E. Dönges, Z. Anorg. Allgem. Chem. **263**, 280-291 (1950).
5. P. Blaha, K. Schwarz, G. Madsen, D. Kvasnicka, and J. Luitz, WIEN 2k, N. Augmented Plane Wave + Local Orbitals Program for Calculating Crystals Properties Katlheinz Schwarz Techn. Universitat Wien, Austria, 2001.

PP9

SPECTROSCOPY OF THE INTRINSIC AND RADIATION INDUCED DEFECTS IN Si BY COMBINING INFRARED ABSORPTION AND CAPACITANCE TRANSIENT TECHNIQUES

J. Pavlovas, A.Uleckas, and E.Gaubas

Institute of Applied Research, Vilnius University, Sauletekio Ave. 9-III, LT-10222 Vilnius, Lithuania

Jevgenijus.Pavlovas@ff.stud.vu.lt

In order to modify functional parameters of a semiconductor power device, radiation technologies are employed to induce fast carrier traps and to enhance hereby the reverse recovery rate. Irradiations by beams of fast electrons and of protons can be used to create homogeneous distribution of recombination centres or to localize layers of enhanced recombination. However, interactions of intrinsic and radiation defects complicate steady-state characteristics of devices by increasing leakage current, forward voltage drop etc. those are non-acceptable during device operation. Therefore, defect engineering is usually exploited to activate beneficial defects and to suppress harmful ones, when, spectroscopy of defects is important technological procedure.

Deep level transient spectroscopy (DLTS) is a standard method to identify traps associated with defects by evaluating the density of traps, the activation energy and carrier capture cross-section. However, the DLTS spectroscopy is an integral technique which is based on measurements of capacitance relaxation due to change of filling of deep traps. On the other hand, the identification of defects by DLTS method is based on correlation between structure of DLTS peaks and microscopic analysis of defects made by other methods, such as EPR. Therefore DLTS technique is inappropriate to identify nomenclature of new defects, e.g. VOH complexes and vacancy clusters. Additionally, the DLTS is non-operational when density of defect exceeds that of impurities. The infrared transmission spectroscopy (IRTS) is based on analysis of vibrational modes of defects, and, hereby, it is a microscopic technique for examination of defects. Thus, the IRTS is appropriate method to identify new defects by measurements and simulations of spectra. Therefore, the combining infrared absorption and capacitance deep level transient techniques have been employed in this work for identification and control of new, the intrinsic and radiation induced defects.

The improved IRT spectrometer and commercial DLTS instruments had been used for combined spectral analysis in wide range of temperatures. The silicon PiN diodes and wafer samples irradiated by protons and neutrons have been investigated after various technological procedures. The beneficial anneal of the rather shallow traps ascribed to radiation induced vacancy complexes has been unveiled under isochronal heat treatments of proton irradiated Si diodes in temperature range below 240 °C. Peculiarities of identification of defects will be discussed.

PP10

TECHNIQUES AND INSTRUMENTATION FOR CARRIER LIFETIME MEASUREMENTS WITHIN WIDE RANGE OF EXCITATION DENSITIES

K. Žilinskas, A. Uleckas, E. Gaubas

Institute of Applied Research, Vilnius University, Sauletekio Ave. 9-III, LT-10222 Vilnius, Lithuania

kestutis.zilinskas@ff.stud.vu.lt

Carrier lifetime is one of the most sensitive parameters to defects in material. On the other hand, carrier lifetime is the main parameter which determines the dynamic characteristics of semiconductor devices. Therefore, control of carrier lifetime in differently doped and under various carrier injection conditions are widely used as a technological procedure within modifications of power rectifiers designed for operation in the range of high frequencies. Complementarily, carrier lifetime reduction is the limiting factor in functioning of high energy particle detectors. In this work, the comprehensive techniques and instrumentation have been developed for contact-less control of carrier lifetime in substrate materials and in device structures covering wide range of the excess carrier densities from 10^{11} to 10^{19} cm^{-3} by combining various techniques and by implementing specific measurements regimes.

The measurement techniques based on free carrier absorption transients have been combined. The pulsed excited photoconductivity transients probed by 10 and 22 GHz microwaves have been employed to carry out the carrier lifetime measurements at low injection densities. The instrument for planar and cross-sectional mapping of recombination lifetime distribution has been developed. An additional to pulsed 0.5 – 5 ns excitation at 1.06 μm wavelength the steady-state spectrally varied bias illumination has been applied to separate carrier trapping and photoconductivity quenching effects. These regimes combined with temperature scans of carrier lifetime variations comprise the spectroscopic instrumentation for technological control of recombination centres in material. The photoconductivity transients probed by continuous wave infrared light in the range of 1.55 – 2.6 μm served as a tool for carrier lifetime measurements in the range of high excitation densities. The instrument for simultaneous control of carrier lifetime at low and high excitation conditions has been designed and fabricated for express control of dominant recombination deep levels by using the satellite samples of the same material.

The specific recombination lifetime variations obtained in Si, Ge and GaAs materials will be illustrated. The modifications of the instrument for in situ carrier lifetime control in Si within harsh environment of irradiation chamber during exposure under 2- 9 MeV protons will be discussed.

PP11

PHOTOPHYSICAL PROPERTIES OF TRIPHENYLAMINE BASED DERIVATIVES

S. Raišys[1], A. Miasojedovas[1], K. Kazlauskas[1], S. Juršėnas[1], I. Petrikytė[2], M. Daškevičienė[2], V. Getautis[2]

[1] *Institute of Applied Research, Vilnius University, Sauletekio Ave. 9-III, LT-10222 Vilnius, Lithuania*

[2]*Department of Organic Chemistry, Kaunas University of Technology, Radvilenu pl. 19, LT-50279 Kaunas, Lithuania*

raisys@gmail.com

Triphenylamine (TPA) derivatives are widely investigated organic electronics compounds expressing excellent thermal and electrochemical stability, electron donating and optoelectronic properties [1]. Triphenyldiamine (TPD) is probably the best known TPA derivative, commonly used in organic light emitting devices (OLED) as an excellent hole transporting material. Typically, OLED device contains three or more layers of organic materials with each layer designed to perform only a certain function, e.g. to transport either holes or electrons, or emit light. Therefore, synthesis of new materials featuring multifunctional properties is attractive alternative leading to simplification of the device structure and fabrication.

In this study a series of TPA-based derivatives in solution, solid state and aggregates were investigated by measuring their absorption and photoluminescence (PL) spectra, PL quantum yields (QY) and PL lifetimes.

Experimental results indicate that derivatives in solution are less emissive (QY up to 1.8%) as compared to solid state (QY up to 5.5%) due to intramolecular torsions of phenyl groups. The presence of efficient non-radiative deactivation in solutions is additionally proved by very fast PL decay times (<0.08 ns), whereas decay times obtained for the films are slower, yet not exceeding 0.7 ns. The results obtained in the self-assembled nanoaggregates demonstrate significant increase in QY (up to 4 times) indicating suppression of torsional motions of the phenyl groups [2]. The shape and maximum (500 nm) of the emission spectrum in solution and solid state was found to be independent of a number of the phenyl groups attached. However, higher QY was estimated in the solutions and films of the TPA derivatives possessing more phenyl rings.

1. Y. Shirota, Y. J. Mater. Chem. **10**, 1-25 (2000).
2. Z. Zhao, S. Chen, X. Shen, F. Mahtab, Y. Yu, P. Lu, J. W. Y. Lam, H.S. Kwok. B. Z. Tang, Chem. Commun., **46**, 686–688 (2010).

PP12

INFLUENCE OF ISOELECTRONIC IMPURITIES ON A DEEP LEVEL RELATED LUMINESCENCE IN ZnSe SCINTILLATORS

D.Shevchenko

Institute of Applied Research, Vilnius University, Sauletekio Ave. 9-III, LT-10222 Vilnius, Lithuania
sevcenkoff@gmail.com

Recently, zinc selenide attracted considerable attention as scintillating material for X ray detection. Isoelectronically doped ZnSe exhibits high conversion efficiency due to strong emission below its band gap, high radiation hardness, low hygroscopicity and small afterglow, which is 20-100 times lower than that in conventional scintillator CsI(Tl). Moreover, the deep-level-related emission peaking at 600- 650 nm is convenient for detection by high sensitivity silicon photodiodes. To receive thermally stabile crystals with strong emission and weak reabsorption, ZnSe single crystals can be doped with isoelectronic impurities and thermally annealed in properly selected atmosphere after growth. These properties of ZnSe single crystals enabled their application in X-ray and ionizing radiation detectors to be used in medicine, environment monitoring, and security, although luminescence mechanisms of zinc selenide crystals are still not conclusively explained.

Radiative recombination channel efficiency can be improved by isoelectronic doping with tellurium and oxygen. Introduction of these impurities creates thermally stabile defects. Crystal annealing in Zn vapor enables one to stabilize defects responsible for radiative recombination and accelerate the charge carrier recombination through the radiative recombination channels. Therefore it is important to understand the radiative and non-radiative recombination mechanisms and their relation with the crystal growth conditions.

In this work, a study of deep level related photoluminescence in four isoelectronicaly doped ZnSe scintillating crystals is presented. One sample was doped with tellurium, the second sample was doped with oxygen by annealing in oxygen rich atmosphere, the third sample was doped with oxygen by mixing Al_2O_3 into the melt for crystal growth, while undoped ZnSe was also studied as the fourth sample for reference.

To study carrier dynamics at low density of nonequilibrium carriers, what is typical for operation of high-sensitivity ZnSe-based radiation detectors, frequency domain luminescence lifetime measurement technique was applied. Photoluminescence and quantum yield spectra were measured using photoluminescence spectroscopy technique.

Investigation of photoluminescence properties of isoelectronically doped ZnSe(Te), ZnSe(O) and ZnSe(O,Al) shows that doping of ZnSe with tellurium is most effective and increases luminescence intensity by a factor of ~30. Crystal annealing in Zn vapor additionally increases the photoluminescence intensity by 4 times. Isoelectronic doping with oxygen does almost not influence the luminescence intensity, but ZnSe(O) crystals annealed in Zn vapor have stronger luminescence intensity by ~ 40 times. ZnSe doping with aluminum and oxygen increases luminescence intensity about 15 times, while subsequent annealing of this sample in Zn vapor increases luminescence intensity by ~ 4 times.

Studies of decay kinetics showed that luminescence decay of the annealed samples is faster than that of unannealead samples. The fastest luminescence decay was observed in ZnSe(O,Al) sample annealed in Zn vapor. The luminescence of this sample is dominated by radiative recombination through donor-acceptor pairs, which characteristic decay time is ~ 3.9 μs. A less significant exponential component with characteristic decay time ~ 0.19 μs is also observed.

Annealing of the crystals in Zn vapor increases their photoluminescence quantum yield several times. The highest quantum yield (~ 15 %) is observed in ZnSe(O,Al) sample, when excitation photon energy is larger than the band gap of zinc selenide.

The quantum yield rapidly increases when the excitation photon energy is reduced below the ZnSe band gap. The highest quantum yield (~ 42.5 %) is observed in ZnSe(Te) sample annealed in Zn vapors, when the luminescence is excited at 2.58 eV photon energy (band gap of ZnSe at room temperature is Eg = 2.68 eV). This behavior is explained by the influence of nonradiative surface recombination and direct excitation of shallow donors in donor-acceptor pair luminescence.

PP13

ILLUMINATION WITH A COMPUTER CONTROLLED TRADE-OFF BETWEEN COLOUR FIDELITY AND SATURATION

A. Tuzikas

Institute of Applied Research, Vilnius University, Sauletekio Ave. 9-III, LT-10222 Vilnius, Lithuania

arunas.tuzikas@gmail.com

Lighting sources, which are based on additive colour mixing of emissions from several light emitting diodes (LEDs), offer versatility in colour quality of illumination Tetrachromatic (red-amber-green-blue) solid-state lamps with a particular correlated colour temperature can be optimized in respect of colour rendering index (CRI), luminous efficiency of radiation (LER), colour fidelity index (CFI) and colour saturation index (CSI) [1]. The possibility in varying the spectral power distribution (SPD) of the lamp allows illumination with a trade-off between fidelity and saturation of object colours (Figure 1).

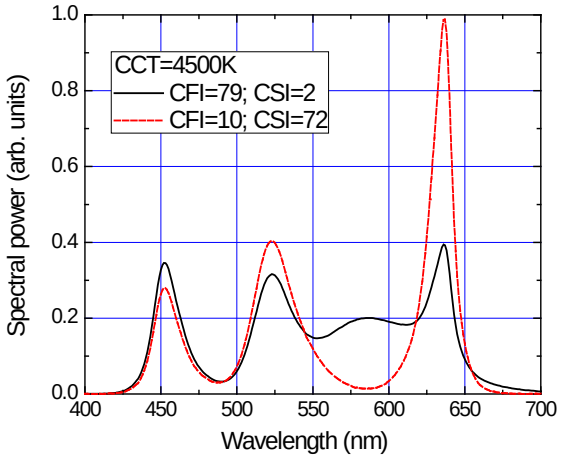

Fig. 1. Spectral power distributions of a tetrachromatic lighting source composed of red, amber, green, and blue LEDs. Solid line, high-fidelity lamp; dashed line, colour-saturating lamp.

A white solid state lamp with variable SPD was assembled of Philips Lumileds Lighting Luxeon® Rebel royal-blue 452 nm and green 523 nm InGaN LEDs, phosphor converted amber 589 nm LEDs, and red AlGaInP 637 nm LEDs. A computer-controlled electronic circuit for the variation of the partial fluxes of each group of LEDs was developed using the principle of pulse width modulation. To mitigate the temperature drifts of the LED output due to the heating of the chips, a feedback was introduced into the driving circuit. Uniform distribution of the colour-mixed emission was provided by means of plastic colour mixers. The developed “smart” solid-state lamp can find numerous applications in lighting where individual needs in colour quality are to be met.

1. A. Žukauskas, R. Vaicekauskas, A. Tuzikas, and M. Shur, Int. J. High Speed Electron. Syst., in press.

PP14

MODELING OF ALL-OPTICALLY PHOTOINDUCED MOLECULAR POLAR ALIGNMENT IN AZO-POLYMERS

L. Kučinskaitė[1], R. Petruškevičius[2]

[1] *Faculty of Physics, Vilnius University, Sauletekio ave. 9-III, LT-10222 Vilnius, Lithuania*

Lina.Kucinskaite@ff.stud.vu.lt

[2] *Institute of Physics, Savanoriu ave. 231, LT-02300 Vilnius, Lithuania*

Optical poling of azobenzene containing polymers enables us to break centrosymmetry of optically isotropic media creating the second-order nonlinear optical effect [1]. It is important to find new materials, in which the second order susceptibility can be induced. The micro patterning of the second order susceptibility $\chi^{(2)}$ of azo-dye doped polymer films by optical poling is performed by coherent combination of a fundamental field E_ω and the second harmonic field $E_{2\omega}$. The coherent pumping of the electro-optic polymer film results in an orientational hole burning through the quantum interference of two-photon absorption at the fundamental frequency ω and one-photon absorption at the second-harmonic frequency 2ω. The orientation hole burning is followed by a reversible trans-cis-trans isomerization process, which drives optical orientation motion, finally leading to a net permanent molecular polar order and automatically produces quasi-phase-matched $\chi^{(2)}$ micro-pattern for generation of the second harmonic.

Phenomenological model of photoinduced poling dynamics is developed. Given the intensities of the fundamental field and the second harmonic field used in the poling process, generation and relaxation of $\chi^{(2)}$ and $\chi^{(3)}$ nonlinear susceptibilities are described by this model. The physical origin of all-optical poling is attributed to orientational hole burning and molecular reorientation. It includes three parts: the first one is the isomerization of trans transforming to cis back to trans, the third one is the molecular thermal – induced orientational diffusion. The theory developed below is more general for considering the influence of cis on the poling process. Even though the direct contribution of cis to the induced susceptibility $\chi^{(2)}$ is negligible, the population of cis affects obviously the polar order of trans, thus it affects the induced susceptibility $\chi^{(2)}$ [2]. To derive the time – dependent expression of photoinduced poling, we consider the elementary contribution to the polar order made by the fraction of the molecules $dn(\Omega)$ whose representative moment of transition is presented in an elementary solid angle $d\Omega$ near the direction $\Omega(\Theta, \varphi)$. Obviously, time evolutions of the molecular density of trans $n_t(\Omega)$ and cis $n_c(\Omega)$ (Fig.1.) presented in the solid angle $\Omega(\Theta, \varphi)$ are given by

$$\frac{\mathrm{d}n_t(\Omega)}{\mathrm{d}t} = -\xi I(\Theta) n_t(\Omega) + \frac{1}{\tau_c}\iint P(\Omega' \to \Omega) n_c(\Omega')\mathrm{d}\Omega' + D_t \nabla^2 n_t(\Omega) \quad , \tag{1}$$

$$\frac{\mathrm{d}n_c(\Omega)}{\mathrm{d}t} = -\frac{1}{\tau_c} n_c(\Omega) + \xi\iint Q(\Omega' \to \Omega) I(\Theta') n_t(\Omega')\mathrm{d}\Omega' + D_c \nabla^2 n_c(\Omega) \quad . \tag{2}$$

The three terms in the right sides of (1) and (2) correspond to the three parts described above for trans and cis , respectively. ξ is the quantum efficiency of trans-to-cis photoisomerization, which is mainly related to resonant excitation, laser rate and matrix rigidity. τ_c represents the lifetime of cis. $P(\Omega' \to \Omega)$ and $Q(\Omega' \to \Omega)$ are the probabilities for molecules to rotate from Ω' to Ω in the process of cis-to-trans thermal recovery and trans-to-cis optical transition respectively. D_t and D_c are the thermal-induced orientational diffusion constants for trans and cis. $n_t(\Omega)\mathrm{d}\Omega$ and $n_c(\Omega)\mathrm{d}\Omega$ are the number of trans and cis which orient in the elementary solid angle $\mathrm{d}\Omega$ around the direction $\Omega(\Theta, \varphi)$ [2].

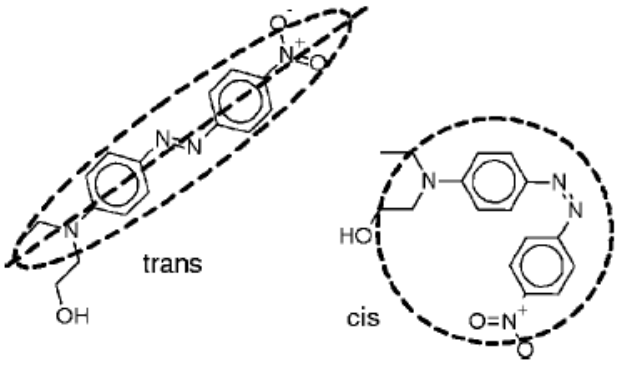

Fig. 1. Trans and cis isomerization of azobenzenes.

The cis and trans orientational order parameters up to the fourth order are used in the calculations. The fact that the laser used in experiments operates in pulses, rather than continuous wave mode, is also taken into account in this model. The necessary parameters for the model are obtained using both recent experimental results discussed here, and the earlier works on dark polar order relaxation [2, 3]. The model could eventually be used to determine the optimal intensities of poling fields for efficient generation of nonlinear optical structures.

1. C. Fiorini, F. Charra, J. M. Nunzi, and P. Raimond, Opt. Soc. Am., **14**, 1984-2003 (1997).
2. G.Xu. X.Liu, J. Si, P. Ye, Zh. Li, Yu. Shen, Opt. Lett., **25**, 329-331 (2000).
3. G. Seniutinas, L. Laipniece, J. Kreicberga, V. Kampars, J. Gražulevičius, R. Petruškevičius, R. Tomašiunas, J. Opt. A: Pure. Appl. Opt. **11**, 034003 (2009).

PP15

DIELECTRIC INVESTIGATIONS OF FERROELECTRIC $Bi_{2.5}Gd_{1.5}Ti_3O_{12}$ CERAMICS

E. Masiukaitė [1], J. Banys[1], D. Kiselev[2]

[1] *Department of Theoretical Physics, Faculty of Physics, Vilnius University, Sauletekio ave. 9-III, LT-10222 Vilnius, Lithuania*

Edita.Masiukaite@ff.stud.vu.lt

[2] *University of Aveiro, 3810-193 Aveiro, Portugal*

For high memory density device applications using ferroelectrics, ferroelectric materials should have a large remanent polarization, low coercive field, and good fatigue resistance at the same time [1–4]. A ferroelectric $Pb(Zr_xTi_{1-x})O_3$ (PZT) has been considered as a strong candidate for future memory applications because of its superior ferroelectricity [2,4]. However, PZT has a few disadvantages, such as environmentally hazardous lead content and poor fatigue endurance. Although the fatigue properties of PZT capacitor can be significantly improved by using metal-oxide electrodes, these electrodes tend to increase complexity of the fabrication procedure and leakage current [5,6]. Therefore, development of a new lead-free material having a superior ferroelectricity comparable to PZT is essential for these applications [2,3]. Lead-free bismuth-layered perovskite ferroelectrics, such as $SrBi_2Ta_2O_9$ (SBT) and $Bi_4Ti_3O_{12}$ (BIT), have been extensively studied as alternative materials for memory applications [2,7–9]. Most promising candidate at the moment looks like $Bi_{2.5}Gd_{1.5}Ti_3O_{12}$ (BGT), due to the high phase transition temperature. The aim of the present work was to investigate newly sintered ceramics with gadolinium substitution of bismuths by broad band dielectric spectroscopy. Measurements have been performed in the frequency range 20 Hz to 1 MHz and temperature range from 20 K to 1050 K. Obtained results can be divided into two parts: the low temperature part, where the glass like dispersion occurs at very low temperatures – below (Fig. 1) – the real part of the dielectric permittivity decreases with temperature increasing like in dipolar glasses or relaxes; the high temperature part. The high temperature part is dominated by conductivity and due to that the real and imaginary parts of dielectric permittivity increases up to $5{,}4 \times 10^7$. The obtained results have been analyzed in the terms of specific resistance, conductivity, and electrical modulus. The first of all we will discuss conductivity calculation results. The total conductivity follows universal law $\sigma(\upsilon) = \sigma_{DC} + A\omega^s$, with $\sigma_{DC} = \sigma_0 \exp(E_A/kT)$. Not to forget that this values are the total conductivity values of the system. To distinguish the grain conductivity from intergrain conductivity the specific resistance has been calculated. The results are presented in the Fig. 2. We can clearly see that we have two semicircles, which can be attributed to the grain conductivity (Higher frequency part) and intergrain conductivity (low frequency part). From the higher frequency semicircle we can calculate the graine DC conductivity at different temperatures. Similar results have been obtained from the electrical modulus representation (Fig. 3).

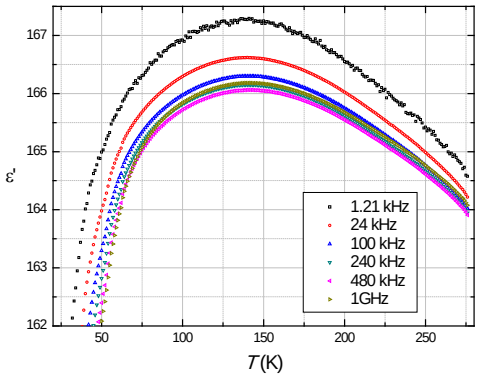

Fig. 1. Temperature dependences of the real part of the dielectric permittivity of BGT ceramics.

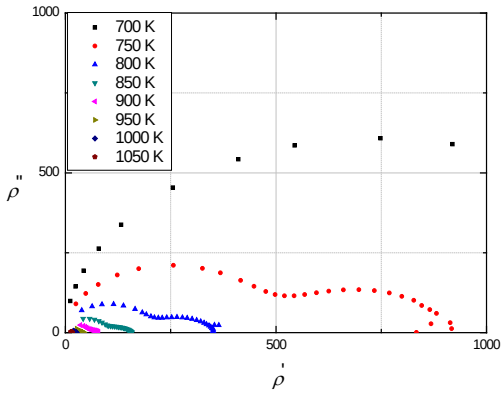

Fig. 2. Cole-Cole diagram for BGT ceramics.

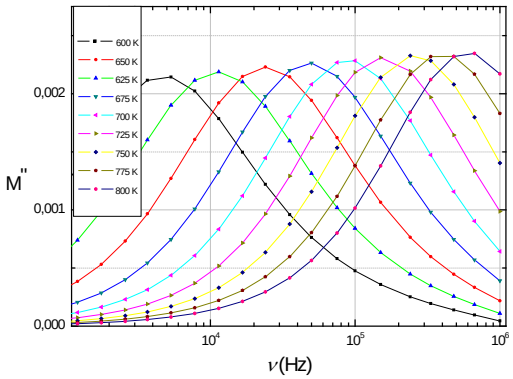

Fig. 3. M'' over the ν in a temperature range for the BGT ceramics.

We can conclude that dielectric spectra of $Bi_{2.5}Gd_{1.5}Ti_3O_{12}$ consist of two parts – low temperature freezing part similar to dipolar glasses and high temperature part dominated by electrical conductivity with sigma dc activation energy 0.9 eV, which most probably is caused by oxygen vacancies in this material.

1. J.F. Scott, *Ferroelectric Memories*, (Springer, Berlin, 2000).
2. B.H. Park, B.S. Kang, S.D. Bu, T.W. Noh, J. Lee, W. Jo, Nature **401**, 682 (1999).
3. T. Watanabe, T. Kojima, T. Sakai, H. Funakubo, M.Osada, Y. Noguchi, M. Miyayama, J. Appl. Phys. **92**, 1518 (2002).
4. D. Wu, A. Li, T. Zhu, Z. Liu, N. Ming, J. Appl. Phys. **88**, 5941 (2000).
5. U. Chon, K.B. Kim, H.M. Jang, G.C. Yi, Appl. Phys. Lett. **79**, 3137 (2001).
6. H.N. Al-Shareef, K.R. Bellur, A.I. Kingon, O. Auciello, Appl. Phys. Lett. **66**, 239 (1995).
7. C.A. Paz deAraujo, J.D. Cuchiaro, L.D. McMillan, M.C. Scott, J.F. Scott, Nature **374**, 12(1995).
8. D. Wu, A.D. Li, H.Q. Lin, T. Yu, Z.G. Liu, N.B. Ming, Appl. Phys. Lett. **76**, 2208 (2000).
9. S.O. Ryu, P.C. Joshi, S.B. Desu, Appl. Phys. Lett. **75**, 2126 (1999).

PP16

STUDY OF NON-EQUILIBRIUM CARRIER DIFFUSION AND RECOMBINATION IN $GaBi_XAs_{1-X}$ BY FOUR-WAVE MIXING TECHNIQUE

L. Lubys, S. Nargelas, R. Aleksiejūnas

Department of Semiconductor Optoelectronics, Institute of Applied Research, Vilnius University, Sauletekio Ave. 9-III, LT-10222 Vilnius, Lithuania

laurynas.lubys@ff.stud.vu.lt

Isoelectronic doping of GaAs allows significant modification of its electronic parameters. By substituting As atoms with larger Bi atoms, bandgap narrowing (of up to -62 meV/%Bi) and sub-picosecond carrier lifetimes are observed, thus making GaBiAs a potential material for ultrafast photodetectors for the use in infrared communication, as well as for optoelectronic emitters and detectors of terahertz radiation [1]. A bandgap as narrow as 0.74 eV and Bi content of x=11% has been achieved [2].

Non-equilibrium carrier lifetime and bipolar diffusion coefficient was measured in low-temperature grown (LTG) GaBiAs epilayers and in the LTG GaAs substrate on which they were grown by MBE. The exact Bi content in the samples is not known, however, using data from photoluminescence measurements, it has been estimated to be in the range of 3% to 5.5% in different samples.

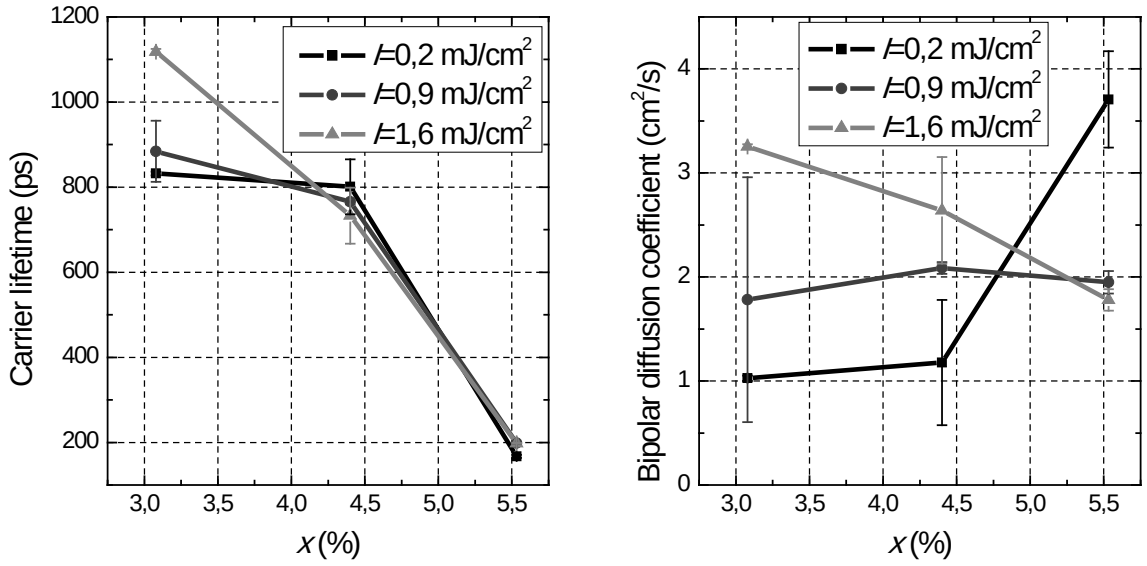

Fig 1. Carrier lifetime and bipolar diffusion coefficient measured in samples with different Bi content *x* at different excitation intensities *I*.

The four-wave mixing technique was used in measurements. A transient diffraction grating was induced using the 2nd harmonic (532 nm) of a YAG:Nd laser (PL 2143, Ekspla) and was probed using the 1st harmonic (1064 nm) of the same laser. Time resolution was achieved by increasing the optical path of the probe beam and was limited by the duration of the laser pulse (~25 ps). Diffraction efficiency as a function of excitation intensity was measured in order to investigate recombination processes in the samples.

Carrier lifetimes and diffusion coefficients measured at different excitation levels are presented in Fig. 1. Carrier lifetimes decrease with increasing Bi content which can be explained by Bi atoms forming fast recombination centers. The longest observed carrier lifetime was 850-1150 ps and the shortest –180-200 ps. For comparison, the carrier lifetime in the substrate was ~400 ps.

The measured value of bipolar diffusion coefficient (1÷4 cm^2/s, which corresponds to hole mobility of 20÷80 $cm^2/(V \cdot s)$) does not change significantly with increasing Bi content, however, it is much lower than that in the substrate (~40 cm^2/s) or in GaAs (~20 cm^2/s), therefore, Bi incorporation greatly reduces the quality of the crystal.

At excitation intensities above 0,4 mJ/cm^2 a faster induced grating decay component has been observed. This effect was not observed in the substrate within the intensity limits of the experiment (up to 4,5 mJ/cm^2), therefore, it can be assumed that Bi incorporation increases the non-linear carrier recombination coefficients.

1. V. Pačebutas, K. Bertulis, L. Dapkus, G. Aleksejenko, A. Krotkus, K. M. Yu,W. Walukiewicz, Semicond. Sci. Technol. Vol. **22,** 819–823 (2007).
2. A. Krotkus, V. Pačebutas, K. Bertulis, G. Aleksejenko**,** Journal of Materials Science: Materials in Electronics Vol. **20**, 363-366 (2009).

PP17

STUDY OF THE AUGER RECOMBINATION PROCESSES BY FREE CARRIER ABSORPTION TRANSIENT TECHNIQUES

A. Balčytis, T. Čeponis, E. Gaubas

Institute of Applied Research, Vilnius University, Sauletekio Ave. 9-III, LT-10222 Vilnius, Lithuania Armandas.Balcytis@ff.stud.vu.lt

Due to its high electron mobility germanium is experiencing resurgence as a promising material in the production of high frequency field effect transistors, efficient GaAs/Ge solar cells as well as in power electronics that operate at cryogenic temperatures. At high excitation conditions, Auger recombination is a limiting factor for carrier lifetime in the indirect-band semiconductors [1]. However, parameters of the Auger recombination in germanium up-to-now have been determined with poor precision. Therefore, study of Auger processes by using modern measurement techniques is important for the technology of state-of-the-art Ge based devices that operate at high carrier density.

In this work the characteristics of carrier recombination in pure crystalline Ge wafers have been studied by varying excitation and doping level in a wide range of carrier densities. The free carrier decay transients have been examined by combining free carrier absorption transient techniques based on pulsed photoconductivity probed by the continuous infrared (at 2.4 μm) radiation, employed at high excitation levels, and microwave (at 22 GHz) radiation, at low carrier injection regime [2]. The carrier decay transients in Si and Ge materials have been recorded in for comparative purposes in order to reliably identify the Auger recombination regimes. Shockley-Read-Hall type and Auger recombination processes have been clearly unveiled in Si wafers. However, the band-to-band Auger transitions in germanium appeared to be un-detectable at excitation densities close to the value of surface damage threshold. This leads to the conclusion that the Auger coefficient values for germanium determined by other researchers have been overestimated [3]. Thus, the value of the coefficient for Auger recombination does not exceed 10^{-32} cm^6/s order of magnitude.

The obtained doping and excitation density dependent carrier recombination lifetime variations in Ge are analysed. The possible improvements for extraction of the parameters of Auger recombination in germanium by varied excitation wavelength spectroscopy will be discussed.

1. P. T. Landsberg, *The band-band Auger effect in semiconductors, Solid – State Electronics*, vol. **30** no. 11, (1987).

2. N. G. Nilsson,, Physica Scripta, **8**, 165 – 176, (1973).

3 D. Poelman, P. Clauws and B. Depuydt, , Solar Energy Materials and Solar Cells, **76** 167-173 (2003).

PP18

KINETIC PROPERTIES OF INDOLO-BENZOXAZINE PHOTOCHROMIC COMPOUNDS INVESTIGATED BY NANOSECOND TIME-RESOLVED SPECTROSCOPY

V. Pranculis[1], L. Ivanauskas[1], V. Martynaitis[2], A. Šačkus[2], M. Vengris[1]

[1] *Laser Research Center, Department of Quantum Electronics, Faculty of Physics of Vilnius University, Saulėtekio ave. 10, LT-10223 Vilnius, Lithuania*

[2] *Institute of Synthetic Chemistry, Kaunas University of Technology, Radvilėnų Rd. 19, LT-50254 Kaunas, Lithuania*

Vytenis.Pranculis@ff.vu.lt

Photochromism is light-induced reversible transformation of a chemical species between two forms having different absorption spectra.

The phenomenon of photochromism was noted as early as 1867 [1], yet the research of the field are still bringing up new facts and results. One of these was the invention of the new organic photochromic compounds of spirooxazine class in 2005 [2].

Derivatives of this new dye (indolo [2,1-b] [1,3] benzoxazine, VA 07-01 in Fig. 1) were analyzed by means of nanosecond flash-photolysis in order to estimate the effect of structural modifications of the basic structure (VA 07-01 in Fig. 1). Chemical formulas of analyzed compounds are shown in figure 1.

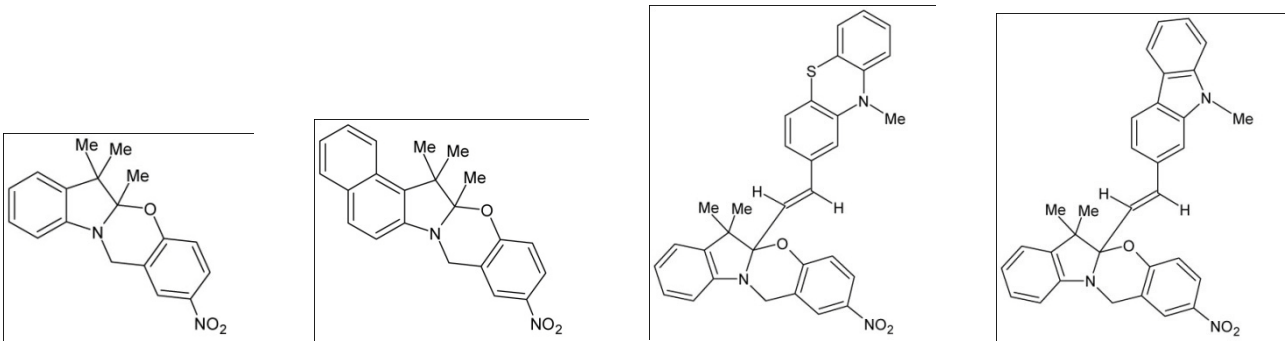

VA 07-01 RS 15-03 VA 03-09 VA 03-13

Fig. 1. Chemical formulas of analyzed spirooxazines.

Samples were dissolved in MeCN and excited by 3rd harmonic of Nd: YAG laser (Ekspla NL301). High-speed photodiodes and 1 GHz bandwidth oscilloscope were used to detect transient absorption of the solution in the selected wavelength. Time resolution of the experiments was limited by the duration of laser pulse (5 ns).

Comparison of time-gated absorption spectra of VA 07-01 and RS 15-03 (Fig. 2.) shows that the absorption maximum at ~425nm is due to nitrophenolate. This is also confirmed by the

nitrophenolate absorption spectra presented in [3]. The strong RS 15-03 absorption band at 525nm could be due to benzene ring addition to the indoline moiety because it is much weaker in other analyzed compounds.

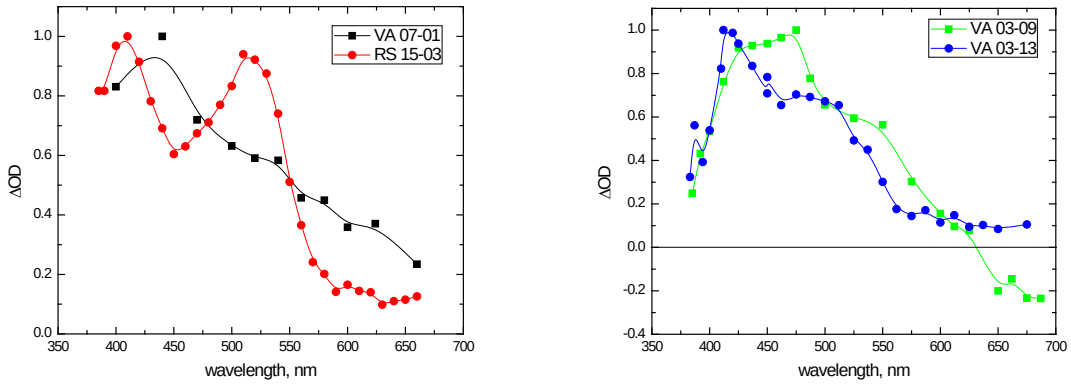

Fig. 2. Time-gated spectra of analyzed spirooxazines.

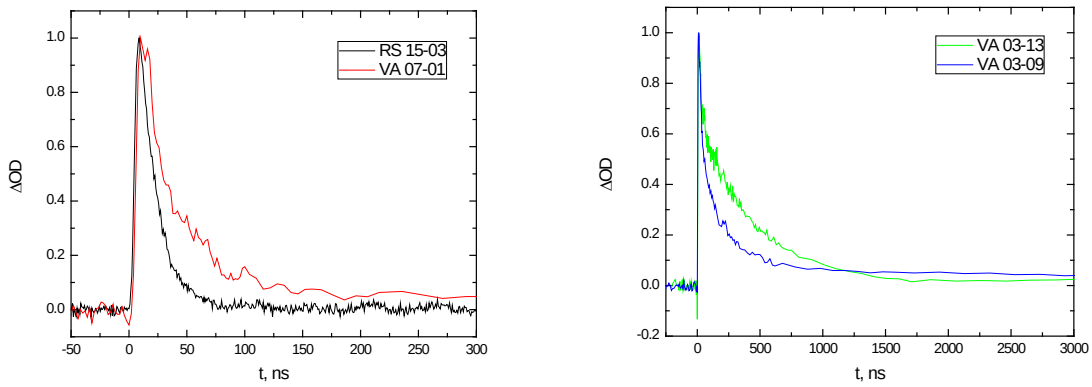

Fig. 3. Transient absorption kinetics of analyzed spirooxazines. Note the different time-span of right and left graphs.

Transient absorption kinetics shown in Fig. 3 imposes that massive chemical groups linked to spiro atom through ethylene bridge prolongs relaxation time to microsecond domain. This can be explained by more complicated geometrical transformation required for returning back to the original form.

Collected data is helpful for understanding and distinguishing roles of different moieties of spirooxazine in photochromic reaction. This roughly allows predicting the parameters of newly designed photochromes.

1. J. Fritzsche. Comptes Rendus Acad. Sci., Paris, **69**, 1035 (1867).
2. M. Tomasulo, S. Sortino and F. M. Raymo; Org. Lett. **Vol. 7, Nr. 6**, 2005, 1109-1112
3. M. Barkauskas, Lithuanian Journal of Physics, **Vol. 48, No. 3**, pp. 231-242 (2008).

PP19

THEORETICAL MODELLING OF BACTERIORHODOPSIN

K. Redeckas, M. Mačernis

Department of Theoretical Physics, Faculty of Physics, Vilnius University,
Saulėtekio al. 9 LT-10222 Vilnius, Lithuania
kipras.redeckas@ff.stud.vu.lt

Theoretical modelling of biomolecular structures allows us to learn more about their properties and to determine their distinct features. The main object of interest of this work was the bacteriorhodopsin protein which known as a molecular proton pump. Bacteriorhodopsin undergoes a unique photocycle which occurs after the absorption of a photon. During this photocycle bacteriorhodopsin experiences structural and spectral changes.

Methods of both high level quantum mechanics and molecular dynamics were used in this work. We used the molecular dynamics force field and software package AMBER [1] to create a functional model of the whole protein system. The lysine amino acid with it bounding retinal chromophore were reparametrised for hybrid quantum mechanics/molecular mechanics (QM/MM) simulations. Geometry optimization with the implementation of the semi-empirical self-consistent charge density functional tight binding method (DFTB/SCC-DFTB) for the amino acid-ligand complex was successfully performed on the complete bacteriorhodopsin structure with its lipid surroundings.

The retinal chromophore was also investigated using quantum mechanics software package ORCA [2]. This package was used for high level geometry optimization and electronic spectra calculations. We applied the density functional theory (DTF) methods for optimal geometry computation and time-dependent density functional theory (TD-DFT) methods for estimation of the first four excited states of the chromophore. A series of calculations was performed alternating some of the primary parameters of TD-DFT in order to acknowledge their influence for the simulated spectra. Several different functionals were used (BLYP, B3LYP) with the inclusion of Tamm-Dancoff approximation (TDA).

The calculated values of the first excited state S_1 agree nicely both with experimental data and theoretical results from other publications [3][4]. The computed oscillator strengths show that transitions to this state are expected to be allowed. This leads us to believe that density functional methods using BLYP and B3LYP functionals are suitable for modelling bacteriorhodopsin in its first state of the photocycle. Both AMBER and ORCA packages have good tools for modelling the

system. Our future goal is to apply these methods for further analysis and to investigate the effects of the hydrogen bond network and the consequent intermediates of bacteriorhodopsin.

1. http://ambermd.org/
2. http://www.thch.uni-bonn.de/tc/orca/
3. K. Fujimoto, J. Hasegawa, S. Hayashi, S. Kato, H. Nakatsuji. *Mechanism of color tuning in retinal protein: SAC-CI and QM/MM study.* Elsevier, 2005.
4. S. Hayashi, I. Ohmine. Journal of Physical Chemistry B, **104(5)**, 10678–10691 (2001).

PP20

DEFECTS REACTIONS IN IRRADIATED CdTe CRYSTALS

P.Malinovskis[1]

[1]*Vilnius university, Applied science institute*

paulius.malinovskis@ff.vu.lt

The technology of x-ray and γ detectors, optical components for IR applications and communication systems requires bulk CdTe single crystals with the lowest possible equilibrium carrier concentration. One way of preparing high-resistivity CdTe is by growing highest purity crystals. Another, more cheap and easier, way is by compensating self defects and residual impurities by doping with antimony (Sb), lead (Pb) and tin (Sn) – impurities that produce midgap energy levels in CdTe and compensate residual impurities[1., 2.].

The purpose of this work was to analyse the origin of near-intrinsing conduction in CdTe crystals doped with Sb, Pb, and Sn. The electrical conductivity, magnetoresistivity and Hall mobility of the samples were measured before and after x-ray illumination. It was measured by a standard dc technique using an electrometer amplifier with an input resistance of 10^{14} Ω. The samples were rectangular in shape, 5,75· 1,75 · 0,6 mm in dimensions, and have two pairs of ohmic probe contacts.

After the analyzes of the Hall coefficient temperature dependencies, the charge carrier mobility and magnetoresistivity before and after the excitation by x-ray ($h\nu \geq E_K$ (Cd K-shell absorption edge)) activation energy values were determined, which was similar to those in scientific literature [3,4]. After the excitation with x-ray we observed the defect created by x-ray radiation reactions with former defects, their recharge and clusters formation.

1. Glenn F. Knoll. *Radiation detection and measurement* (John Wiley and sons, 1989).
2. T.Fukura, H.J.Schee. *Crystal Growth technology* (John Wiley & Sons Ltd, 2003).
3. P. N. Gorlei, O. A. Parfenyuk, M. I. Ilashchuk, I. V. Nikolaevich. Inorganic Materials, **Vol. 41. No. 12 (**2005).
4. P.Fochuk, R.Grill, Ye.Nykonyuk, J.Krustok, Z.Zakharuk, M.Grossberg, O.Panchuk. High temperature properties of CdTe crystals, doped by Sb. IEEE Nuclear Science Symposium Conference Record R01-5. 2006.

PP21

STUDY OF LIQUID STRUCTURE OF ACETONITRILE CLUSTER FORMATION IN AQUEOUS SOLUTIONS BY 2D CORRELATION VIBRATIONAL SPECTROSCOPY

M. Pareigis, V. Aleksa

Vilnius University, Faculty of Physics, Department of General Physic and Spectroscopy, Saulėtekio al. 9 – 3, LT – 10222 Vilnius, Lithuania

martynas.pareigis@ff.stud.vu.lt

Vibrational spectroscopy is very powerful tool to probe the association and interaction of acetonitrile molecules in water and ionic liquids. The structure of acetonitrile - water mixtures has been investigated by Raman and FT-IR spectroscopy methods over wide range of acetonitrile mole fractions (0 % ≤ X_{AN} ≤ 100 %, Fig. 1.).

Two dimensional (2D) asynchronous Raman spectra in the region of C≡N vibrations of acetonitrile revealed two peaks which are located at 2252 and 2256 cm^{-1}. Spectral parameters of the C≡N vibration of complexes were studied in H_2O-CH_3CN mixture.

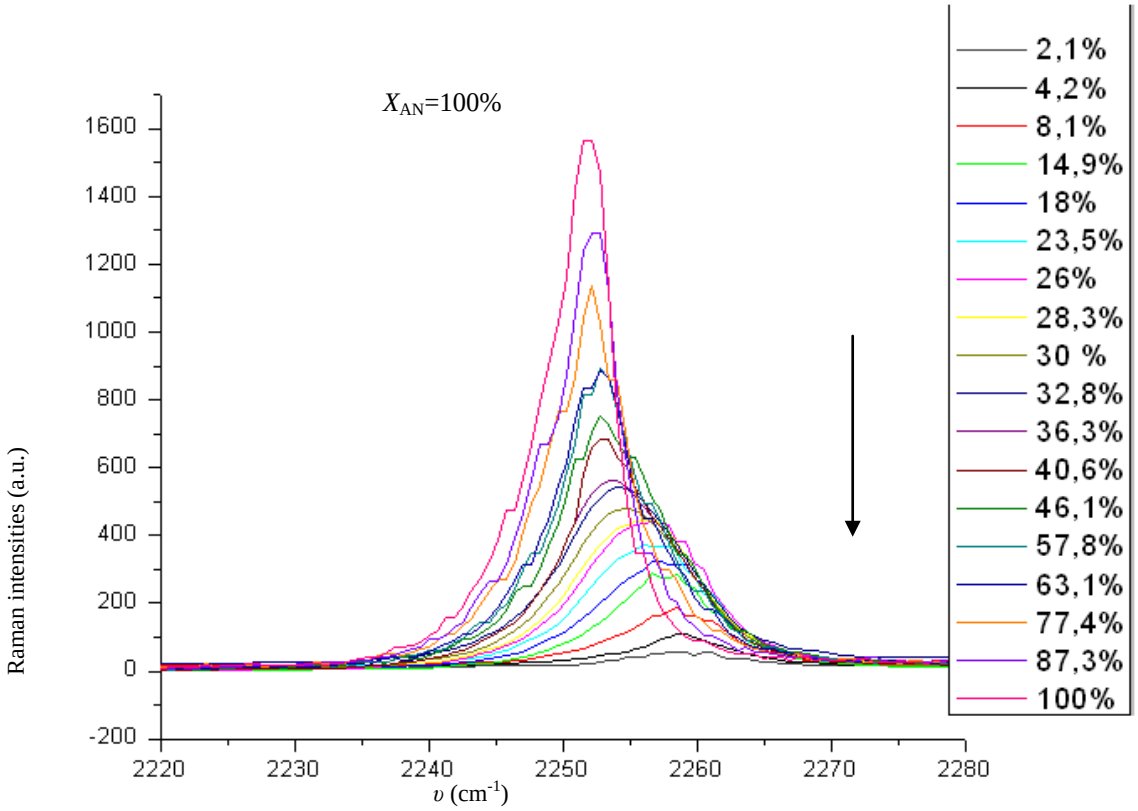

Fig. 1. C≡N symmetric stretching Raman shift plotted as a function of the acetonitrile molar fraction in the H_2O-CH_3CN mixtures

The high-wavenumber part of the band begins to broaden, but the position of the band‘s maximum in the spectrum is not changed. This broadening can be explained if one supposes that the band consist of more two or more bands. It can be related with formation of acetonitrile clusters in mixture.

1. I. Noda. Applied spectroscopy. **54(7)**, 994-999 (2000).
2. M. Stoev, A. Makarow, J.M.A. Robledo. Spectroscopy Letters, **28(8)**, 1251–1258 (1995).
3. F.H. Tukhvatilin, A. Jumabaev, G. Muradov, H.A. Hushvaktov and A.A. Absanov. Journal Of Raman Spectroscopy. **36**, 932-937 (2005).

PP22

INVESTIGATION OF SCANNING PROBE MICROSCOPE ELECTROMECHANICAL SYSTEM DYNAMICS

I. Morkvėnaitė-Vilkončienė

Kaunas University of Technology

inga.klajune@gmail.com

In-depth knowledge of scanning probe microscopy (SPM) dynamics is necessary when interpreting obtained images and especially when the sources of artifacts are to be identified. The aim of this research was to build and test the dynamic model of SPM electromechanical system. For simplicity reasons only atomic force microscopy (AFM) contact mode dynamics was explored.

The sensor part of AFM electromechanical system, most affecting the image quality, is subjected by the following forces: cantilever spring force, friction force, inertia and the force of interaction with the sample:

$$F_{inertia} + F_{spring} + F_{friction} = F(z); \tag{1}$$

The most simple approach, which nevertheless leads to a realistic description of most tip movements, is to start with Newton's equation of motion: [1,2]:

$$m\frac{\mathrm{d}^2 z}{\mathrm{d}t^2} + \gamma\frac{\mathrm{dz}}{\mathrm{d}t} + kz = F(z); \tag{2}$$

m - the effective mass of the cantilever,k - the spring constant of the cantilever, and $\gamma = 2\sqrt{\frac{k}{m}}$ - the dissipation term.

A linear second order differential equations is written as [3]:

$$\frac{\mathrm{d}^2 z}{\mathrm{d}t^2} + 2\xi\omega_n\frac{\mathrm{dz}}{\mathrm{d}t} + \omega^2{}_n z = \omega^2{}_n x \tag{3}$$

where $\omega_n = \sqrt{k/m}$ is the undamped angular frequency of the cantilever and ζ is a constant called the damping ratio.

The transfer function of (3) is[3]:

$$\frac{Z(s)}{X(s)} = \frac{\omega^2{}_n}{s^2 + 2\xi\,\omega_n s + \omega^2{}_n} \tag{4}$$

From (1), (2), (3) and (4), we obtain the transfer function, from which a model of Matlab/Simulink model was created (Fig. 1.).

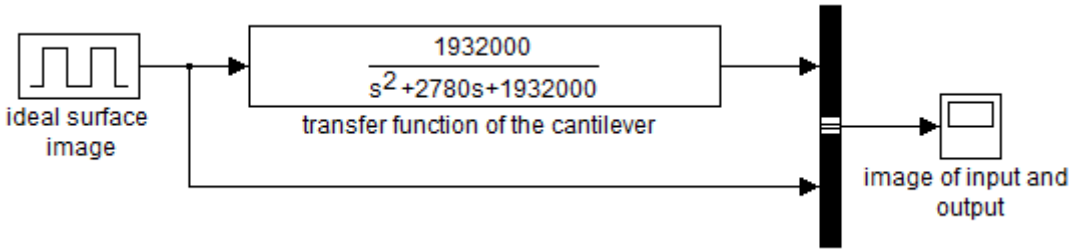

Fig. 1. Simulink model of the cantilever movement.

Rectangular 5 ms 1 μm hight pulses simulate the ideal surface profile. Coefficients were obtained by the manufacturer‘s data available on the Nanosurf EasyScan 2 SPM, working with CONTR cantilever. Coefficients obtained for a contact mode have following values: $k = 0.2N/m$, $b = 50\mu m$, $h = 2\mu m$, $l = 450\mu m$. On the Fig. 2 the system output is compared with an input. Dynamic errors can be explicitly observed.

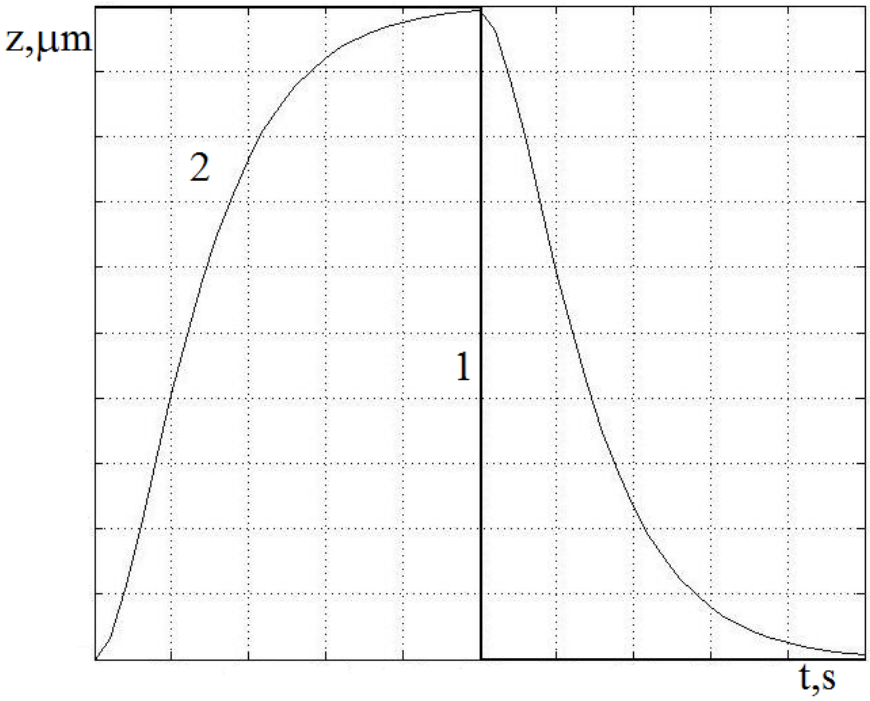

Fig. 2. Simulation of profile scan: 1– ideal surface image, 2 – the obtained image.

1. Hans-Jugen Butt, Brunero Cappella, Michael Kappl. Surface Science Reports, **59,** 1–152 (2005).
2. D. Sarid, *Scanning Force Microscopy: With Applications to Electric, Magnetic, and Atomic Forces* (Oxford University Press US, 1994).
3. V.S.Januševičius, *Automatinis valdymas* (Kaunas, 2003).

PP23

PHOTOELECTRICAL PROPERTIES AND AGEING OF ZnPC/C60 SOLAR CELLS

V. Kažukauskas[1], A. Arlauskas[1], M. Pranaitis[1], Rudolf Lessmann[2], Moritz Riede[2], Karl Leo[2]

[1] *Semiconductor Physics Department and Institute of Applied Research*

andrius.arlauskas@ff.stud.vu.lt

[2] *Tecnische Universität Dresden, Institut für Angewande Photophysik*

Copper and zinc Phtalocyanines (CuPc and ZnPc), and C60 are frequently used for organic solar cell engineering. Their energy levels form a donor-acceptor junction, which leads to charge separation; they have high absorption coefficients and a complementary absorption of the Sun spectrum. Yet, the lifetime of high efficiency organic solar cells is still in the range of 1000 h. This is mainly attributed to contamination with oxygen and moisture that can react with excited molecules. We have investigated the ageing properties of ZnPc/C60 solar cells and the corresponding changes of energetic parameters characterizing material conductivity, potential barrier height and charge carrier mobility.

The devices were aged for 1300 hours under constant illumination by blue LED, with peak emission at 475 nm, and incident light power density of 10 mW/cm^2. The devices aged under light showed a fast initial degradation of the short circuit current and of the fill factor followed by the much slower, nearly linear decay of these values.

The potential barrier height giving the diode-like behavior and the activation energy value of material conductivity were evaluated from the IV dependencies at different temperatures. The potential barrier of about 0.55 eV evaluated in the reference sample, increased after degradation up to 0.63 eV. Meanwhile the thermal activation energy values of the electrical conductivity grew from about 0.28 eV prior to degradation up to about 0.34 eV after ageing.

Carrier mobility dependencies on electric field at different temperatures were measured by CELIV. It was demonstrated that the mobility decrease during degradation is caused by the increase of both energetic (σ) and positional disorder (Σ) parameters within the Gaussian Disorder Model. Therefore, hopping carrier transport becomes aggravated, resulting in decrease of the sample conductivity as well as growth of its activation energy. This means that the jumps of the carriers between hopping states have to be energized more to move in a greater energetic and spatial disorder in order to take part in conductivity. Moreover, increasing material disorder also causes growth of the mean potential barrier at the interface.

PP24

FLUCTUATIONS OF INDIUM CONCENTRATION IN In-RICH-InGaN EPITAXIAL LAYERS

Vilmantas Šukauskas and Darius Dobrovolskas

Semiconductor Physics Department, Vilnius University, Vilnius, Lithuania

vil.sukauskas@gmail.com

Ternary compounds of InGaN are of great interest for applications in nearly all commercial light emission systems since they allow bandgap tunability from the UV to the visible region of the spectrum [1]. However, their optical properties including radiative recombination peculiarities still need further investigation in order to reveal details of fundamental processes and recombination mechanisms which are far from complete understanding in order to optimize device operation regimes and even to extend their usage. In this paper, investigation of In-rich $In_xGa_{1-x}N$ (x is close to ~30%) epitaxial layers grown by MOCVD technique over sapphire substrate was performed using laser scanning confocal microscopy (LSCM) technique. This method provides unique possibility to analyze spatial distribution of photoluminescence (PL) with high (submicron) spatial resolution and to study carrier localization problems. Since the band gap of ternary compound $In_xGa_{1-x}N$ depends on In fraction x [1] the near-band edge (NBE) emission spectra can also provide information on In space distribution in the layer. Band gap was determined by wavelength of the PL intensity maximum. These spectra revealed that In concentration is not uniform throughout the sample surface. Besides, PL intensity is distributed non-homogeneously, too. Typical image of spatially distributed PL intensity with high and low intensity areas is illustrated in Fig. 1.

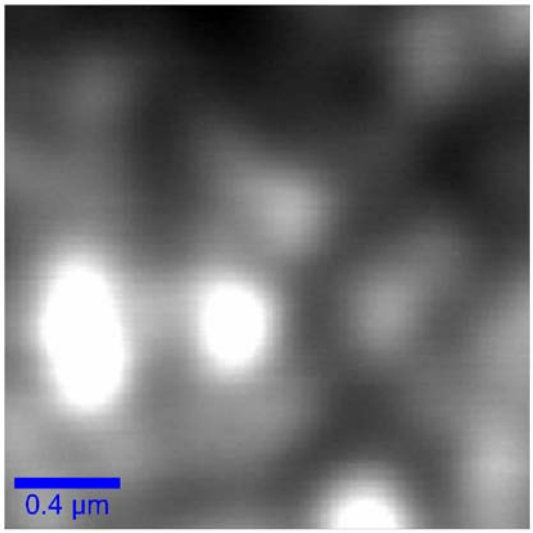

Fig. 1. Image of spatially distributed PL intensity in the area of 2x2µm of $In_xGa_{1-x}N$ sample.

In our experiments using LSCM technique it was reached spatial resolution up to ~200 nm. Meanwhile, the size of scanning step was 10 nm, thus 40 thousands spectra were collected from

2x2μm area of the sample surface. The sample surface was excited by 200 nm-diameter spot of the focused He-Cd laser beam (λ = 442 nm) whereas PL was collected at each adjacent point with the 10-nm-scanning step. The PL spectra demonstrated that NBE maximum position varies within the excited spot.

It is known that higher indium concentration in InGaN compound leads to lower band gap [2]. Thus it is naturally assumed that In content spatial fluctuations in ternary compound InGaN leading to band-gap variations may lead to the corresponding PL intensity fluctuations: areas with lower band-gap (higher In concentration) should demonstrate higher PL intensity and vice versa. This idea was verified by analyzing PL space-integrated and spectrally-resolved intensity in bright (high PL intensity) and dark (low PL intensity) areas of InGaN layer. Fig. 2 shows the typical spectra of low and high PL intensity areas. Interestingly, usually dark PL areas demonstrate NBE maximum at slightly longer wavelength in comparison to that of bright ones. This means that fluctuations of In concentration are not responsible for non-uniform spatial (at leas for this scale) of the PL intensity. Meanwhile the analysis of the observed NBE maximum fluctuations within the bright and dark areas of the excited spot with the step of 10 nm showed variations in In concentration from $x \approx 0.32$ to $x \approx 0.35$.

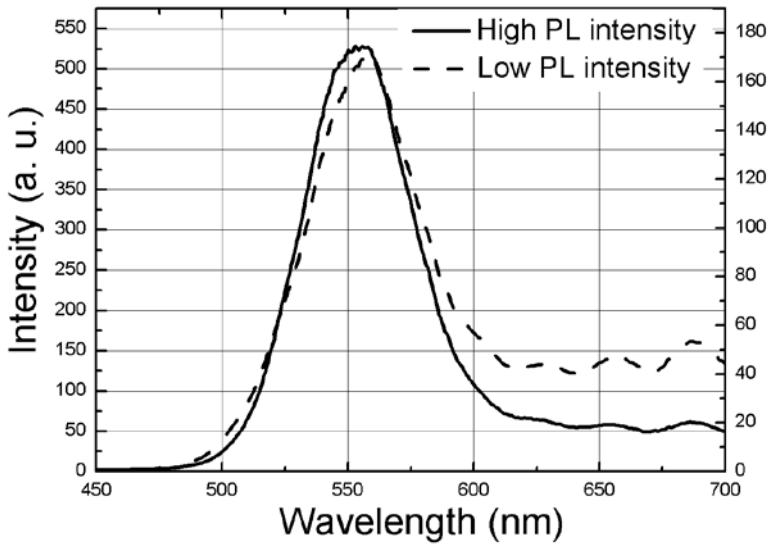

Fig. 2. Average spectra of high and low PL intensity areas.

Presumably, the PL intensity spatial distribution as bright and dark spots is caused by corresponding non-homogeneous distribution of non-radiative recombination centers. The details of radiative and non-radiative recombination processes in InGaN layers are discussed.

1. S. J. Pearton, J. C. Zolper, R. J. Shul, and F. Ren, J. Appl. Phys. **86**, 1 (1999).
2. www.semiconductors.co.uk

PP25

POPULATION INVERSION IN OPTICALY EXCITED ZnO CRYSTALS

T. Gulbinas , M. Karaliūnas

Semiconductor Physics Department and Institute of Applied Research, Vilnius University

tadas@gulbinas.lt

Wide-band-gap semiconductors have attracted a great deal of attention because of ever-increasing commercial desire for light emitting devices in blue-UV spectral region. ZnO is one of these wide-band-gap (E_g = 3.37 eV) semiconductors with characteristics promising for UV optoelectronics. One exceptionally interesting feature of ZnO is a huge exciton binding energy (60 meV) which makes possible existence of excitons and emission mechanisms involving these quasiparticles even at room temperature and above. Many of light-emitting devices operate under extreme conditions, in particular, at high pumping levels, which determine a variety of different optical transitions involving excitons especially at the threshold of population inversion. However, due to complexity of the processes many mechanisms still are far from understanding.

Here we present results of population inversion and optical gain (OG) experimental measurements in high-quality ZnO epitaxial films, growth on sapphire substrates with GaN buffer layers using molecular beam epitaxy. All measurements are performed at room temperature. The aim of this work is to analyze conditions of population inversion in ZnO, in particular, to determine the lasing threshold for excitation power density, as well as analysis of radiative transition mechanisms.

Photoluminescence (PL) and optical gain spectra have been analyzed over a wide range of excitation intensities using laser radiation with photon energy 3.49 eV and 4.66 eV. Stimulated emission peak was observed at E_{ph}= 3.175 eV. The PL analysis shows that mechanisms of stimulated emission involve exciton recombination. In particular interaction of excitons among themselves and with optical phonons is discussed. Measurements also show strong photon re-emission in ZnO epitaxial layers. This phenomenon was observed when underneath GaN buffer layer was exited and its emission lines could be resolved in PL spectra. Investigation of the PL dependence on excitation indicates that the threshold pumping power density is around ~700 kW/cm^2, exceeding of which optical gain was observed.

OG coefficient was measured using so-called thin stripe technique (Shaklee method). Measurements with variable stripe length indicated maximum OG coefficient value of 190 cm^{-1} . OG measurements by comparing two spectra for two different stripe lengths indicate blueshift of the gain maximum position when excitation increases. The reasons of OG dynamics in ZnO are discussed.

PP26

MODELLING OF CHARGE CARRIERS TRANSPORT IN DISORDERED MATERIALS IN THE CASE OF DOUBLE INJECTION

V.Valentinavičius[1], N. Nekrašas[1], G. Juška[1]

[1] *Vilnius University, Faculty of Physics, Department of Solid State Electronics*

vytis.valentinavicius@gmail.com

Lately organic disordered materials have drawn increasingly more attention. Cheap production and specific features of organic materials made them suitable for LED and solar panel applications. This is why it is very important to fully investigate the properties of these materials. In this paper, the chosen method of investigation is double injection (DoI) current transient analysis, which enables to measure charge carriers recombination and transport properties within material [1]. Theoretical equations of the charge carriers transport and recombination in general can not be solved, only individual cases can be analysed [2], thus computer simulations are used to obtain results.

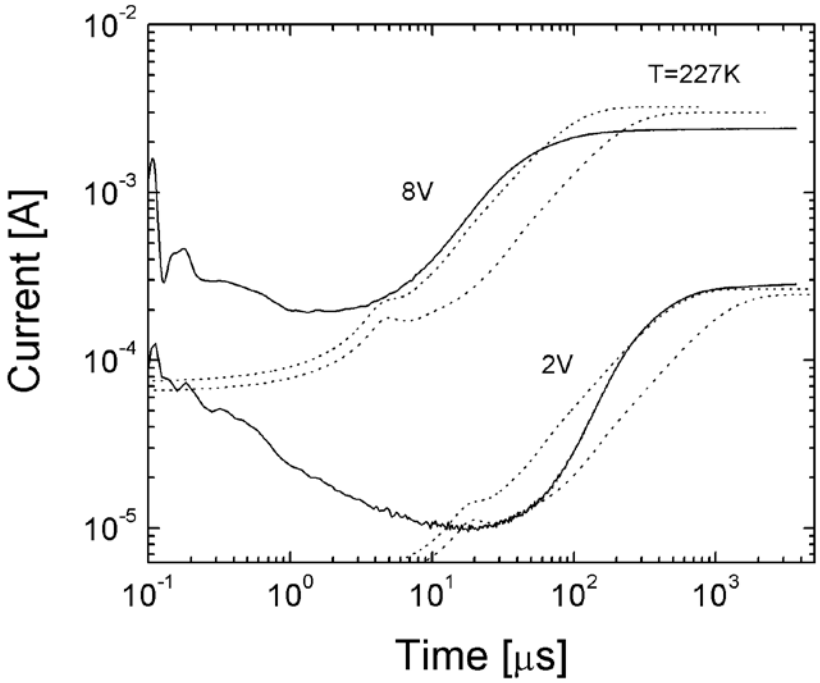

Fig. 1 Double injection current transients in RR-P3HT/PCBM blend at different voltages compared with the modelled ones.

The main goal of this work is to model numerically the transport and recombination of charge carriers in disordered materials in the case of DoI. Currently existing models [3] do not cover all significant processes that effect charge carriers transport. In Fig. 1, experimentally obtained DoI current transients in (RR-P3HT/PCBM) blend are compared with the ones obtained by currently existing model, and significant difference between them can be seen. The new model includes more physical effects which are influential on charge carriers distribution within material and, consequently, DoI current transient. Furthermore, the cases where diffusion is essential to DoI current transient are analysed.

1. G. Juška, K. Genevičius, G. Sliaužys, N. Nekrašas, IEEE Journal of Selected Topics in Quantum Electronics, **PP**, Issue 99, 1-6 (2010).
2. M.A. Lampert, P. *Mark, Current Injection in Solids* (New York, Academic Press, 1970).
3. G. Juška, K. Genevičius, G. Sliaužys, N. Nekrašas, R. Österbacka, Journal of Non-Crystalline Solids, **354**, Issues 19-25, 2858-2861 (2008).

PP27

DIELECTRIC PROPERTIES OF $PBFE_{0.5}TA_{0.5}O_3$ CERAMICS

M. Šimėnas[1], K.Bormanis[2], J.Banys[1], R.Grigalaitis[1]

[1] *Vilnius University, Physics faculty, Saulėtekio av. 9, III b., LT-10222 Vilnius, Lithuania*

mantas.simenas@ff.stud.vu.lt

[2] *Institute of Solid State Physics, Latvia University, Latvia*

Materials that are both ferroelectric and magnetic—multiferroics—are rare. This is because in most ferroelectrics, such as $BaTiO_3$, the ferroelectricity is driven by a hybridization of empty *d* orbitals with occupied *p* orbitals of the octahedrally coordinated oxygen ions. This mechanism requires empty *d* orbitals and thus cannot lead to multiferroic behavior. There are consequently very few ferroelectrics that exhibit long range magnetic order, and rarer still are materials where these two disparate order parameters exist and exhibit significant coupling. Multiferroics have been of particular interest recently both to understand the fundamental aspects of the novel mechanism that gives rise to this magnetic-ferroelectric coupling, as well as because of the intriguing possibility of using these coupled order parameters in novel device applications. In particular, recent "proof of principle" work has shown that it is possible to control the magnetic phase with an applied electric field, and control the electric polarization with an applied magnetic field. One of the most promising candidates of this type is $PbFe_{0.5}Ta_{0.5}O_3$. In this contribution we present dielectric properties of $PbFe_{0.5}Ta_{0.5}O_3$ ceramics in wide temperature (130 – 450K) and frequency (0.2- 2000 kHz) range.

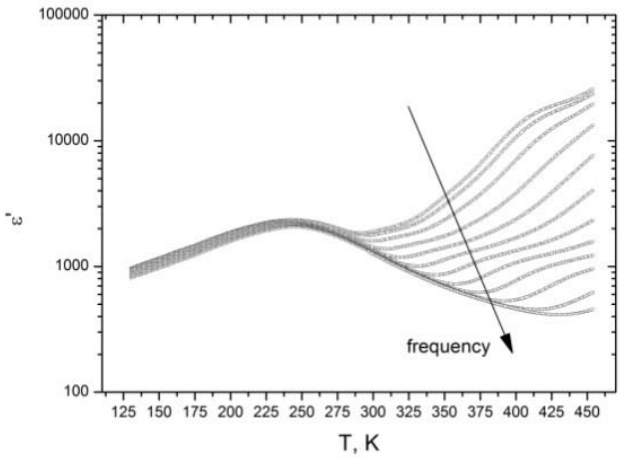

Fig. 1. Temperature dependence of the real part of complex dielectric permittivity of $PbFe_{0.5}Ta_{0.5}O_3$. Arrow shows the increasing frequencies from 20 Hz to 1 MHz.

Dielectric measurements of complex dielectric permittivity $\varepsilon^* = \varepsilon' - i\varepsilon''$ of the $PbFe_{0.5}Ta_{0.5}O_3$ show only one phase transition at a Curie temperature ~ 240 K (Fig. 1). At this temperature real part of dielectric permittivity ε' reaches a maximum value (around 2250), which is dependent on frequency.

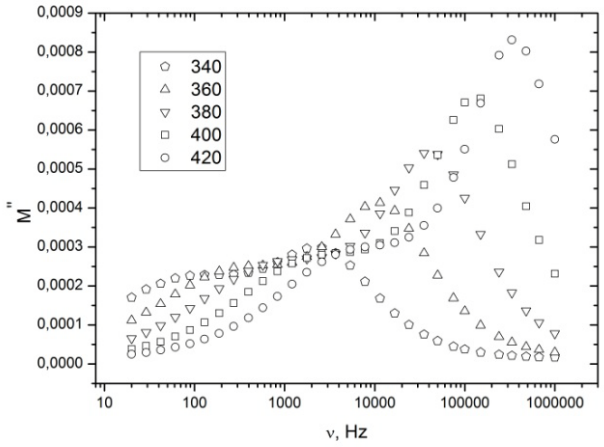

Fig. 2. Frequency dependence of imaginary part of complex electric modulus of $PbFe_{0.5}Ta_{0.5}O_3$ at various temperatures.

As it is possible to see from the fig.1., the dielectric properties at high temperatures are dominated by electrical conductivity. Due to that, the complex electric modulus of $PbFe_{0.5}Ta_{0.5}O_3$ has been calculated at the high temperatures according to the equation $M^* = 1/\varepsilon^*$. The obtained frequencies dependencies of imaginary part of electric modulus are presented in Fig. 2.

In Fig. 3 the peaks positions of M'' are presented versus the temperature. Using this plot the activation energy has been calculated: $E_A/k_B = 9064$ K.

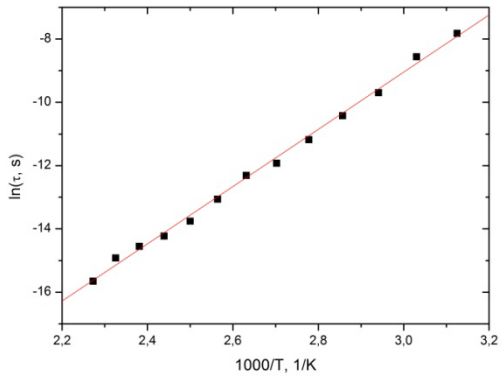

Fig. 3. Temperature dependence of peaks positions of M''

The obtained value of the activation energy show, that conductivity is caused by oxygen vacancies migrating in the $PbFe_{0.5}Ta_{0.5}O_3$ lattice.

PP28

INVESTIGATION OF Fe_xAl_{100-X} PREPARED BY HIGH - ENERGY BALL MILLING

V. Bėčytė[1], K. Mažeika[1], J. Reklaitis[1]

[1] *Institute of Physics, Savanorių 231, 02300, Vilnius, Lithuania*

violeta.becyte@gmail.com

High - energy ball milling is an extensively used technique for preparation of the nanocrystalline solid solutions, amorphous alloys or composites which are in particular interest because of the potential technological application [1, 2]. Restricting our attention on the Fe - Al systems Al - rich region, it has been found that the milling process depends critically on the type of mill and on the milling conditions [3]. Moreover, it has been reported that it is possible to make the nanogranular ferromagnetic Fe-Al systems with Fe concentration as low as 1 % at due to the formation of Fe clusters on the grain boundaries [4].

In this work we present our research done on synthesis of the Fe - Al alloys and their investigation by means of Mössbauer spectroscopy.

Fe and Al powder were mixed in compositions with 98.5 and 99.5 % at Al. Milling was performed using planetary mono mill Pulverisette 6 under nitrogen atmosphere with hardened steel vial and steel balls of 5mm diameter (ball to powder ratio 20:1) for a fixed time of 20 h. Ethanol (0.05 ml/g of powder) was added as a lubricant agent to avoid aluminum sticking to the milling media. Mössbauer spectroscopy studies were used to trace the evolution of phase structure of the system.

1. J.R. Dahn, N.S Dechamps, R.E Mar, S.P. Farrel, Journal of Physics: Condensed Matter **18**, 4907-4920 (2006).
2. J.D. McGraw, M.D Fleischauer, J.R Dahn, R.A Dunlap, Philosophical Magazine **86**, 5017-5030 (2006).
3. F. Cardellini, V. Contini, G. Mazzone and A. Montone, Philosophical Magazine **B 76**, 629-638 (1997).
4. Varkey Sebastian, N. Lakshmi, K. Venugopalan, Journal of Magnetism and. Magnetic Materials **309**, 153-159 (2007).

PP29

RELAXATION DYNAMICS OF OPTICALLY ORIENTED DENDRIMERS

G. Navickaitė[1], G. Seniutinas[1], R. Tomašiūnas[1], R. Petruškevičius[2]

[1] *Institute of Applied Research, Vilnius University, Saulėtekio 10, LT-10223 Vilnius, Lithuania*

gabriele.navickaite@ff.stud.vu.lt

[2] *Institute of Physics, Savanorių 231, LT-02300 Vilnius, Lithuania*

All-optical poling is an important experiment, because it creates noncentrosymmetry in optically isotropic material and as a result nonlinear optical effect is observed. Noncentrosymmetry is created using first (ω) and second (2ω) harmonic's beams of nanosecond Nd:YAG laser. The orientation hole burning is followed by a reversible *trans-cis-trans* isomerization process, which drives optical orientation motion, finally leading to a net permanent molecular polar order [1].

Three different generations of polyester type dendrimers (G0, G1, G2) containing azobenzene in the core were investigated. Dendrimers were inserted into polycarbonate matrix and formed guest-host system.

We were interested in the effect of the reading beam's energy to the relaxation process. The maximum signal of second harmonic generation is reached and then relaxation process is recorded using different ω beam's energy.

We managed to create noncentrosymmetry in G0 and G1 dendrimers and discovered that the higher reading beam's energy the quicker relaxation. G2 dendrimer is much larger so it faces greater resistance while moving in the matrix.

1. G. Seniutinas, L. Laipniece, J. Kreicberga, V. Kampars, J. Gražulevičius, R. Petruškevičius, R. Tomašiūnas, J. Opt. A: Pure Appl. Opt. **11**, 034003(2009).

PP30

TRIPLET EMITTING COMPLEXES WITH CHARGE TRANSPORTING UNITS

L. Skardžiūtė[1], K. Kazlauskas[1], S. Juršėnas[1], D. Tomkutė-Lukšienė[2], T. Malinauskas[2], V. Getautis[2]

[1]*Institute of Applied Research, Vilnius University, Saulėtekio 9-III, LT-10222 Vilnius, Lithuania*

lina.skardziute@ff.stud.vu.lt

[2]*Department of Organic Chemistry, Kaunas University of Technology, Radvilėnų pl. 19, LT-50270 Kaunas, Lithuania*

Iridium-based metal-ligand complexes possessing charge transporting units and featuring high emission efficiency and multi-functionality are promising for phosphorescent organic light emitting diodes (OLEDs). The strong spin–orbit coupling of the transition metal provides a unique possibility for such iridium(III) complexes to overcome the forbidden optical transitions from the triplet states, thus leading to an increase of the internal quantum efficiency of OLEDs up to 100%. Another important feature of transition metal-ligand multifunctional complexes is the charge-transport function, which allows simplification of the OLED fabrication. Since a single layer of the mentioned complexes not only emits light, but also acts as a charge carrier, an additional hole-transport layer in the devices can be omitted. This is extremely helpful in producing OLEDs by cheap spin-casting technique.

A series of multifunctional iridium-phenylbenzothiazole complexes bearing different number (from 0 up to 28) of hole-transporting carbazole groups were synthesized and investigated. In this work triplet emitting complexes were characterized by measuring luminescence spectra, decay lifetimes and quantum yields of their dilute solutions and thin films.

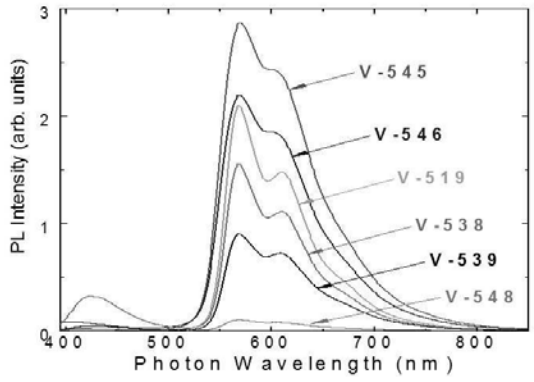

Fig. 1. Phosphorescence spectra of the Multifunctional iridium based metal-ligand complexes

Table 1. Number of Carbazole rings and Quantum yields of the multifuncional complexes in solutions and thin films.

	Number of Carbazole rings	**QY (in a solution)**	**QY (in a thin film)**
V-545	0	65 %	2 – 3 %
V519	8 – lig.	39 %	9 – 10 %
V-538	12 – lig.	32 %	
V-546	16 – acac	50 %	
V-539	8 – lig. 16 – acac	19 %	2 – 2.4 %
V-548	12 – lig. 16 – acac	2 %	

Both the solutions and thin films exhibited similar shape of the luminescence spectra. This proved the origin of the light emission to be molecular-like with concentration quenching due to formation of excimers avoided. However, a noticeable difference between the dependence of the quantum yields on the number of the hole transporting groups in the solutions and films has been observed. Solutions of complexes bearing less carbazole groups exhibited higher quantum yields as the ones with more hole-transport groups. In the thin films, thought, the quantum yields did not depend on the number of the carbazole groups. Most likely, the molecules in the films are packed in such way, that the hole transporting groups separate the emitting centres from each other, and thus, prevent emission quenching. Here, the geometry of the molecule plays more important role than the the number of the hole transport groups does. Complexes with the carbazole groups attached to both the ligand and acethylacetonate (acac) group express 5 times smaller quantum yields as those with the hole-transporting groups attached to only one position in the molecule.

1. M.A. Baldo, D.F. O´Brien, Y. You, A. Shoustikov, S. Sibley, M.E. Thompson, S.R. Forrest, Nature **395**, 151 (1998).

PP31

INVESTIGATION OF LOCALISED CARRIER DYNAMICS IN InGaN-BASED LEDs BY FREQUENCY-RESOLVED ELECTROLUMINESCENCE MEASUREMENTS

V. Jakštas and P. Vitta

Institute of Applied Research, Vilnius University, Sauletekio Ave. 9-III, LT-10222 Vilnius, Lithuania

Vytautas.Jakstas@ff.stud.vu.lt

Recent technological progress in nitride semiconductors opened the way for using them in various applications where short emission wavelength and/or emitter's high-brightness are of vital importance. Relatively high quantum efficiency in the presence of high dislocation density was achieved due to the localization of excited carriers in potential minima and preventing them from reaching nonradiative recombination centres. On the other hand, the physical background of high-indium content InGaN compounds is not fully understood and presents a limiting factor for the use of these materials in longer-wavelength (red to amber) optoelectronics.

Here we report on the technique for the investigation of localized carrier dynamics in the active layer of InGaN light-emitting diodes (LEDs). Electroluminescence decay time measurements were performed for three different InGaN LEDs with the peak wavelength of 460 nm (blue), 505 nm (cyan), and 520 nm (green), respectively. Decay time was measured in the frequency domain by analysing the phase response of harmonically modulated electroluminescence due to localized carriers. The short-wavelength wing of the electroluminescence band, which is due to free-carrier recombination, was used for the phase reference. Modulation of the LED driving current was provided by means of a low-phase-jitter signal generator (IFR 2023A) and the the phase response was measured using a radio-frequency lock-in amplifier (Stanford Research Systems SR 844). A double monochromator (Yobin Yvon H-10) was used for the spectral resolution (less than 0.5 nm) within a high dynamic range. The phase-resolved electroluminescence signal exhibited biexponential emission decay law with one component in the range of tens of nanoseconds and another extremely short component. The longer component can be attributed to recombination of the localized carries, while the short component is due to free-carrier recombination. For further analysis only the localized-carriers emission lifetime (longer one) was considered and the phase shift data as a function of frequency was analyzed by a non-linear least squares fitting method. The emission decay time exhibited a decrease with increasing quantum energy. Such behaviour was found to be in a qualitative agreement with the model of weak localization [1].

1. S. Nakamura, S. F. Chichibu, *Introduction to Nitride Semiconductor Blue Lasers and Light Emitting Diodes* (CRC Press, Boca Raton, Florida, USA, 2000).

PP32

EXCITED STATES AND THEIR RELAXATION IN MULTIFUNCTIONAL COMPOUNDS

S. Puzinas, R. Karpicz, V. Gulbinas

Institute of Physics, Savanorių Ave. 231, LT-02300 Vilnius, Lithuania

Skomantas.Puzinas@ff.stud.vu.lt

Due to their unique physical properties organic multifunctional compounds are attractive for application in optoelectronic devices such as organic light emitting diodes and photovoltaic cells. Solutions and thin films of studied compounds (Scheme 1) were investigated by means of steady-state absorption and fluorescence measurements.

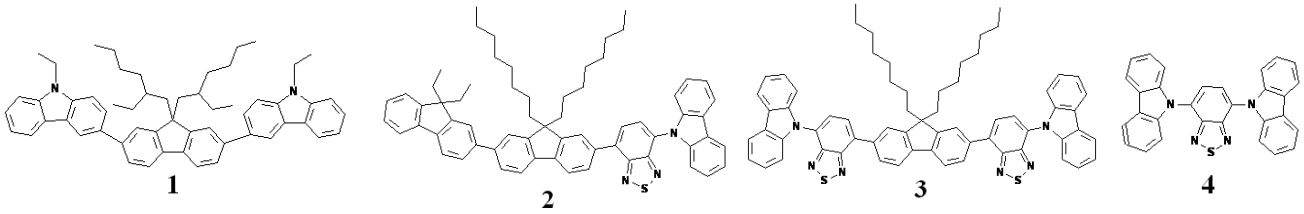

Scheme 1. Structure of compounds **1**, **2**, **3** and **4**.

Optical properties of **2**, **3** and **4** compounds are similar. In UV-VIS absorption spectra of these compounds in THF solution are some typical absorption bands: a strong at 277 nm, which could be attributed to a carbazole (Cz) functional group, and at 430-455 nm - attributed to a low-band-gap [2,1,3]–benzothiadiazole (BT) moiety. Absorption spectra of thin films differ to these in THF solutions: the 277 nm absorption band is several times weaker and about 10 nm red-shifted; the 430-455 nm absorption band differ slightly.

Fluorescence spectra of **2**, **3**, **4** THF solutions have one strong emission band, located at 555 nm. The emission band of **3** and **4** compounds thin films is red-shifted by 10 and 20 nm respectively. It could be related to different environment for molecules in solid films. Optical properties of these compounds are mostly induced by BT chromophore.

However, optical properties of compound **1** are different to **2**, **3**, **4** compounds and can be attributed to fluorene and Cz chromophores.

Results show that these molecules are promising materials for use in heterostructure light emitting devices.

PP33

INVESTIGATION OF INTERACTION OF GOLD AND RADIATION INDUCED DEFECTS IN SI PIN DIODES BY COMBINING CURRENT-CAPACITANCE-VOLTAGE AND CAPACITANCE DEEP LEVEL TRANSIENT TECHNIQUES

Mikhail Bozhenok, T. Čeponis, and E.Gaubas

Institute of Applied Research, Vilnius University

Michail.Bozenok@ff.stud.vu.lt

Introduction of gold impurities and radiation defects become the widely used technological methods to create fast carrier traps in order to modify functional parameters of a semiconductor power device operating in the range of high frequencies. Rather intricate structure of spectrum of deep traps in the band-gap of Si appears under in-diffusion of gold and irradiations by high energy particles. Only several traps show beneficial behaviour as the fast recombination centres, when single either in-diffusion or irradiation procedures are applied. Therefore, in this work, the combined gold doping and irradiation by 2-3 MeV protons beam have been performed on commercial Si power pin diodes. To reveal the structure of deep traps spectrum and their impact of functional characteristics of power devices, the correlated investigation of interaction of gold and radiation induced defects in Si pin diodes has been carried out by combining current-capacitance-voltage and capacitance deep level transient techniques.

Capacitance deep level transient spectroscopy (DLTS) has been applied to evaluate the density of traps, the activation energy and carrier capture cross-section ascribed to specific deep traps in well-known nomenclature associated with gold impurities and vacancy-complexes formed by irradiations. The current-voltage (I-V) and capacitance–voltage (C-V) characteristics have been simultaneously examined after each technological step (gold in-diffusion, irradiation by protons, anneal) to control changes in steady-state characteristics of processed diodes.

Three-four DLTS peaks appeared after doping with gold relatively to a flat background in the initial Si pin diodes. The DLTS spectrum has been considerably transformed after irradiation by protons of the gold doped Si diodes. The VOH complex ascribed peak became dominant in the DLTS spectra. The increase of leakage current and changes in C-V characteristics have been observed synchronously with variation of structure of DLTS spectra after each technological step. Further transforms in DLTS and I-C-V characteristics have been obtained after heat treatments in the temperature range of 80-400 °C due to evolution of gold and radiation induced defects. Peculiarities of formation of the complexes of gold and radiation defects will be discussed. It has been shown in this work, that combined gold in-diffusion and irradiation by protons can be an advanced technology for enhancement of operation frequency of pin diodes keeping appropriate steady-state parameters of power devices.

PP34

THERMAL AND CHROMATICITY CHARACTERIZATION OF HIGH-POWER LEDs UNDER PULSED DRIVING

A.Stonkus, Z. Vaitonis

Institute of Applied Research, Vilnius University,
stonkusandrius@gmail.com

Breakthrough in application of solid-state lighting sources offers considerable power savings. Narrow-band light-emitting diodes (LEDs) are widely used in automotive signage, traffic lighting LCD backlighting, and full-colour video displays. However, Joule heat released in the cladding and active layers of LEDs may noticeably affect the output flux and move the chromaticity out of the ranges determined by signage and display standards. This effect is especially important in the conditions when the average driving current is varied. The output and chromaticity drifts can be minimized by the selection of optimal methods of LED driving. A common method of driving LEDs is application of rectangular pulses with a variable duty cycle and a constant forward current. In this case, LED output is controlled by the duration and frequency of the pulses. Usually, pulse width modulation at a constant repetition frequency (PWM) is used [1]. Another method of controlling LED output is frequency modulation (FM) at a constant width of the pulses.

In this work, thermal and spectral characteristics of LEDs driven in the PWM and FM modes were investigated and compared. High-power, red (AlInGaP), amber (AlInGaP), and blue (InGaN) LEDs were studied. In order to estimate the temperature of the LED chip, a forward-voltage method was applied and the dominant wavelength and chromaticity coordinates of the LEDs were found from electroluminescence spectra. All measurements were performed within a cryostat/oven in order to stabilize the temperature of the LED mounting pad. The analysis of the experimental results revealed a difference in dominant wavelength for PWM and FM driving methods. Different average temperatures were revealed during the current pulse for the two driving methods. Meanwhile, the average temperature during whole period was the same. Significant changes in spectral characteristics and chromaticity coordinates were determined for amber AlInGaP LED. This phenomenon can be explained by the sensitivity of emission properties of high-aluminium-content AlGaInP alloy to temperature.

1. Žukauskas, A. *Puslaidininkiniai šviestukai* (Vilnius: Progretus, 231p. 2008)

PP35

UPDATE OF PHOTOELECTRICAL SPECTROSCOPY EQUIPMENT AND INVESTIGATION OF DEFECT LEVELS IN SILICON

N. Vainorius, V. Kažukauskas, J. V. Vaitkus

Vilnius University, Institute of Applied Research, Saulėtekio al. 9-III, Vilnius 10222

neimantas.vainorius@ff.stud.vu.lt

Ionising radiation detectors are in harsh environment during experiments in Large Hadron Collider (LHC). So they degrade because of it. To develop semiconductor material and create detectors with better properties, such as speed and high radiation hardness, the collaboration program RD50 was started by CERN. Silicon is still the best choice for that purpose. It is believed, that new detectors with better properties, achieved by modification of silicon, will replace the old ones in LHC after 5 years of experiments.

One of the purposes of our work was to upgrade photoelectrical spectroscopy equipment, by tailoring it to photoconductivity spectra (Fig.1) analysis in order to investigate defect levels in silicon. The obtained experimental spectra were modeled numerically by Lucovsky model [1]. The

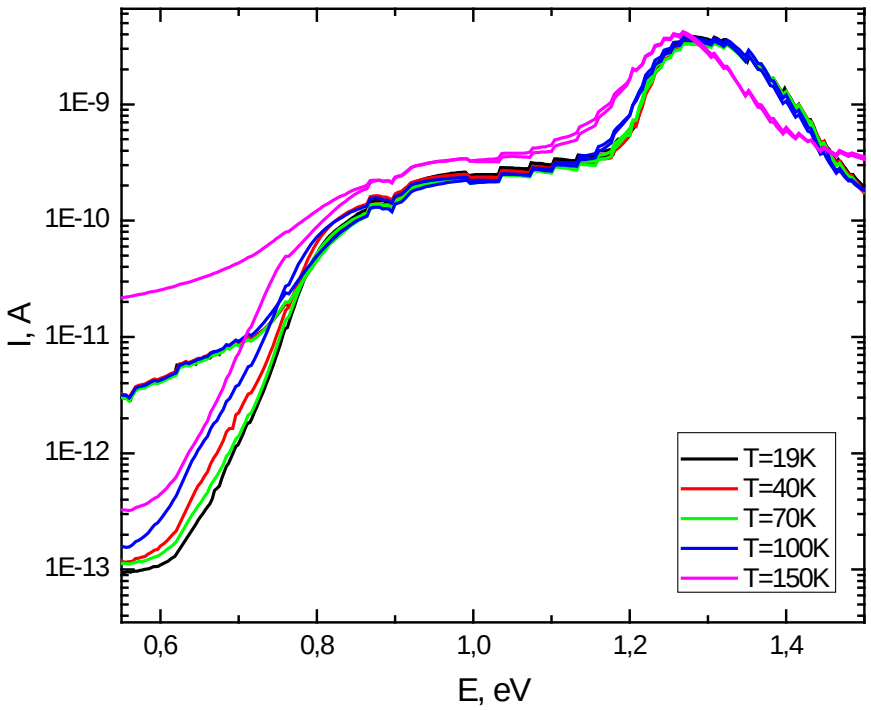

Figure 1. Photoconductivity spectrum of neutron irradiated silicon in different temperatures

following activation energies of neutron irradiated epitaxial silicon were determined: 0,556 eV; 0,612 eV; 0,667 eV; 0,750 eV. After scanning the spectra from high to low energies, persistent

currents were observed that were caused by activation of the level at 0,75 eV. In order to measure shallow levels, thermal stimulated currents method was used. Activation energies of these levels are: 0,14 eV; 0,21 eV; 0,39 eV and 0,45 eV.

1. G. Lucovsky, *Solid State Communications* (299-302, 1965)

PP36

THEORETICAL ELECTRONIC SPECTRA OF CAROTENOIDS' STEREOISOMERS

S. Rekštytė, M. Mačernis

Department of Theoretical Physics, Faculty of Physics, Vilnius University, Saulėtekio al. 9 LT-10222 Vilnius, Lithuania

sima.rekstyte@gmail.com

Carotenoids – organic pigments naturally found in chloroplasts and chromoplasts of plants and other photosynthetic organisms. They are known to be involved in several important aspects of photosynthesis. When investigating pigment-protein complexes from photosynthetic organisms using three-dimensional X-ray crystallography there has been found a number of stereoisomers of carotenoids. It is thought that a natural selection of stereoisomers in protein complexes is due to organisms' need to accomplish specific biological task. However, it is not yet proved. Systematic optical spectroscopic and computational investigations are being carried out to determine the role that different stereoisomers play in physiological functions.

In this work there are presented the results of computational calculations which were carried out for three carotenoids: spirilloxanthin, spheroidene and neurosporene. Also, cis and trans isomers were analyzed. The studied carotenoids are naturally found in photosynthetic bacterium Rhodospirillum rubrum and Rhodobacter sphaeroides. The purpose of this work was to investigate the influence of cis-trans isomerism to carotenoids' electronic spectra. The necessary calculations were carried out using different methods and various computational chemistry software programs on computer cluster in Faculty of Physics at the Vilnius University. Geometry optimization and ground state energy calculations were performed using Gaussian software [1]. Electronic spectra were calculated using three different methods. Spectra of carotenoids were calculated using Time-Dependant Density Functional Theory (TDDFT) with BLYP functional in NWChem [2]. Electronic spectra of spirilloxanthin isomers were also computed using two Configuration Interaction methods - CIS and CISDTQ - with GAMESS software [3]. The acquired results were compared with experimental data [4]. Some differences between them were found. TDDFT calculations produced quite correct excitation energies and properly assessed the forbidden transition to the first excited state. However, they did not show "cis-peaks" that are mentioned in experimental data. Only CIS calculations showed a "cis-peak"; however, both CIS and CISDTQ calculations gave very incorrect energies.

Discrepancy between experimental and theoretical data might have occurred due to the fact that experimental spectra were obtained from samples in solvent. In the performed calculations interaction between stereoisomers and solvent were not included. A future goal is to investigate the contribution of solvents to the electronic spectra of carotenoids' stereoisomers. Necessary calculations are already being carried out.

1. Gaussian 03, Revision D.01, M. J. Frisch et al., Gaussian, Inc., Wallingford CT, 2004.
2. E. J. Bylaska et al., NWChem, A Computational Chemistry Package for Parallel Computers, Version 5.1 (2007) Pacific Northwest National Laboratory, Richland, Washington 99352-0999, USA.
3. M. W. Schmidt et al., J. Comput. Chem. **14**, 1347–1363 (1993).
4. Dariusz M. Niedzwiedzki et al., Ultrafast time resolved absorbtion spectroscopy of geometric isomers of carotenoids, Chemical Physics 357, (2009).

PP37

AUTOMATED DEGRADATION TESTS OF ORGANIC LIGHT EMITTING DIODES

K. A. Krivas, M. Viliūnas, K. Genevičius

Department of Solid State Electronics, Faculty of Physics, Vilnius University

karparas.krivas@gmail.com

In our days, demand for energy saving technologies is constantly growing. Around 20% of world's total electrical power is used for lighting purposes. The growth of new semiconductor lighting technologies enables increase of the effectiveness twice and save up to 10% of total electrical power. There are two competing solid state lighting technologies: based on inorganic semiconductors and organic materials (organic light emitting diodes - OLED). In comparison with "classical" LEDs, OLEDs have several advantages: OLED technology can be used for the large area device, flexible devices, materials and technology for making OLED's are potentially cheaper and devices could be easily recycled. One of the main problems in OLEDs structures is degradation of performance due to the oxidation, which is present in all organic materials. Therefore, time consuming degradation experiments gives essential information on the properties of OLEDs. The aim of this work was development of the two channels device for the automated degradation tests.

Two channels of the device allow direct comparison of the two different structures at the same conditions (moisture, temperature, radiation). Device can operate in three different regimes: constant voltage, constant current and constant light intensity. For the easier sample comparison, both channels of the device are working in the same measurement regime, with the same static parameter. Compact and stand alone device could be used in the glovebox system directly after the end of OLED fabrication. Experimental data is stored in the internal memory of the device, which can be read through the USB interface. The main parameters of the device: maximal voltage – 20 V, maximal current – 50 mA, resolution 12 bits, more than 100000 data points.

PP38

DIELECTRIC PROPERTIES OF $CoFe_2O_4$-$BaTiO_3$ CERAMICS

A.Kuprevičiūtė[1], J.Banys[1], R.Grigalaitis[1]

[1] *Vilnius University, Physics faculty, Saulėtekio av. 9, III b., LT-10222 Vilnius, Lithuania*

a.kupreviciute@ff.stud.vu.lt

Combining cobalt ferrite ($CoFe_2O_4$) which has cubic spinel structure with perovskite-type stuctrure $BaTiO_3$ leads to multiferroic behaviour of the material. $CoFe_2O_4$-$BaTiO_3$ is a multiferroic material, which means that it exhibits more than one order parameter in a single phase. In this case we have magnetic and ferroectric order parameter coupling. This type of materials are uncommon, even though the interconversion mechanisms of energies stored in magnetic and electric fields plays an important role in many devices such as transducers, storage devices, etc. The investigated sample was synthesized during the sol-gel process. Already performed experiments showed that dielectric properties strongly depend on the fabrication mechanisms of sample as in one sample irreversible structure changes after heating was observed and in the other not.

Measurements of dielectric properties of $CoFe_2O_4$-$BaTiO_3$ ceramics were made in the frequency ranging from 20 Hz to 150 MHz and temperature ranging from 120 K to 450 K. The temperature dependence of the real part of complex permittivity $\varepsilon^*=\varepsilon'-i\varepsilon''$ showed that there is only one phase transition at a Curie temperature around 300 K.

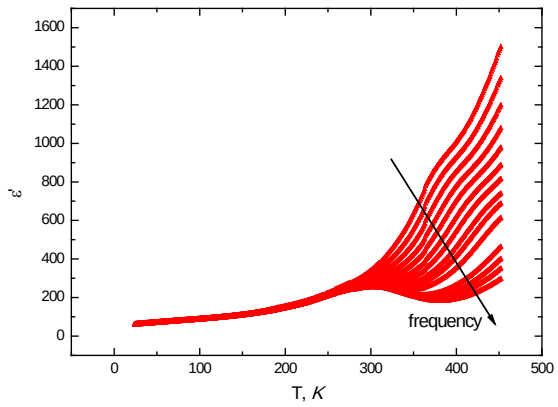

Fig. 1. The dependence of real part of complex dielectric permittivity on temperature. The arrow shows the direction of increasing frequency from 20 Hz to 1 MHz.

Fig.1. shows that at high temperatures the growth of dielectric permittivity is caused by electric conductivity. Accordingly, the complex electric modulus, which is inversely proportional to

complex dielectric permittivity $M^*=1/\varepsilon^*$, of $CoFe_2O_4$-$BaTiO_3$ was calculated. The resulting dependencies on frequency are shown in fig. 2.

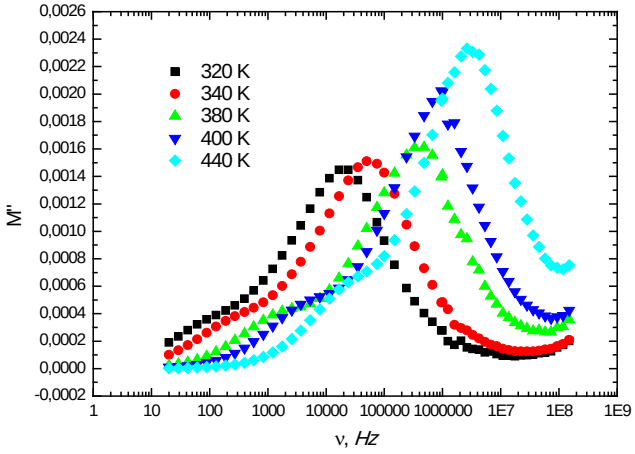

Fig. 2. The dependence of imaginary part of electric modulus on frequency in different temperatures.

In fig. 3 the change of peak positions of imaginary part of complex electric modulus depending on the inverse temperature are shown. Linear regression coefficient of these points corresponds to activation energy E_a, which in this case is $\frac{E_a}{k_b} = 5578$ K.

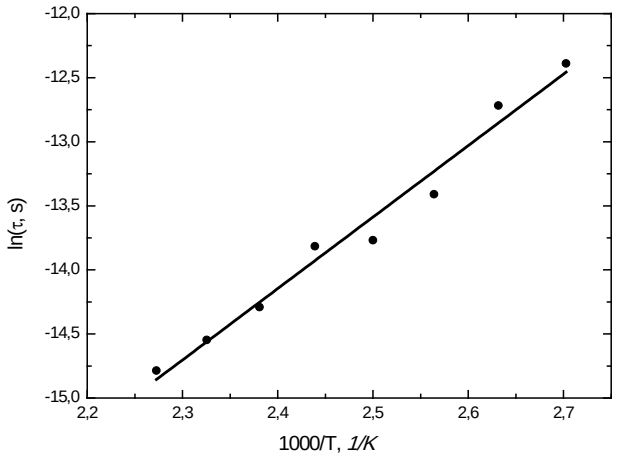

Fig. 3. The peak points of M'' dependence on inverse temperature and its' linear fit.

PP39

TYROSINE-TRYPTOPHAN COMPLEX: ELECTRON TRANSFER MODELING BY MEANS OF QUANTUM CHEMISTRY RULES

N. Galikova, M. Kelminskas, A. Stonkus, A. Gruodis

Faculty of Physics, Vilnius University, Sauletekio 9, korp.3, Vilnius, Lithuania

Nurija.Galikova@ff.stud.vu.lt

Tyrosine (Fig. 1a) and tryptophan (Fig. 1b) molecules are natural π-conjugated luminophores. Tyrosine (Tyr) and tryptophan (Trp) molecular pair [1] belongs to class of 20 standard amino acids, which are essential for biological organisms. Electron transfer (ET) processes between proteins and several cofactors are mostly caused by resonance interaction in the [Tyr..Trp] complex. This ET phenomenon is useful for model verifying purposes when donor-acceptor interactions are expressed in empirical, semi-empirical or *ab-initio* framework.

This work is devoted for modelling of ET processes using advanced quantum chemistry tool *GAUSSIAN03* [2] and *NUVOLA* [3], due to well-known Fermi golden rule [4] and Marcus theory. Total transition rate *W* evaluation is expressed by following equation:

$$W = \frac{2\pi}{\hbar}\sum_{\alpha,\beta}\left|\left\langle \alpha\left|\hat{V}_{\alpha\beta}\right|\beta\right\rangle\right|^2 (FCWD), \qquad (1)$$

where *FCWD* denotes the Franck-Condon-weighted density of one-article electronic states.

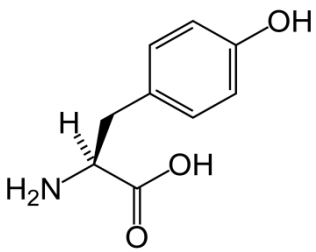

Fig. 1a. Structure of tyrosine (2-Amino-3-(4-hydroxyphenyl)propanoic acid) molecule

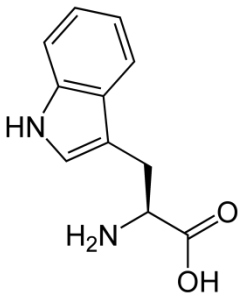

Fig. 1b. Structure of tryptophan (2-Amino-3-(1*H*-indol-3-yl)propanoic acid) molecule

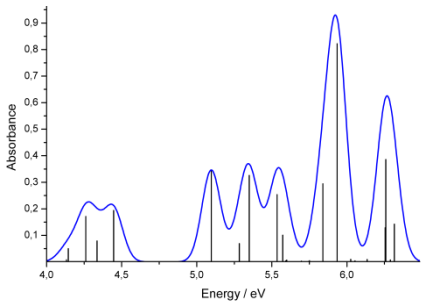

Fig. 2. Simulated Tyr absorbance spectrum using ZINDO method

Simulations of optical absorption spectra were done solving simplified form of Schrödinger equation for ZINDO method:

$$\Psi = \Psi_0 + \sum_{ia} T_{ia}\Psi(i \to a) + \sum_{ijab} T_{ijab}\Psi(ij \to ab) \qquad (2)$$

Calculations are performed for donor system, Tyr, using several highest occupied molecular orbitals (up to ten) and same number of lowest virtual states. Fig. 2 represents simulated Tyr absorbance spectrum using ZINDO method.

Fig. 3 represents the two-dimensional distribution of intermolecular ET rate on atom position number of two interacting molecules. Essential ET rate occurs between 14 atom (belonging to donor, Tyr) and (19, 24) atom (belonging to acceptor, Trp).

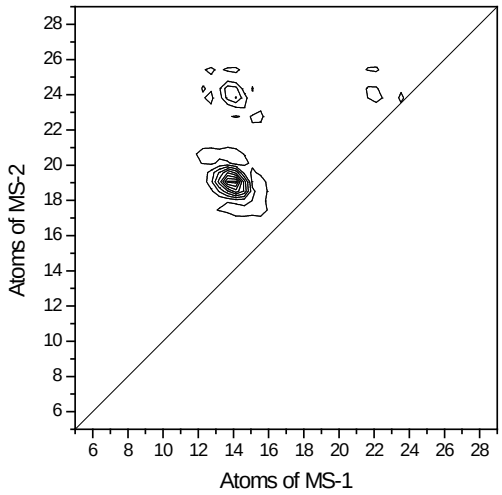

Fig. 3a. Intermolecular ET rate 3D distribution on atom position number of two interacting molecules. The first one is charge donor and the second is charge acceptor.

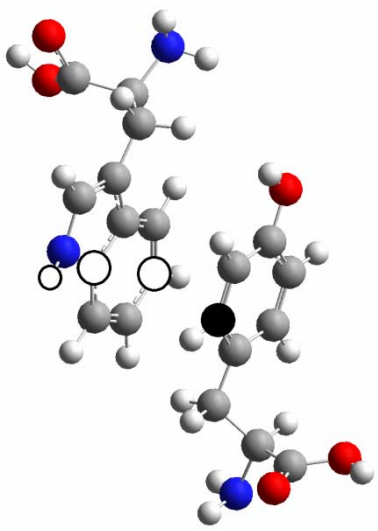

Fig. 3b. Black atom shows charge donor an white, correspondingly, charge acceptor in pending molecules.

1. Chyuan-Yin Lee, FEBS letters **299/2** – 119-123 (1992).
2. Gaussian 03, Revision D.01, M. J. Frisch, G. W. Trucks, et al, and J. A. Pople, Gaussian, Inc., Wallingford CT, (2004).
3. N. Galikova, A. Gruodis, Innovative infotechnologies for science, business and education (IITSBE), 2, 12.1. (2008).
4. R.A. Marcus and N.Sutin, // Biochim.Biophys.Acta **811**, 265 (1992).

PP40

INTERMOLECULAR ELECTRON TRANFER PROCESSES IN DIMETHYLAMINO-STILBAZOL DIMER USING QUANTUM CHEMISTRY APPROACH

M. Kelminskas, N. Galikova, A. Gruodis, J. Šulskus

Faculty of Physics, Vilnius University, Sauletekio 9, korp.3, Vilnius, Lithuania

Mantas.Kelminskas@ff.stud.vu.lt

Stilbazol derivatives belong to the liquid crystal class of *p*-substituted pyridines which exhibit excellent charge donor properties. Due to high sensitivity to the surrounding environment, dimethylamino-stilbazol (DMA-S) monomers and aggregates (for example, dimers, see Fig. 1) exhibit two forms: protonated form and unprotonated (acid) form, which could coexist in dynamic equilibrium (see Fig. 2) This molecular system distinguishes for several unique properties and self-organization - particular capability of molecules to deploy in respect of other chemical compounds in space (for example, adsorbtion on metal surface).

Simulations of electron transfer (ET) processes were made for model object – DMA-S dimer when chlorine anion is localized in surrounding of dimethylamino group. Modeling of adsorption processes through the energetically allowed ET process was made using advanced quantum chemistry tool *GAUSSIAN03* [1] and *NUVOLA* [2]. Ratio of ET was calculated by means of Fermi golden rule equation, overlap of electronic function was estimated only, see Fig. 2.

$$W_{12} = \frac{2\pi}{\hbar}\left\langle \Psi_1 \left| \hat{H}_{12} \right| \Psi_2 \right\rangle^2 \rho(E_1 - E_2) \tag{1}$$

Modeling allows us to conclude that asymmetric (not resonance) intermolecular ET transfer in dimer takes place between pyridine fragment and parabenzene fragment. Two types of dominated ET were estimated: i) along the long axes of dimer, ii) perpendicular to the long axes.

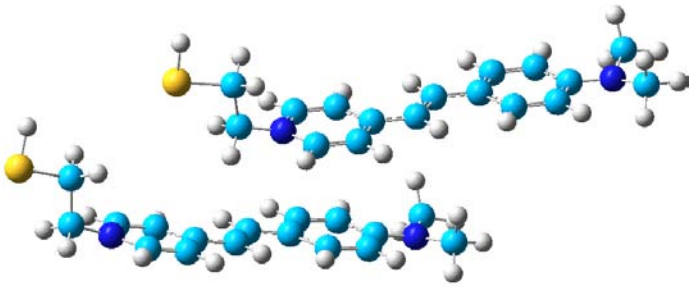

Fig. 1. Dimethylamino-stilbazol (DMA-S)

Presence of CT (0,5-1 electrons) in dimer confirms the possibility of existing acid form of DMA-S in unprotonated solution. This assumption was formulated from IR and UV spectrometric results.

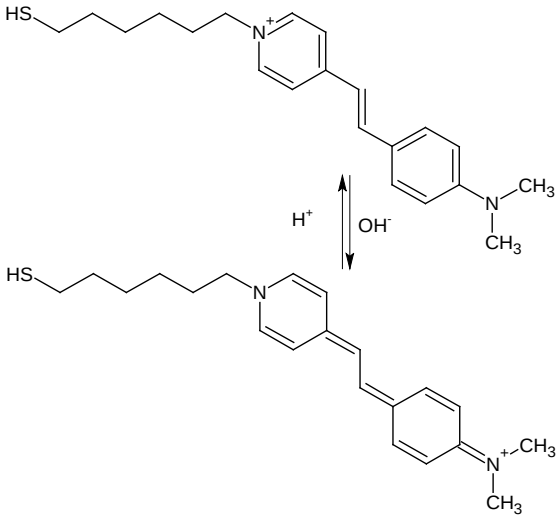

Fig. 2. Stilbazol cation in two cviterionic form: benzenoid and quinoid forms.

1. Gaussian 03, Revision D.01, M. J. Frisch, G. W. Trucks, et al, and J. A. Pople, Gaussian, Inc., Wallingford CT, (2004)
2. N. Galikova, A. Gruodis, Innovative infotechnologies for science, business and education (IITSBE), **2**, 12.1 (2008).

PP41

QUANTUM EFFICIENCY INVESTIGATION OF YAG:CE AND $Y_3MG_2ALSI_2O_{12}$:CE PHOSPHORS

J. Jurkevičius[1]

[1]*Faculty of Physics, Vilnius University, Sauletekio ave. 9, building III, room 718*
LT-10222 Vilnius, Lithuania
getjonas@gmail.com

Yttrium aluminum garnet doped with trivalent cerium (YAG:Ce) is widely used as an efficient phosphor material for InGaN based white LEDs. However, in order to obtain efficient white LEDs which exhibit lower color temperature, other phosphor materials are investigated.

Here are presented results of a study on luminescence quantum efficiency (LQE) of $Y_3Mg_2AlSi_2O_{12}$:Ce. LQE of sol-gel derived $Y_3Mg_2AlSi_2O_{12}$:Ce phosphor was studied in samples with varying cerium concentration (from 0.015 mol% to 0.06 mol%) and annealing temperature (from 1400 °C to 1550 °C). LQE of traditional sol-gel derived YAG:Ce phosphor was studied for comparison.

In order to minimize the influence of light reabsorption, transparent containers for phosphor powders were designed and produced. 440 nm wavelength blue LED was used as the excitation source.

Strong concentration quenching effect for LQE was observed in $Y_3Mg_2AlSi_2O_{12}$:Ce. However, only weak and non-monotonous dependency of LQE on annealing temperature was observed. Highest LQE value for $Y_3Mg_2AlSi_2O_{12}$:Ce (70 %) was observed in sample with lowest cerium content (0.015 mol%) and lowest annealing temperature (1400 °C). This value exceeded the highest value of sol-gel YAG:Ce LQE (46 %) measured during investigation and is comparable to quantum efficiency values for presently commercially available phosphors for white LEDs.

PP42

VACUUM DEPOSITION OF ORGANIC MATERIAL LAYERS AND INVESTIGATION OF PHOTOELECTRIC FEATURES

Bronė Lenkevičiūtė

Department of Solid State Electronics, Vilnius University

Brone.Lenkeviciute@ff.stud.vu.lt

The single layers of organic electron transport material OXD-7 and organic emitter V-417 were vacuum deposited at room temperature onto by ITO covered glass substrates and spectra of absorbance were measured. Using CELIV method the charge carrier mobility dependencies on electric field were measured [1]. The mobility of electrons in OXD-7 layer was of the order of 10^{-5} $cm^2/V \cdot s$, while the mobility of holes of V-417 layer was approximately $5 \cdot 10^{-7} cm^2/V \cdot s$. Using photo-CELIV method the relaxation of charge carrier density was measured, from which the lifetime of charge carriers of both electrons in OXD-7 and holes in V-417 were evaluated [2].

The spectrum of electroluminescence of V-417 single layer demonstrated maximum at 550 nm.

1. G.Juška, K.Arlauskas, M.Viliūnas, K.Genevičius, R.Osterbacka, H.Stubb., Physical Review B **62,** 16235-16238 (2000).
2. G.Juška, K.Genevičius, K.Arlauskas, R.Osterbacka, H.Stubb., Macromolecular Symposia **212**, 209-217 (2004).

PP43

VACUUM DEPOSITION AND PHOTOELECTRIC FEATURES OF CuPc AND C_{60} LAYERS

Armantas Melianas

Department of Solid State Electronics, Vilnius University

Armantas.Melianas@ff.stud.vu.lt

The single layers of CuPc and C_{60} and double layer CuPc/C_{60} structures were vacuum deposited at room temperature onto by ITO covered glass substrates. The spectra of absorbance of single layers were compared with one of CuPc/C_{60} structure, and no special features were obtained. The I-V characteristics of so formed layers and structures were measured and compared with results of Ref. [1]. Using photo-CELIV method [2], from the charge carrier mobility dependencies on electric field and charge carrier density relaxation the mobility-lifetime product was estimated and compared with one evaluated from I-V characteristic.

1. B. Yu, L. Huang, H. Wang and D. Yan., Advanced Materials **22,** 1017-1020 (2010).
2. G.Juška, K.Genevičius, K.Arlauskas, R.Osterbacka, H.Stubb., Macromolecular Symposia **212**, 209-217 (2004).

PP44

THIRD ORDER PROPERTIES OF INDAN-1,3-DIONE MOLECULES

G. G. Seniutinas[1], R. Czaplicki[2], R. Tomašiūnas[1], V. Getautis[3]

[1] *Institute of Applied Research, Vilnius University, Saulėtekio 10, LT-10223 Vilnius, Lithuania*

gediminas.seniutinas@ff.stud.vu.lt

[2] *Laboratory Poma, University of Angers, FRE CNRS 2988, 2 boulevard Lavoisier, F-49045 Angers Cedex 1, France*

[3] *Kaunas University of Technology, Radvilėnų pl. 19, LT-50270 Kaunas, Lithuania*

We report on non-linear optical features of indan-1,3-dione class molecules. These basically flat in an unexcited state molecules have large dipole moment [1]. Magnitude of the dipole moment and it's change under excitation significantly depends on substituents attached. Having more rotational degree of freedom these molecules manifest torsion motion. Twisting around single or double bound responsible for relaxation dynamics and fluorescence properties has been recently investigated by Karpicz [2]. All the features make indan-1,3-dione molecules as high dielectric susceptibility material attractive for application in non-linear optics. In this work we extend the nonlinear optical knowledge about this new material by investigating third order optical nonlinearity. Third harmonic generation (THG) is one of the powerful and almost background free nonlinear optical methods, what allows us to evaluate the third order nonlinear susceptibility. THG was measured for the materials prepared as a guest-host system in polycarbonate matrix spin-coated on silica substrate. Maker fringe technique used enabled to separate the third order non-linear optical property of the material from silica, what was confirmed analytically. $\chi^{(3)}$ values obtained for different stage of synthesis, i.e. monomer, dimmer, let us draw relation between structure and optical nonlinearity. Despite the differences in architecture and phase, all the molecules showed respective non-linear optical susceptibility and the values of $\chi^{(3)}$ deviate from $2{,}25\times10^{-21}$ for monomeric material to $7{,}3\times10^{-21}$ m^2/V^2 for dimmer material, what gave a direct indication about the influence of complexity of the material to optical non-linearity.

1. M. A. Rutkis, A. Vembris, V. Zauls et al., Proc. SPIE 6192-6192Q (2006).
2. R. Karpicz, V. Getautis, K. Kazlauskas, S. Juršėnas, V. Gulbinas, Chem. Phys. **351**, 147-53 (2008).
3. B. Sahraoui, J. Luc, A. Meghea, R. Czaplicki et al., J. Opt. A: Pure Appl. Opt. **11**, 024005(1-26) (2009).
4. F. Kajzar, J. Messier, C. J. Rosilio, Appl. Phys. **60**, 3040-3044 (1986).

PP45

PHOTOELECTRICAL PROPERTIES OF DOUBLE – LAYERS FILMS OF DMABI DERIVATIVES

M. Indrikova[a], J. Latvels[a], K. Pudžs[a], P. Pastors[b], V. Kampars[b]

[a]*Institute of Solid State Physics, University of Latvia*

[b]*Riga Technical University*

Solar cells based on organic materials presently is innovative and at the same time perspective field. To achieve higher efficiency of solar cell, it is important that molecule absorbs light in spectral region close to sun spectrum. Therefore photoelectrical investigations are necessary. To increase a possibility to absorb wider solar spectrum, it is necessary to search new organic molecules with absorption spectrum similar to sun spectrum.

One of such molecules is dimetilaminobenziliden-1,3-indandion (DMABI).

DMABI is organic isolator with wide band gap (~1.9eV) and high photogeneration quantum efficiency. In collaboration with chemists different derivatives of DMABI were studied, trying to find compounds with better photogeneration properties.

In our work we used “sandwich type” samples which were made by vacuum evaporation method.

For electrical measurements a space charge limited current method was used. It describes interdependence of current, voltage and the thickness of sample.

PP46

TWO-DIMENSIONAL OPTICAL SPECTROSCOPY OF LINEAR J-AGGREGATES OF PSEUDOISOCYANINE

A. Gelžinis[1], V. Butkus[1], L. Valkūnas[1,2]

[1] *Department of Theoretical Physics, Faculty of Physics, Vilnius University, Sauletekio ave. 9-III, LT-10222 Vilnius, Lithuania*

[2] *Institute of Physics, Savanoriu ave. 231, LT-02300 Vilnius, Lithuania*

andrius.gelzinis@ff.stud.vu.lt

Two-dimensional (2D) optical spectroscopy is an analogue to multi-dimensional techniques of nuclear magnetic resonance (NMR) as the photon-echo (PE) signal is obtained in a four-wave mixing experiment using ultra-short laser pulses in visible or IR regions. Photon echo signal is then spectrally resolved and plotted against two frequency axis corresponding to two delay times between the laser pulses. 2D PE spectroscopy have been used to probe dynamical phenomena in various multichromophoric complexes. It was the key tool of Engel et al. in proving a wave-like energy transfer within a photosynthetic light-harvesting Fenna – Matthews – Olson (FMO) complex [1].

Theoretical simulations of 2D spectra are computationally expensive and do not scale linearly with a size of the system that is being modeled. The systems that are being investigated most are relatively small. The FMO complex, for example, consists of only 7 chromophores [2]. Here we present simulations of 2D spectra of a much bigger system - J-aggregates consisting of 64 chromophores. Parallel computing on a multi-processor computer cluster had to be implemented.

Molecular aggregates (J-aggregates) are macroscopic clusters of molecules with intermolecular spacing intermediate between crystal lattice and isolated molecules. The scientific interest on J-aggregates is due to the fact that they possess a very narrow absorption band, named the J-band that is red shifted relatively to a monomer band. It is possible that some form of J-aggregates could be used in constructing artificial light harvesting complexes [3].

In this work simulations of 2D spectra of linear J-aggregates of pseudoisocyanine (PIC), 1,1'-diethyl-2,2'-cyanide at 77 K are presented. Many ideas about aggregate structure have been put forward. Here, the spatial configuration model of PIC molecules proposed by Fidder [4] is utilized.

On the left side of Fig. 1 a simulation of 2D spectra at population time T = 0 fs of one elementary cell of J-aggregates (4 chromophores in Fidder‘s model) is presented. As it is expected, the diagonal of 2D spectra mirrors linear absorption spectra. The J-band can be clearly seen at the

lower left corner of the spectra at the diagonal. Other features at the diagonal represent to the third and fourth exciton state respectively. As it is expected, they have much smaller amplitudes than the J-band. If the transition dipoles were all parallel, only the J-band would be visible at the diagonal. Cross-peaks that are present at the spectra are due to non zero coupling between the monomers. It should be noted, that ability to see cross-peaks is one of the biggest advantages of 2D spectroscopy compared to linear spectroscopy. The negative peaks are caused by excited state absorption while positive peaks are caused by ground state bleaching and excited state emission.

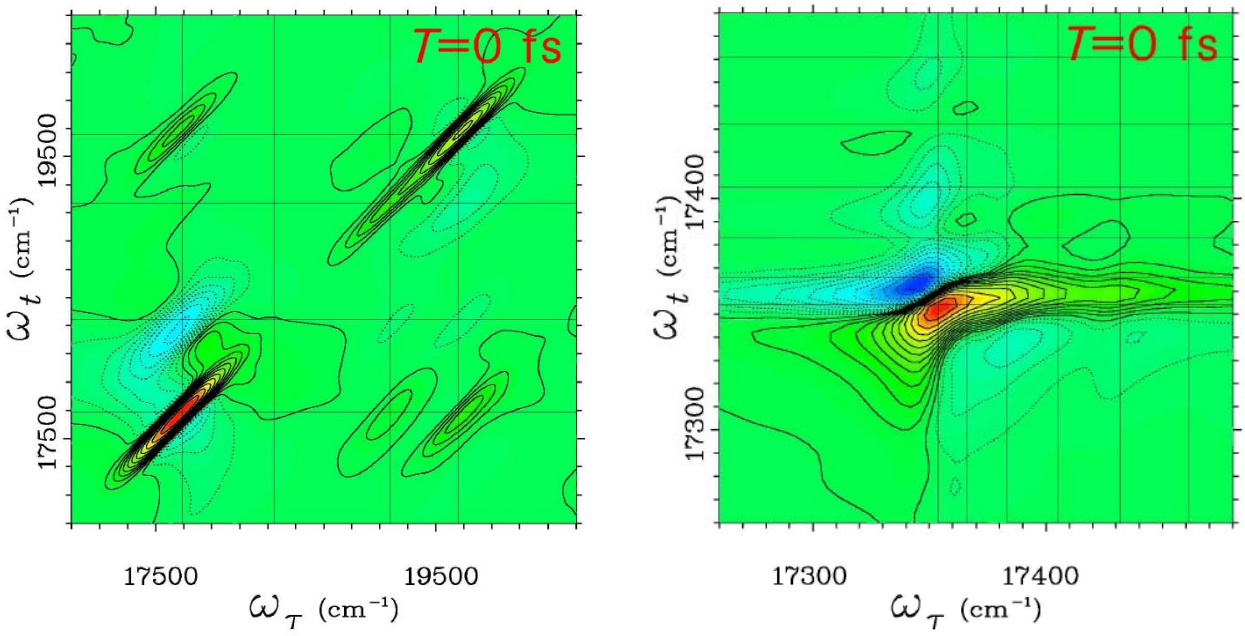

Figure 1**.** Numerically simulated 2D spectra of a single unit cell of 4 molecules of J-aggregate (on the left) and the J-band of a J-aggregate of 64 molecules (on the right) at population time T = 0 fs.

A 2D spectra at population time T = 0 fs of J-aggregates consisting of 64 chromophores is shown at th right side of Fig. 1. Because the J-band is getting narrower with increasing aggregate size, only the J-band region of the spectra is presented. The complexity of this spectra can be explained by the fact that visible elements are a superposition of several elements. Still, the positive J-band peak is dominant. The strongest negative peak is much lower here and it changes the form of the J-band peak. Three other negative peaks are visible above the J-band. As population relaxation does not play any role when T = 0 fs, these peaks are solely due to excited state absorption.

1. G. S. Engel. Nature **446,** 782 (2007).
2. M. Cho, H. M. Vaswani, T. Brixner, J. Stenger, G. R. Fleming. Exciton, J. Phys. Chem. B **21**, 109, 10542–10556 (2005).
3. F. Milota et al. Chem. Phys. **357**, 45-53 (2009)
4. H. Fidder. Chem. Phys. **341**, 158-168 (2007).

PP47

DOUBLY RESONANT OPTICAL PARAMETRIC OSCILLATOR WITH COMPENSATION OF SIGNAL AND IDLER WAVE'S CAVITY LENGTH

Mindaugas Gecevičius, dr. Vygandas Jarutis, prof. habil. dr. Valerijus Smilgevičius

Vilnius University, Quantum Electronics Department, Saulėtekio al. 9, LT-10222 Vilnius

mindaugas.gecevicius@ff.stud.vu.lt

Optical parametric generation in nonlinear crystals now is mostly useful as a widely tunable

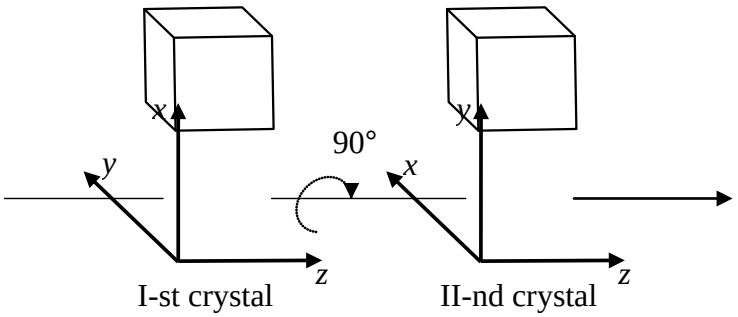

Fig. 1. KTP crystals in OPO cavity configuration

source in UV, VIS and IR spectrum regions. Optical parametric oscillators (OPO) are extremely used in spectroscopy and analytical applications. There are two types of OPO`s: singly and doubly resonant. Doubly resonant OPO`s has lower generation threshold in comparison with singly resonant OPO`s, but radiation has cluster structure caused by different longitudinal mode spacing for signal and idler waves. In [1] it was shown possibility to realize clusterless radiation of doubly resonant OPO using different cavities for signal and idler waves (for type-II phase-matching case). Unfortunately the stability of radiation in such OPO`s configuration are unstable in order different cavities mode beating.

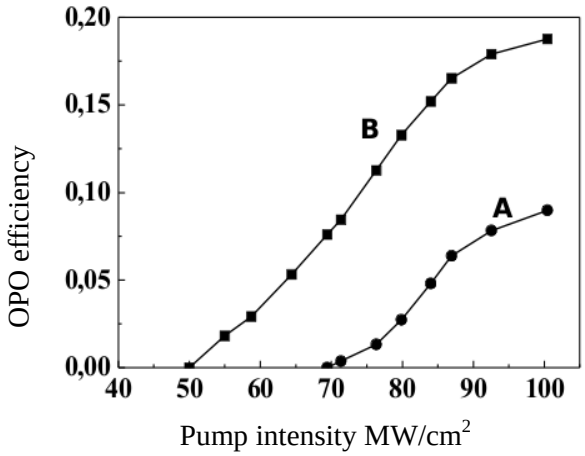

Fig. 2. OPO efficiency versus pump intensity for one crystal OPO – A, and for two crystals OPO – B

In this report we present results of new configuration design OPO investigation (type-II interaction). In this case into traditional KTP OPO cavity the same length second KTP (10 mm) crystal was inserted. This crystal orientation was orthogonal to first one as shown in fig.1. In this case in the first KTP crystal generated signal (o-polarized) and idler (e-polarized) in second KTP crystal propagates as e-polarized – signal, and o-polarized idler waves. And as a result the cavity

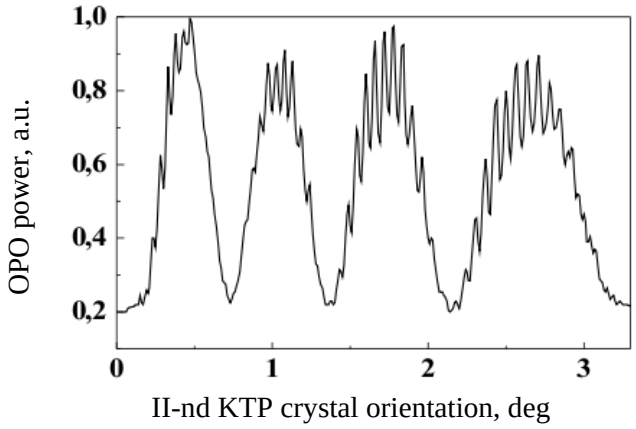

Fig. 3. OPO average power dependence versus *II*-nd KTP crystal orientation

lengths for signal and idler waves are compensated.

For the KTP OPO pump the laser system consists of microchip laser and Yb doubted fiber amplifier were used. Pulse duration was 1.2 ns, maximum energy – 100 μJ, repetition rate – 2 kHz. It well known that efficiency and generation threshold of OPO strongly depends on the cavity length. In our case only few passes of pump radiation in OPO cavity was realised. Fig. 2 shows OPO efficiency versus pump intensity for one KTP crystal OPO – A, and B – two KTP crystal OPO. In both cases the OPO cavity optical lengths were the same. Traditional OPO generation threshold was ~70 MW/cm^2 (efficiency – ~9 %); two crystals OPO threshold was approximately two times lower (efficiency – 18 %).

The OPO output intensity strongly depends on the *II*-nd KTP crystal orientation. It is necessary select direction of signal and idler waves propagation how are shown in fig. 3.

Presented results shows that proposed OPO`s configuration allows to decrease generation threshold and increase efficiency of doubly resonant OPO.

1. A.Marcinkevičius, A.Piskarskas, and V.Smilgevičius, Lithuanian J. of Physics **36**, 315 (1996).

PP48

Yb DOPED FIBER AMPLIFIER FOR OPO PUMP

Mindaugas Gecevičius, Valerijus Smilgevičius

Vilnius University, Quantum Electronics Department, Saulėtekio al. 9, LT-10222 Vilnius

mindaugas.gecevicius@ff.stud.vu.lt

In the last years pulsed fiber lasers and amplifiers attract great attention for applications required high repetition rate and average power. At 2006 4.5 MW peak-power Yb-doped fiber amplifier emitting near diffraction-limited output beam have been reported [1]. These results were enabled by double clad large-core amplifier fibers and 100 mm core rode-like Yb-doped photonic crystal fiber.

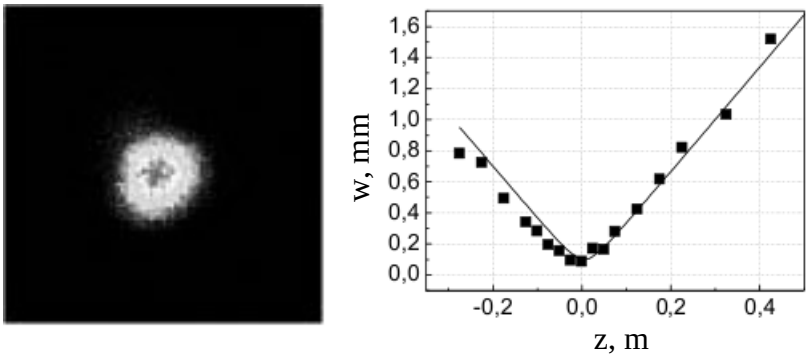

Fig.1. Intensity distribution of amplified radiation (a), and beam radius w versus distance z (b), solid curve - calculated.

In this report we present experimental results of the investigation of one-stage Yb-doped double-clad large-core fiber amplifier using as a seed the radiation of microchip Nd:LSB (duration 0.6 ns) and Nd:YAG (duration 1.2 ns) (both UAB „Standa“ product). From the other hand laser system based on the seed laser and the fiber amplifier could be perspective source for the nonlinear frequency converters pump, and find more important applications. The amplified seed laser radiation was used for pump KTP optical parametric oscillator (OPO).

In fiber amplifier 3 meter long, 30 mm core diameter double-clad Yb-doped NUFERN production fiber were used. Fiber amplifier was pumped by 8.8 W power diode-laser radiation (975 nm). For higher transversal mode discrimination the fiber was rolled-up into 8.5 cm diameter bobbin. Fig. 1. shows intensity distribution of amplified radiation (a), and M^2 measurements results (b). Amplified radiation was close to diffraction limited: M^2_x=1.05; M^2_y=1.1.

Fig.2. shows amplified signal energy versus fiber amplifier pump power for different seed

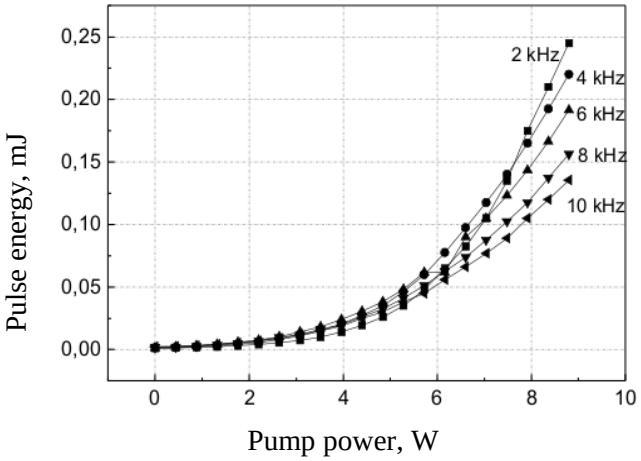

Fig. 2. Amplified signal energy versus fiber amplifier pump power for different seed pulses repetition rate

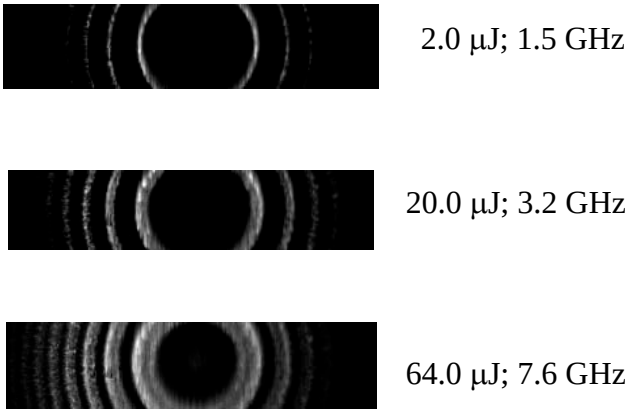

Fig. 3. Spectra of the fiber amplifier output

pulses repetition rate. As seen from the figure maximum energy (~250 μJ) was achieved when the repetition rate was 2-4 kHz (for 1.2 ns pulses). For the maximum amplified pulse energy intensity was ~0.4 MW, the spectrum of the radiation was increased from 1 to 3.5 GHz by nonlinear processes as phase-modulation and SRS. The spectrum width of 0.6 ns duration pulses increased to 7 GHz. In both cases stimulated Brillouin scattering were not observed. Fig. 2. presents fiber amplifier output radiation spectra measured by Fabri-Perot interferometer for different signal energy.

Good amplified beam quality allows with 60% efficiency generate second harmonics (8 mm KTP crystal; $\theta = 90^o$, $\varphi = 24^o$). This radiation for doubly resonant KTP OPO pump was used. Tuning range of OPO was 1.02-1.08 μm and was limited by KTP crystal aperture. OPO efficiency reached 55%.

Experimental results shows that investigated microlaser – fiber amplifier system could be perspective source for nonlinear frequency converters pump.

1. Brooks C.D., Di Teodoro F., Appl. Phys. Lett., v.**89**, 111119 (2006).

PP49

FEMTOSECOND PULSES INDUCED SELF-POLYMERIZATION AT NANO-SCALE

G. Bičkauskaitė, M. Malinauskas

Vilnius University, Physics Faculty, Department of Quantum Electronics,
Laser Research Center, Saulėtekio ave. 10, LT-10223 Vilnius, Lithuania
mangirdas.malinauskas@ff.vu.lt

When exposing a photopolymer by a tightly focused laser beam two-photon absorption is induced and ultra-localized polymerization reaction is initiated. By pin-point scanning the trace of virtually designed object features of desirable architecture can be materialized. After rinsing in a solvent only the exposed part of material is left and in this way 3D microobjects are produced [1, 2]. Recently, self-polymerization of fiber-like features has been reported [3]. Such nano-features form in-between rigid polymeric supports when the distance between them is smaller than critical (D_{cr} < 1 μm) [4, 5]. In this paper, results of self-polymerization of nano-fibers (diameter < 100 nm) and nano-membranes (thickness ~ 100 nm) in acrylate based photopolymers AKRE37, PEG-DA and SCR500 are presented. By femtosecond laser (80 fs, 800 nm, 80 MHz) beam radicals are generated in-between the fabricated "X" walls when writing parallel lines at light intensity close to polymerization threshold. The conditions (average laser power P and period of laser written lines L) required for self-polymerized features (nano-fibers and nano-membranes) to form in a certain photopolymer are experimentally obtained. A model describing self-polymerization conditions including the influence of laser beam intensity I, radical concentration C, feature rigidity F and critical distance D_{cr} between the supports is proposed [6].

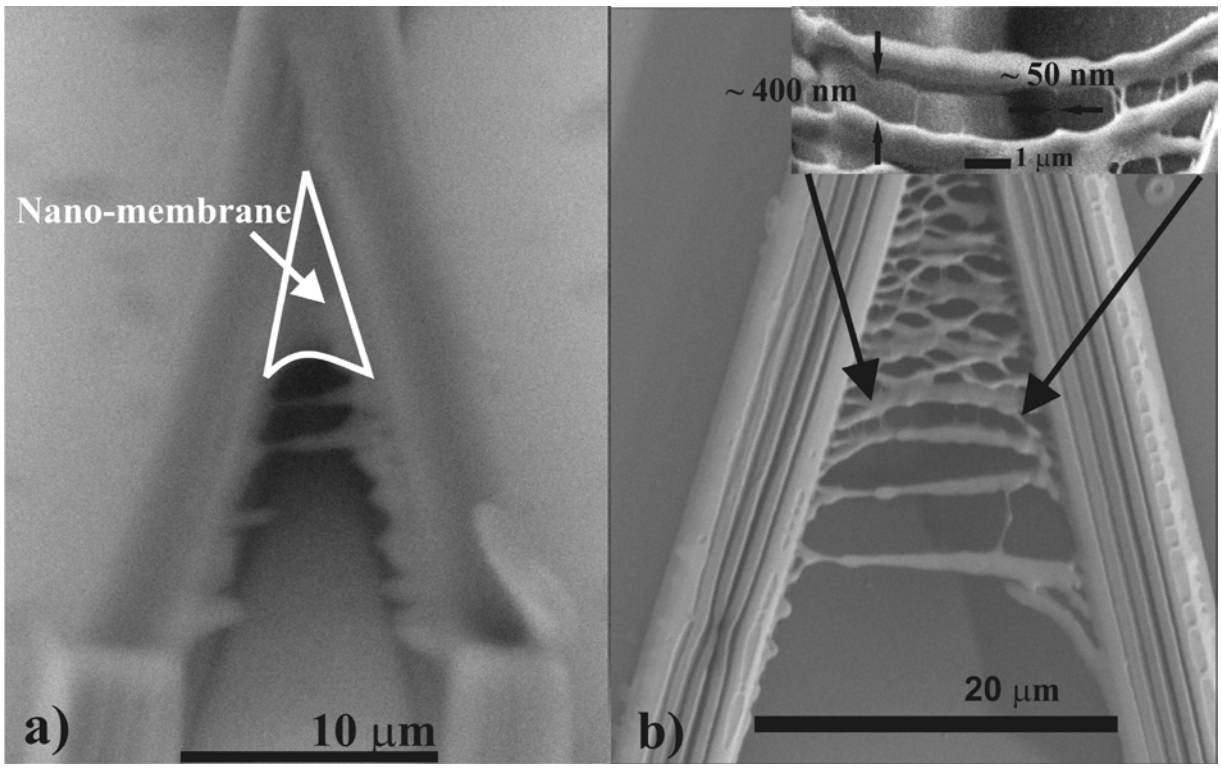

Fig. 1. Self-formed nano-features in-between the supporting walls in AKRE37: a) nano-membrane; b) periodic nano-fibers in a gap between the fabricated lines.

1. H. -B. Sun and S. Kawata, Adv. Polym. Sci. **170**, 169-273 (2004).
2. M. Malinauskas, H. Gilbergs *et al.*, Proc. of SPIE **7366**, 736622 (2009).
3. H. -B. Sun, A. Nakamura *et al.*, Adv. Mater. **23**, 2011-2014 (2003).
4. S. -H. Park, T. -W. Lim *et al.*, Appl. Phys. Lett. **89**, 173133 (2006).
5. D. Tan, Y. Li *et al.*, Appl. Phys. Lett. **90**, 071106 (2007).
6. M. Malinauskas, G. Bičkauskaitė, M. Rutkauskas, D. Paipulas, V. Purlys and R. Gadonas, Lithuanian J. Phys. (to be printed 2010).

PP50

SELF-FOCUSING IN LARGE MODE AREA OPTICAL FIBER

J. Želudevičius[1], V. Vosylius[2], K. Regelskis[3]

[1,2,3] *Laboratory for Applied Research, Institute of Physics, Vilnius, Lithuania*

[1,2] *Faculty of Physics, Vilnius University, Vilnius, Lithuania*

[1] ckjulek@gmail.com

Developments in fiber technologies made fiber lasers and amplifiers capable of providing high output powers, thus allowing these sources to displace conventional lasers in variety of applications. However, high beam powers induce in fiber different nonlinear effects, which reduce overall performance. Highest attainable peak power in fiber amplifier is limited by self-focusing, which arises from intensity dependent refractive index component. When peak power in fiber approaches some critical value ($P_{crit.}$) self-focusing makes the beam collapse, with intensity becoming high enough for optical damage of fiber to occur. Despite there are many theoretical studies ([1], [2], [3]) investigating beam propagation in fibers at powers approaching $P_{crit.}$, there is no reliable experimental data approving theoretical calculations. So objective of this work was to investigate experimentally self-focusing in large mode area fiber.

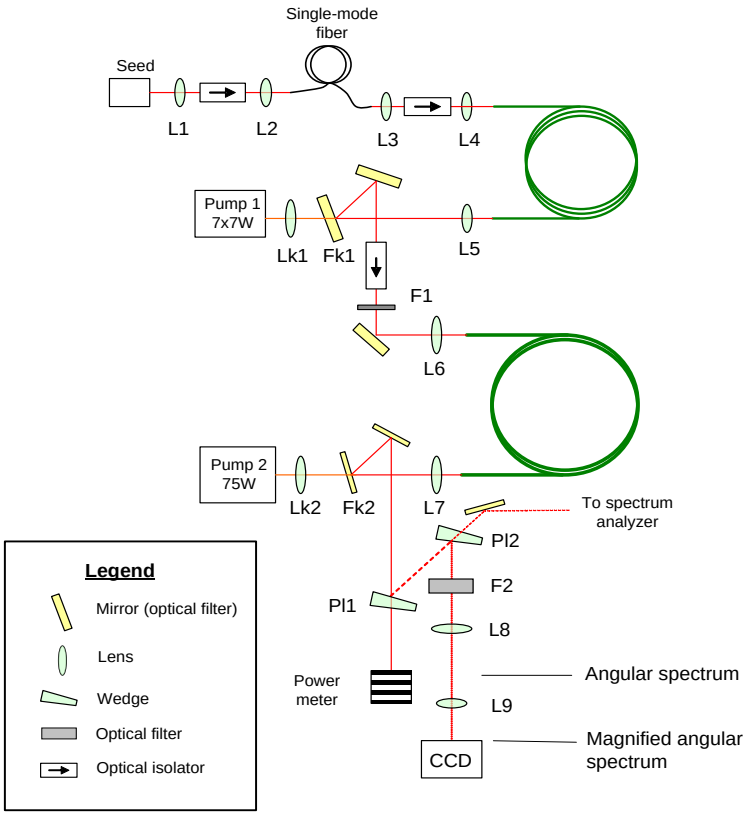

Fig. 1. Schematic diagram

In order to induce self-focusing we amplified 400 ps pulses (generated by passively Q - switched microchip laser, repetition rate - 5 kHz) of 1063 nm light using two fiber amplifier stages (**Fig.1**). In first amplification stage we used 30 μm core diameter, double-clad, ytterbium doped fiber and in second stage - 65 μm core diameter (effective mode diameter – 50 μm), double-clad, ytterbium doped fiber. We tried to excite fundamental mode in both active fibers. In first stage fiber beam intensity distribution very similar to Gaussian was achieved and in second stage fiber we had some difficulties exciting fundamental mode so beam intensity distribution was not ideal.

We monitored mode diameter changes in last stage fiber using CCD camera set in angular spectrum field. In angular spectrum field mode diameter changes are inversely proportional to fiber mode diameter changes. Our results showed that usually beyond 2 MW peak power optical breakdown occurred in last stage fiber. Highest peak power reached is 2.5 MW. We were able to record possibly self-focusing induced fiber mode diameter decrease (in angular spectrum field mode diameter increased) at peak powers from 1 MW to 2.5 MW (Fig. 2).

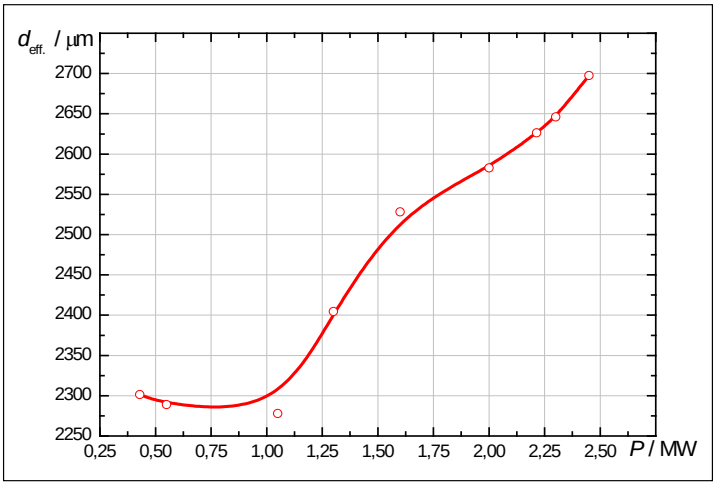

Fig. 2. Measured fiber mode diameter $d_{eff.}$ in angular spectrum field at different pulse peak powers P

Recorded pulse peak power of optical breakdown is approximately two times smaller than peak power of self-focusing predicted by theory. Most theoretical simulations predict self-focusing critical power for similar fiber configuration of about 4.3 MW ([1], [2], [3]). Some additional research is needed to clarify these results and state real reasons for this.

1. G. Ronald Hadley, Roger L. Farrow and Arlee V. Smith, Proc. of SPIE Vol. **6102**, 61021S-7, (2006).
2. Roger L. Farrow, G. Ronald Hadley and Arlee V. Smith, Dahv A.V. Kliner, Proc. of SPIE Vol. **6453**, 645309 (2007).
3. G. Ronald Hadley and Arlee V. Smith, Proc. of SPIE Vol. **6475**, 64750G (2007).

PP51

FEMTOSECOND LASER INDUCED PLASMA ANALYSIS

K. Stankevičiūtė, O. Balachninaitė, V. Sirutkaitis

Laser Research Center, Department of Quantum Electronics, Faculty of Physics of Vilnius University, Saulėtekio ave. 10, LT-10223 Vilnius, Lithuania

karolina.stankeviciute@ff.stud.vu.lt

Laser - induced breakdown spectroscopy (LIBS) is a spectroscopic analysis technique that uses optical emission of laser - induced plasmas to determine the composition of the sample [1]. During the past few years there has been great interest in femtosecond lasers induced plasmas because of low continuum radiation intensity in comparison with nanosecond regime [2]. This feature allows to use LIBS as an inspection technique in micromachining, where high repetition rate lasers are used. To produce reliable information from plasma emission spectra requires good understanding of plasmas properties dependence on various lasers parameters such as pulse energy and fluence, pulse duration and wavelength.

The aim of this work is to compare the spectral information gained by using different wavelengths high repetition rate femtosecond laser pulses as it was previously noticed that laser radiation wavelength has influence on line intensity. Plasma emission spectrum shows higher intensity in visible region, if it is induced by UV radiation rather than IR [3].

The experimental setup consist of Yb:KGW laser producing 1030 nm wavelength 280 fs pulses at 50kHz pulse repetition rate with the maximum output power of 6 W. The BBO crystals were used to generate 257 nm radiation. The experiments were carried out by focusing laser beam with the 50 mm focal length quartz lens on the surface of stainless steal specimen. Another quartz lens (50,8 mm diameter, 100 mm focal length) collects the emission from plasma and focuses it into a fiber. The fiber transfers the emission signal to a four channels (AvaSpec – USB2 – DT, 200 nm – 664 nm spectral range) spectrometer equipped with a charge – couple device (each channel is provided with Sony ILX554 detector). All experiments were conducted in air at atmospheric pressure.

Ultra short pulses were used to reduce the continuous emission background intensity. The region of the spectra distinguishing the highest intensity lines were used for the later analysis. The dependence of spectral lines intensities of plasmas induced by the laser beams of different wavelengths (1060 nm and 257 nm) on energy and fluence was investigated.

The results of the experiments have shown that plasmas induced by UV and IR radiation spectra exhibit the same nature. The inspection of rare elements in the sample needs high energy pulses in order to the increase the amount of excited atoms in plasma as more material is ablated from the sample.

1. A. W. Miziolek, V. Palleschi and I. Schechter, Editors, Laser Induced Breakdown Spectroscopy (LIBS): Fundamentals and Applications (Cambridge University Press, Cambridge, UK, 2006).
2. V. Margetic, A. Pakulev, A. Stockhaus, M. Balshov, K. Niemax, R. Hergeröder, Spectrochimica Acta, Part **B 55**, 1771 – 1785 (2000).
3. L. Formarini, V. Spizzichino, F. Colao, R. Fantoni, V. Lazic, Anal Bioanal Chem **385**, 272 – 280 (2006).

PP52

LASER-INDUCED BACKSIDE WET ETCHING USING FEMTOSECOND LASER PULSES

T.Gertus[1,2], R.Razgaitis[1]

[1] *Laser Research Center, Department of Quantum Electronics, Faculty of Physics of Vilnius University, Saulėtekio ave. 10, LT-10223 Vilnius, Lithuania*

[2] *ALTECHNA Co.Ltd., Konstitucijos ave. 23C-604, Vilnius, LT-08105, Lithuania*

titas.gertus@ff.vu.lt

Laser-**I**nduced **B**ackside **W**et **E**tching (acronym LIBWE) method is a very promising method for micro structuring of transparent materials, for example fused silica, Pyrex, CaF_2, BaF_2, sapphire and different types of glasses using ultraviolet nanosecond excimer laser pulses [1]. Similarly, to LIBWE with nanosecond laser pulses, the irradiation of the solid/liquid interface of transparent material with femtosecond near infrared (NIR) laser pulses results in etching of the material surface and deposition of decomposition products from liquid [2]. The most important advantages of the LIBWE procedure in contrast with other methods of transparent material micromachining are the relatively low etching threshold fluence, sub micrometer depth control, quasi smooth etched hole bottoms, and micro-patterns free of micro-cracks and debris [3].

For LIBWE experiments we use AltSCA femtosecond micromachining system (ALTECHNA Co.Ltd., Lithuania), which integrates high precision 3 - axis XYZ sample positioning linear stages (Aerotech, Inc., USA) and Yb:KGW femtosecond laser PHAROS (Light Conversion GmbH, Lithuania). SCA (**S**ystem **C**ontrol **A**pplication) software was used to compile and execute fabrication algorithms. The synchronization between the high resolution (2,5 nm) positioning system and the laser's firing pattern is precisely (with ±0,3 μm accuracy) controlled with the advanced PSO (**P**osition **S**ynchronized **O**utput). PHAROS laser emits λ = 1030 nm, τ = 300 fs radiation. Pulse repetition rate can be tuned from f_{min} = 1 kHz to f_{max} = 350 kHz and average power can be set up to P = 6 W.

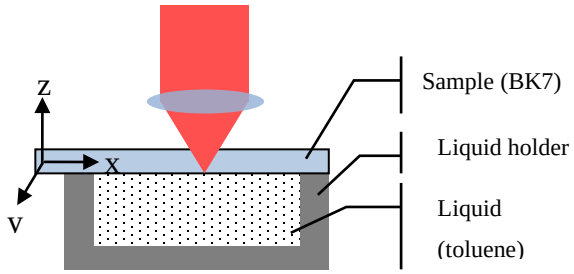

Fig.1 basic experimental set-up for LIBWE.

Special sample holder was made to guaranty solid/liquid interface condition. We use $f = 11$ mm aspheric lens (0.25 NA) to focus laser beam to the back side of h = 1 mm thickness borosilicate glass (BK7) (Fig.1).

We used toluene (C_7H_8 or $C_6H_5CH_3$), also known as methylbenzene or toluol, as „absorbing"-etching liquid. We do not use any absorbers (such as pyrene), which are used for standard LIBWE using nanosecond laser pulses. Toluene is a colorless liquid transparent for $\lambda = 1030$ nm irradiation. It can be exited only through multi-photon excitation, so LIBWE using femtosecond laser pulses can be realized only by means of multi-photon absorption.

Without liquid, h = 1 mm thickness BK7 glass front surface measured damage threshold - Φ_{front} = 1,87 J/cm^2, when incident pulse count is less than P_D <100 and back surface – Φ_{back} = 3,57 J/cm^2, then P_D < 1000. If toluene is in contact with sample back surface etching threshold becomes less than Φ_{LIBWE} = 1,04 J/cm^2, for 125 pulses.

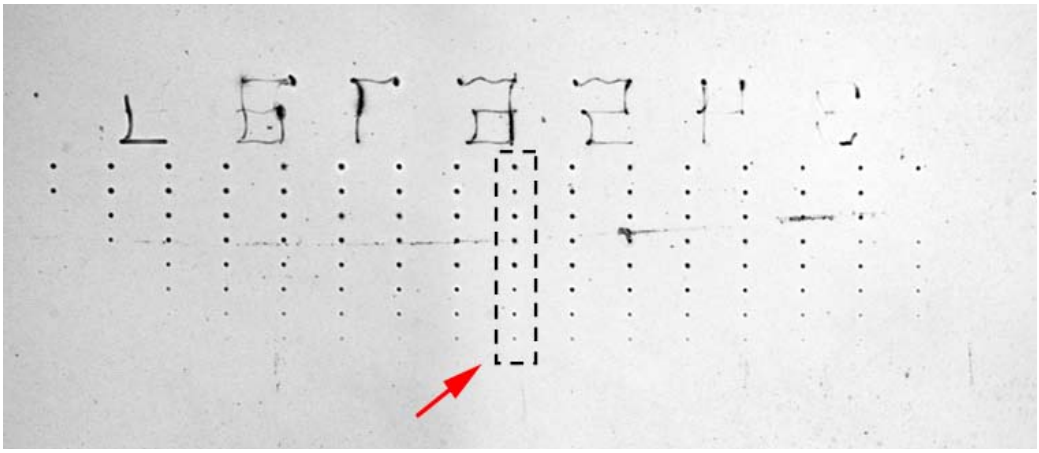

Fig. 2 Back surface of BK7 glass sample micro-machined using LIBWE technology. Fabrication parameters: energy density Φ = 2,09 J/cm^2, pulse repetition rate f = 200 kHz. Different columns represent different focus planes according to the back surface (steps Δz = 2 μm), different rows – different amount of incident pulses ($N = n^3$ (there n – is cycle number)).

We have demonstrated, that back surface of h = 1 mm thickness BK7 glass "damage" - etching threshold becomes lower, when toluene is applied in contact to back surface. Depth of etched structures varies from 50 nm to 1 μm and can be controlled by changing incident pulse amount or energy.

1. Wang J, Niino H and Yabe A 1999 Appl. Phys. A **68** 111–3
2. R Bohme, S Pissadakis, M Ehrhardt, D Ruthe and K Zimmer; J. Phys. D: Appl. Phys**. 39** (2006) 1398–1404
3. Cs.Vass, D. Sebok, B. Hopp, Applied Surface Science **252** (2006) 4768–4772.

PP53

PULSE STRETCHING USING INTRACAVITY FABRY–PÉROT ETALON AND ITS INTENSITY AUTOCORRELATION CHARACTERIZATION

M. Malcius, D. Urbonas, V. Smilgevičius

Laser Research Center, Department of Quantum Electronics, Faculty of Physics of Vilnius University, Saulėtekio ave. 10, LT-10223 Vilnius, Lithuania

mindaugas.malcius@ff.stud.vu.lt

We present results of investigation on Nd:YAG regenerative amplifier (RA) output pulse stretching using different intracavity Fabry–Pérot etalons. Short pulses may lead to self-phase modulation and possible optical damage of active laser medium so it is important to control the pulse duration inside the RA cavity. The relation between pulse duration and its bandwidth is well known:

$$\Delta\nu \cdot \Delta\tau = \text{const} \tag{1}$$

From Eq.1. it is clear that reduction of pulse bandwidth will stretch it in time. Pulse stretching can be accomplished by inserting an etalon in laser cavity. Etalon (also known as Fabry–Pérot etalon) is a transparent material with highly parallel surfaces. When laser beam enters an etalon it works as an optical resonator (Fabry–Pérot interferometer) which transparency changes depending on optical frequency (but is not very periodic according to frequency due to chromatic dispersion). The propagation of rays is depicted in Fig.1.

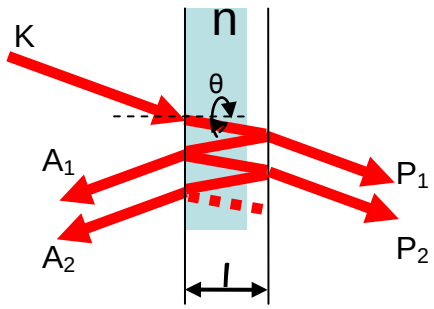

Fig. 1. Ray propagation in etalon

Spectrum narrowing occurs when pulses are propagating through the etalon so the duration of pulses increase. The wavelength separation between adjacent transmission peaks is called the free spectral range of the etalon, Δλ, and is given by [1]:

$$\Delta\lambda = \frac{\lambda_0^2}{2 \cdot n \cdot l \cdot \cos\theta_0} \tag{2}$$

Our goal was to stretch pulses of Nd:YAG RA up to 50 ps. We tested different etalons and measured the output pulse duration using intensity autocorrelation (AC). It is important to know the shape of a pulse, however, the phase still can not be measured using this method [2]. For a Gaussian time profile the autocorrelation width is 1.41 wider than the width of the intensity. This numerical factor, which depends on the shape of the pulse, is sometimes called a deconvolution factor.

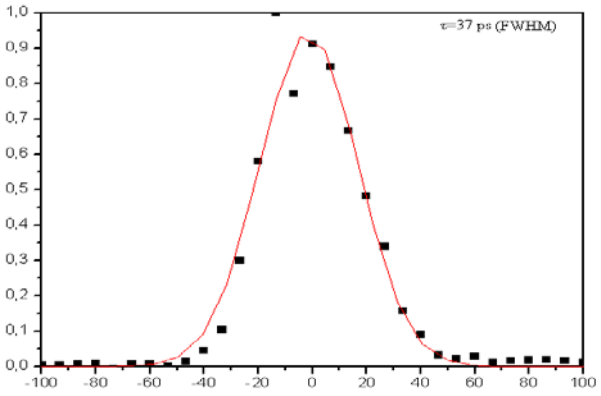

Fig. 2. AC function without etalon

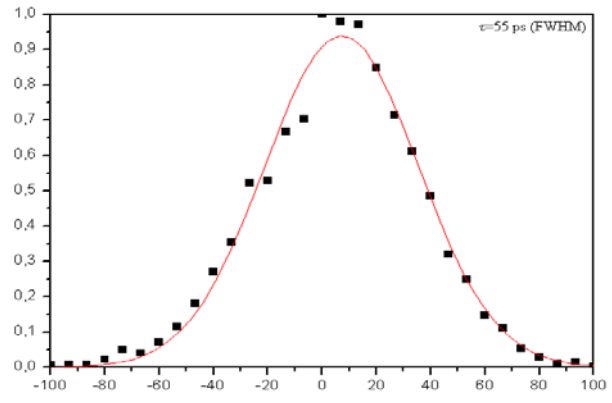

Fig. 3. AC function with 3mm etalon

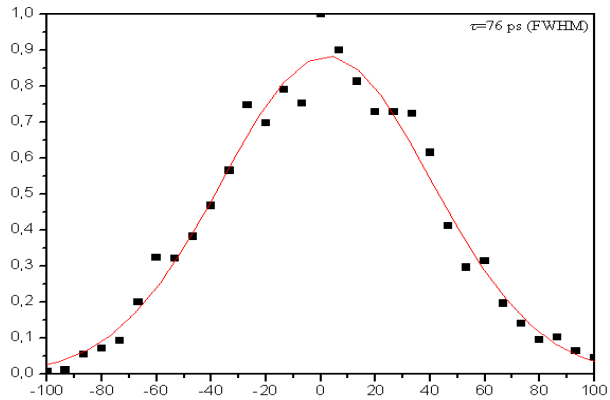

Fig. 4.AC function with 2mm etalon with anti-reflectance coatings

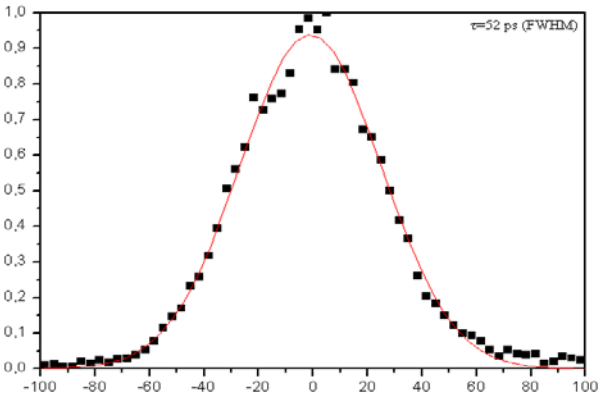

Fig. 5. AC function with 2mm etalon

Making an assumption that the laser generates Gaussian pulses, the durations of a pulse in different configurations were measured: 26 ps without etalon (Fig.2.), 39 ps with 3mm etalon without coatings (Fig.3.), 54 ps using 2 mm etalon with anti-reflection (at 1064nm) coatings (Fig.4.) and 37 ps using 2 mm etalon without coatings (Fig.5.).

1. V. A. Šalna, Optika (Enciklopedija, Vilnius, 2004).
2. V. Sirutkaitis *et al*., Lazerinė technologija (VUL, Vilnius, 2008).

PP54

ACOUSTO OPTICALLY Q-SWITCHED, CONTINUOUSLY PUMPED YB: YAG MINI LASER

Vytautas Stočkus [1, 2], Arūnas Varanavičius[2], Eugenijus Murauskas [3], Marius Leišis [1, 2]

[1] *Altechna Co. Ltd. Konstitucijos ave. 23C-604, LT-08105, Vilnius, Lithuania*

[2] *Department of Quantum Electronics, Faculty of Physics, Vilnius University, Sauletekio ave. 9-III, LT-10222 Vilnius, Lithuania*

vytautas@altechna.com

[3] *Institute of Physics, Savanoriu ave. 231, LT-02300 Vilnius, Lithuania*

In order to achieve higher level of synchronization and low timing jitter various active Q-switching techniques are used. Acousto - optic device applications can be divided into two categories: zero-beam order applications and diffracted beam applications. One of the zero-order beam applications is A-O Q-switching [1]. Q-switches are typically fabricated Tellurium Dioxide, Fused Quartz, or other acousto-optic materials [1].

Q-switches are designed for the conversion of RF energy into acoustic energy by attaching the transducer to the crystal with an vacuum metallized process. Transducers, placed on acousto-optic materials, forms standing acoustical wave, which works as diffraction grating with the period of acoustical wave. This effect causes appropriate losses inside the laser resonator, as part of incident photons diffracts to higher order maximums [2, 3].

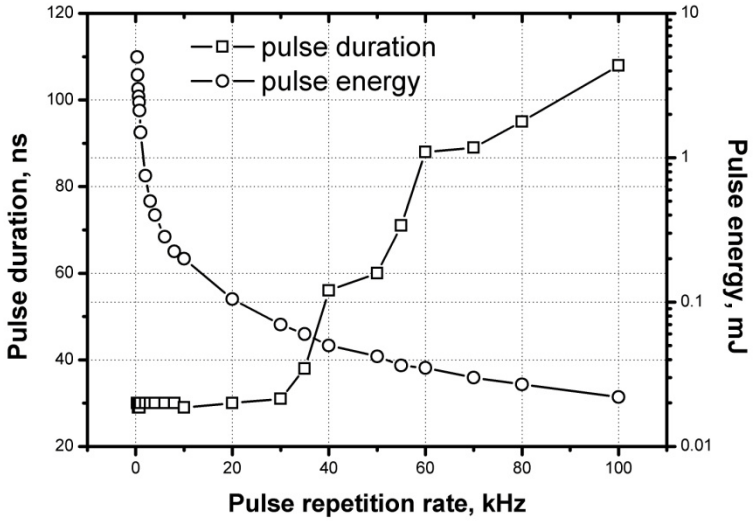

Fig. 1. Measured laser pulse energy and duration dependence over pulse repetition rate

Experimental setup consisted from 2mm. thick Yb (10%): YAG crystal, continuously pumped with 10W fiber coupled 940 nm laser diode, acousto optical Q-switch and partial reflection curved output coupler. The laser was tested under various pulsing frequencies. The highest pulse repetition frequency was 100 kHz with pulse energy 22 μJ and duration 108 ns. The decrement of pulse repetition rate leaded to higher energy and shorter pulse pulses. The average power remained constant around 2 W in the region of 10 kHz – 100 kHz. When the pulse repetition frequency was set below 10 kHz, average power decreased to 1.5 W. Pulse duration dropped from 108 ns at 100kHz, to 31 ns at 30 kHz and remained constant till the end of measurements at 300 Hz. The highest pulse energy achieved was 5 mJ at repetition rate of 300 Hz and pulse peak power of 167 kW.

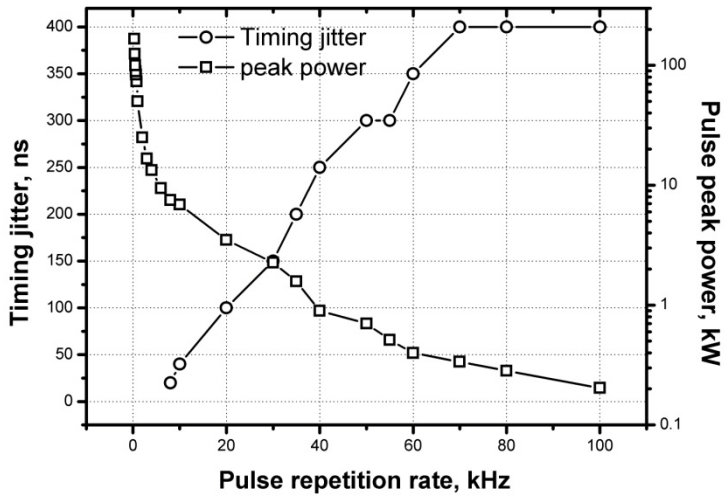

Fig. 1. Measured laser pulse peak power and timing jitter dependence over pulse repetition rate

The timing jitter at 100 kHz pulse repetition was 400 ns, at 8 kHz it decreased to 20 ns. Forward decrement of pulse repetition leaded to timing jitter decrement, which was difficult to measure with equipment, used during experiment. The temporal profile of the laser pulse remained symmetrical in all operation frequencies. This can be explained by properties of Yb: YAG - relatively low emission crossection, which causes low gain in laser resonator. During whole experiment laser was emitting single - TEM00 - transversal mode.

1. W. Koechner, Solid-State Laser Engineering, 6th Ed.(Springer-Verlag, Berlin, 1999), pp. 97-102, 488-529.
2. J. Liu, J. M. Yang, X. W. Fan, and G. G. Wang. Laser Physics, 2010, **Vol. 20, No. 1**, pp. 222–225.
3. J.H. Garcia-Lopez, V. Aboites, A.V. Kiryanov, M.J. Damzen, A. Minassian. Optics Communications, 2003, **Vol. 218**, pp. 155–160.

PP55

DESIGN AND TEST OF TOTAL INTEGRATED SCATTERING APPARATUS FOR OPTICAL COMPONENTS

L. Žitkutė, V. Sirutkaitis

Vilnius University, Quantum Electronics Department, Saulėtekio al. 9, LT – 10222 Vilnius

lina.zitkute@stud.ff.vu.lt

Light scattering is one of the factors that limit quality of optical components. Light scattering of optical components has been interesting since 1970 when laser technologies started to grow [1]. Surface roughness, contaminations, micro scratches, fractures, various defects and fluctuations of the density in the bulk reduce quality of the optical components and increase scattering from them [2]. Measurement of light scattering gives opportunity to explore quality of surface faster than other techniques and it allows testing of larger surfaces. A standard procedure according ISO standard 13696 [3] based on total integrated scattering has been developed for this purpose in the characterization of the laser components. Surface roughness in range from 0.1 to 600 nm can be easy extrapolated from total integrated scattering data [4].

We report design and test of total integrated scattering apparatus based on 1 kHz repetition rate Q-switched laser and capable to perform measurements at 532 and 355 nm wavelengths. Our total scattering measurement facility is equipped with an Ulbricht sphere and designed in way presented on Fig. 1. For the generation of 532 and 355 nm radiation from the laser with fundamental harmonic at 1064 nm are used harmonic generators. The maximum pulse energy at 532 nm is ~0.9 mJ and at 355 nm ~0.6 mJ. For initial pulse energy attenuation by factor up to 100 was used half wavelength plate and thin film polarizer. The laser beam is focused to the ~0.4 mm spot on the investigated sample with 1 m focal lens. The reflected from the sample and transmitted through the sample laser beams are taken away from the specially designed chamber. For the air pollution decreasing in apparatus chamber close loop air cleaning system

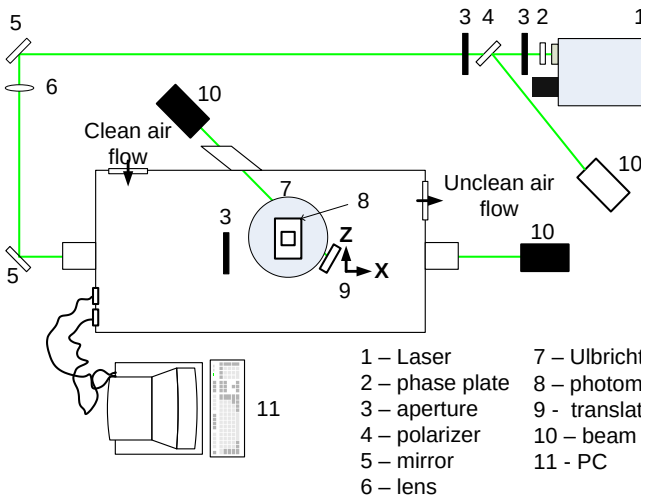

Figure 1: Experimental set-up for total integrated scattering measurements

with Heppa 14 filter was used. It allowed achieve ISO clean class 6 in the chamber and totally avoid particles larger than 5□m. The chamber additionally lets avoid undesirable light that could influence measurements. The scattered signal was registred by Hamamatsu H5784-20 photomultiplier and proceed by NI data accusation card and computer. Software based on the programming package LabView were created to speed up measurements with minimum human resources. We use calibration routine be insertion of a diffuse reflectance standard with known Lambertian scattering characteristics. To keep the photomultiplier signal at level ~100 mV (much lower than saturation level) in the case of reflectance standard and high scattering samples additional attenuator based on neutral filters was used. It attenuated laser beam by factor in range from 1 to 10^5. The sample was placed on the two-axis translation stage for the scattering losses measurement of the whole sample. The sensitivity of the facility was determined by measurements of unloaded sphere. For 532-nm beam the sensitivity was better than 10^{-4} % or 1 ppm and was caused by Rayleight scattering in air and by scattering on small (<1□m) particles. The possibilities of the developed scattering apparatus in scattering losses measurements of the whole surface are presented in Figure 2 and on comparison of the scattering losses of the different coating materials coated on fused silica by IBS method is presented in Figure 3.

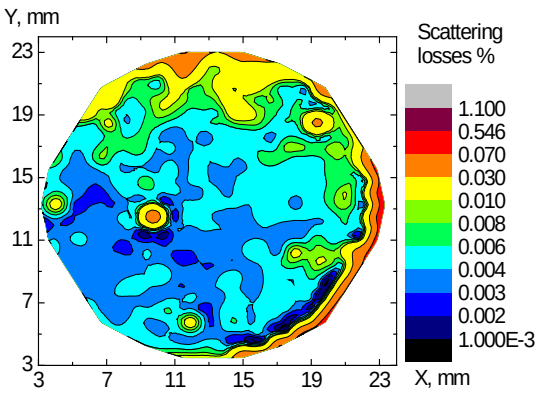

Figure 2: Map of scattering losses for e-beam coated fused silica substrate

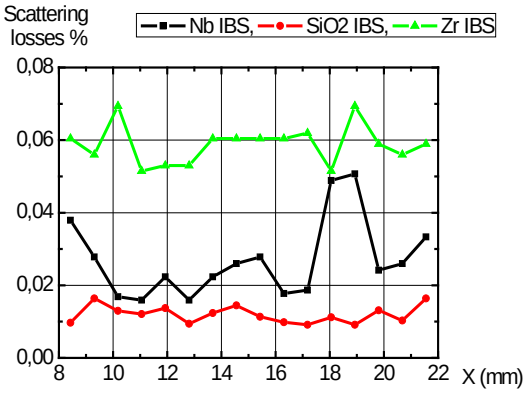

Figure 3: Scattering losses for three different samples coated by IBS method

1. Stover, J.C., *Optical Scattering: Measurement and Analysis*. 2 ed, ed. P.M. Series. (Bellingham, Washington, USA: S P I E-International Society for Optical Engineering. 340, 1995)
2. Hou, H., et al., Appl. Opt., **44**(29): p. 6163-6166 (2005)
3. Standardization, I.O.f., International Standard ISO 13696, Optics and optical instruments - Test methods for radiation scattered by optical components. 2002: Geneva, Switzerland. p. 26.
4. Bennett, J.M. and L. Mattsson, *Introduction to surface roughness and scattering*. (Washington, D.C.: Optical Society of America. 130 1999,).

PP56

THE BROADBAND PULSE COMPRESSION IN DISPERSIVE MEDIUM

K.Kristinaitytė, A.Varanavičius, R.Antipenkov

Faculty of Physics of Vilnius University, Sauletekio ave. 9-III, LT-10222 Vilnius, Lithuania

Kristina.Kristinaityte@ff.stud.vu.lt

Pulse compressor is one of the most crucial components in optical parametric chirped-pulse amplification systems. Employment of bulk media allows to design a relatively inexpensive, compact and low loss set up for broad band pulse compression.

A broadband pulse compression was simulated using the algorithm of pulse stretching when it propagates through a dispersive medium. The main goal is to find optimum conditions for compression of 200 nm bandwidth, 30 mJ and 50 ps pulses to their transform limit using different glasses as a dispersive media.

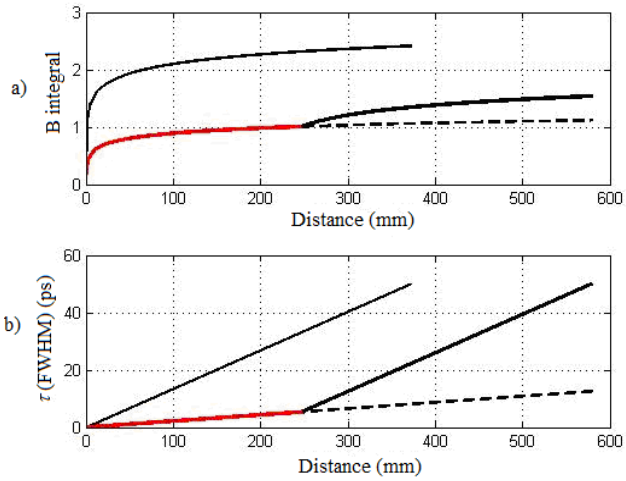

Fig. 1. B-integral (a) and pulse duration τ (b) change over distance in compressor of one material: SF57 (solid thin line) or FS (dashed line), and in compressor of two materials (solid thick line): FS and SF57.

In many high-power lasers, when the pulse energy gets compressed into shorter pulses with higher peak intensities, the nonlinear effects grow exponentially [1]. B-integral is a measure of the nonlinear interaction and it was accepted that B-integral must be kept below the value $B < 1$.

The simulation results presented in Fig. 1 shows, that in order to get lower B-integral values and to use less material under the same conditions, the compressor consisting of two different materials is more preferable.

The contribution present results on number of numerical experiments performed for optimization of compressor characteristics by altering lengths of different materials and employment of chirped mirrors for final compression [2]. It was shown, that such stepwise pulse compression considerably reduces pulse phase characteristic distortions caused by nonlinear effects arising during intense pulse propagation in bulk media.

1. Siegman A.E. *Lasers*. (University Science Books, Mill Valley, CA 1986)
2. Gavin D. Reid, Klaas Wynne. *Ultrafast Laser Technology and Spectroscopy* in *Encyclopedia of Analytical Chemistry*. (John Wiley & Sons Ltd, Chichester, 2000)

PP57

PICOSECOND PULSES DURATION CHARACTERIZATION AND MEASUREMENT AUTOMATION

D. Urbonas, M. Malcius, V. Smilgevicius

Laser Research Center, Department of Quantum Electronics, Faculty of Physics of Vilnius University, Saulėtekio ave. 10, LT-10223 Vilnius, Lithuania

darius.urbonas@ff.stud.vu.lt

Pulse duration is one of the main characteristics of coherent laser radiation, however it has always been a difficult parameter to evaluate since standard electronic detectors are not capable of measuring processes on shorter than sub-nanosecond time scale. That is why it is necessary to use methods that are able to measure events as short as a few optical cycles. Also most measurement devices include nonlinear optical elements.

The intensity autocorrelation (AC) was one of the first attempts to measure sub-nanosecond pulse duration. In our work we used second-order AC. This method involves splitting the pulse into two of equal intensity, variably delaying one pulse with respect to the other, and spatially overlapping the two pulses in some directly responding nonlinear-optical medium (Fig.1).

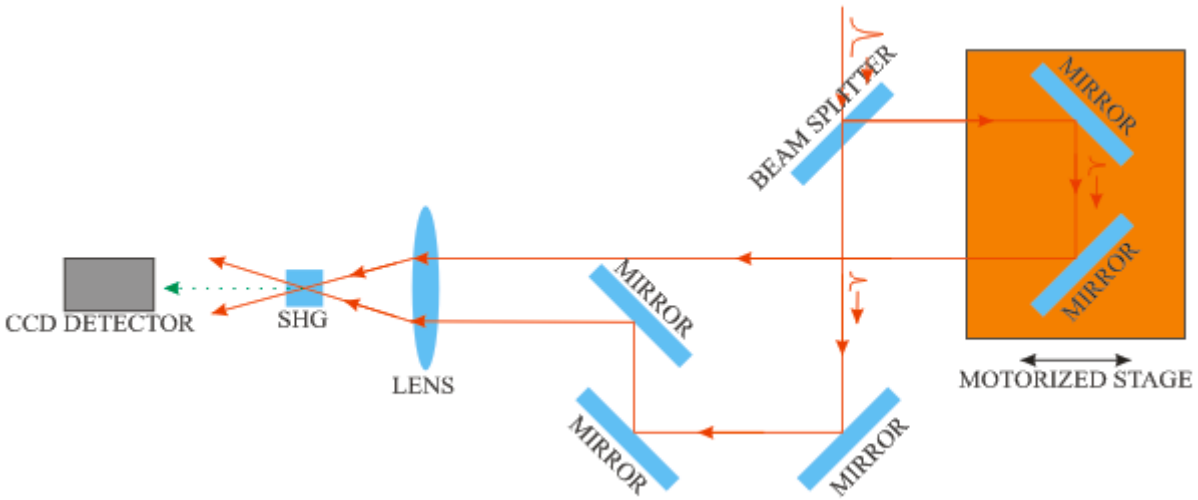

Fig. 1. Basic scheme of automated second order autocorrelator

A second - harmonic crystal will radiate “signal light” at twice the frequency of input light with a field envelope that is given by:

$$E_{sig}^{SHG}(t,\tau) \sim E(t)E(t-\tau) \quad (1)$$

where τ is the delay. This field has an intensity that is proportional to the product of the intensities of two input pulses:

$$I_{sig}^{SHG}(t,\tau) \sim I(t)I(t-\tau) \tag{2}$$

Detectors are too slow to resolve this beam in time so they will measure:

$$A^2(\tau) = \int_{-\infty}^{\infty} I(t)I(t-\tau)\mathrm{d}t \tag{3}$$

This is the intensity autocorrelation. The superscript (2) Eq.3 implies that it is a second order autocorrelation. Here we assume that our pulse profile is Gaussian. For a Gaussian time profile, the autocorrelation width is $\sqrt{2}$ wider than the width of the intensity.

In this work we set a goal to make this measurement precise and fast. We did this by adding motorized stage (delay line) and implementing a program that moves delay line and collects data from photo-diodes. This program was written using "LabVIEW 8.0". It also allows saving and opening data and calculates the duration of a pulse.

The drawbacks of this method are:

1. Minimum and maximum value of pulse duration that can be measured with this method depends on delay line parameters. Short motor step allows to measure very short pulses and long motorized stage – long pulses
2. Speed depends on data acquisition card and motor speed;
3. Requires relatively high peak power in order to generate second harmonic.

Picosecond pulses duration was measured using second order intensity AC and the experiment was automated using delay line with servo engine and LabVIEW to control it. This method was used to characterize pulse stretching using intracavity Fabry-Pérot etalon.

1. V. Sirutkaitis et al., Lazerinė technologija (VUL, Vilnius, 2008).
2. J.C. Diels, W. Rudolph, *Ultrashort Laser Pulse Phenomena: Fundamentals, Techniques, and Applications on a Femtosecond Time Scale. 2nd ed.* (Albuquerque, New Mexico, pp. 457-490, 2006).

PP58

FREQUENCY BANDWIDTH CONTROL OF NARROW BANDWIDTH PARAMETRIC LIGHT AMPLIFIER PUMPED BY CONICAL WAVES

D. Birenis, V. Šiburskis, A. Matijošius

Department of Quantum Electronics, Faculty of Physics, Vilnius University, Sauletekio ave. 9-III, LT-10222 Vilnius, Lithuania

domas.birenis@ff.stud.vu.lt

An important aspect of the optical parametric amplification (OPA) is the ability to be pumped by multiple beams. The multiple-beam pump was first introduced as a technique, which enabled to reduce the spatial bandwidth of the signal in the parametric generation process [1,2]. Some of the present authors have demonstrated highly efficient performance of the OPA pumped by three 1 ps pulses yielding almost 80% energy conversion [3]. The principle was named “energy combining”, as the signal gained energy from the combined pump field. In the case of several noncollinear pump beams, the gain bandwidth of the OPA and the amplified spectral region are determined by the intersection geometry and the crystal orientation, i.e. phase-matching condition. The gain bandwidth of the continuum-seeded single-pass optical parametric amplifier was easily extended using several pump beams amplifying neighboring regions of the seed signal spectrum [4].

In our work we shown that the gain bandwidth of the continuum-seeded single-pass narrow bandwidth optical parametric amplifier may be easily and tunable extended using elliptically-conical pump beams amplifying neighboring regions of the seed signal spectrum. The gain bandwidth broadening of OPA depends on the tilted axicon created difference of spatial frequencies $\theta - \phi$.

1. V. Smilgevičius, A. Stabinis, Opt. Commun. **106**, 69-74 (1994).
2. A. Baltuška, A. Beržanskis, R. Gadonas, A. Pugžlys, V. Smilgevičius, A. Stabinis, Opt. Lett. **20**, 2174-2176 (1995).
3. A. Dubietis, R. Danielius, G. Tamošauskas, A. Piskarskas, J. Opt. Soc. Am. B **15**, 1135-1139 (1998).
4. E. Žeromskis, A. Dubietis, G. Tamošauskas, A. Piskarskas, Opt. Commun. **203**, 435-440 (2002).

PP59

OPTICAL AND ELECTRICAL NOISE CHARACTERISTICS OF FABRY - PEROT LASER DIODES

Ignas Stasevičius

Vilnius University, Physics faculty, Radiophysics department

Ignas.st@gmail.com

Laser diodes represent a key element in the emerging field of optoelectronics which includes, for example, optical communication, optical sensors or optical disc systems. For all these applications, information is either transmitted, stored or read out. The performance of these systems depends to a great deal on the performance of the laser diode with regard to its modulation and noise characteristics [1]. Infrared multimode Fabry – Perot laser diodes are employed as light source in short – haul optical communication systems, where stable narrow radiation spectrum under variable ambience conditions is desired.

The goal of this project is investigation of the impact of low - frequency to certain characteristics of Fabry - Perot laser diodes. Low frequency noise is usually vivid below the margin of 20 kHz depending on the material and its investigations are inevitable part of determining the quality of laser structures and likely reliability. The noise spectrum is 1/*f* type and noise is caused by various growth and processing defects [2].

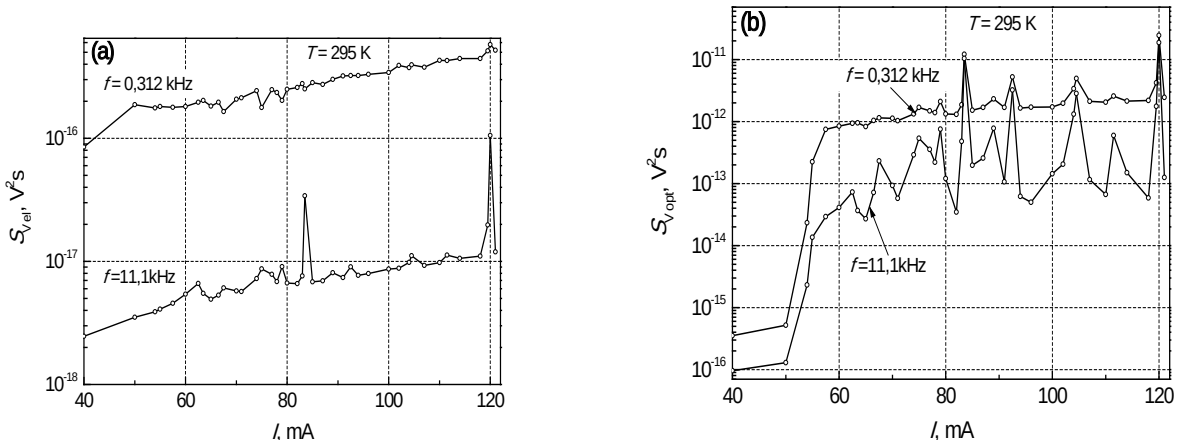

Fig. 1. Laser diode electrical (a) and optical (b) noise spectral density (0,312 kHz and 11,1 kHz) from the reference over injection current in laser diode.

The probing of laser diode is performed in a shielded space so that measurement would not be affected by external noise. The voltage fluctuations, or electrical noise, and radiation power fluctuations, or optical noise, are the characteristics of laser diode measured simultaneously during

the process. Investigation of electrical and optical noise is made by noise analysis program which receives the data through computer sound card.

Optical noise grows rapidly whenever threshold current is reached. This increase is due the instability of lasing-mode operation – in the active layer spontaneous emission is randomly changed with stimulated emission, the number of free carriers and emitted photons is fluctuating.

As the injected current is enhanced, the growth of optical and electrical noise spectral density is observed. Whenever specific values of current are present, the growth of electrical and optical noise is abrupt and vivid. After investigation of optical spectra it was determined that as these values are present the generating modes set is changed, the spectrum is composed of not one, but several modes sets that randomly change. The fluctuations of light intensity evoked by the generation of random modes are called mode hopping noise [3]. During these mode leaps the spectral density of electrical and optical noise grow rapidly and their form is more analogous to the one of white noise rather than $1/f$ noise. What is more, during this effect the noise spectrum is composed of higher frequency components. The main reason of mode hopping effect is that of carriers recombination in barriers and in the cladding layer [4].

The correlation factor between electrical and optical noise spectral densities is positive but close to zero as long as current is below the threshold value. During mode hopping effect, correlation factor grows abruptly.

The effect of mode hopping and its range depend on the temperature, after research it was identified that higher temperature evokes the mode hopping effect with a lower current. Higher temperature and higher injected current lead to the increase of wavelength of generated modes. However, higher temperature also leads to lower correlation factor between electrical and optical noise. The reason of the shift of wavelengths is due to the change of laser voltage, temperature and quantum well population which evokes the shift of laser energy levels [4].

1. K. Petermann, *Laser diode modulation and noise* (Kluwer Academic Publishers, the Netherlands, 1991).
2. R. Sobiestianskas, J. Simmons, S. Smetona, J. Evans, S. Pralgauskaitė, J. Matukas, V. Palenskis, Optical and electrical noise of ridge waveguide InGaAsP/InP F-P and DFB MQW lasers, 16th International Conference ICNF 2001: Noise in Physical Systems and 1/*f* fluctuations. Gainesville, Florida, USA, 22-25 October, 2001.
3. K V. Palenskis, J. Matukas, S. Pralgauskaitė. *Laser diodes* (Vilnius, 2000).
4. S. Pralgauskaitė. Optical and Electrical Low-Frequency Noise Characteristics of Multimode and Singlemode InGaAsP/InP Multiple-Quantum Well Laser Diodes: Doctoral dissertation. Vilnius, p.110, (2003).

PP60

COMPLEX PROFILE MICROOPTICAL COMPONENTS FOR LIGHT FLOW CONTROL FORMED USING NONLINEAR LASER LITHOGRAPHY

K.Belazaras, M.Malinauskas and R.Gadonas

Vilnius University, Faculty of Physics, Department of Quantum electronics, Laser Research Center
Sauletekio av. 10, LT-10223 Vilnius
kastytis.belazaras@ff.stud.vu.lt

The field of microoptics grew drastically in the last decades making great progress in transition from laboratory demonstrations to a broad range of commercial applications. Naturally a variety of microstructuring technologies for optical elements formation have been developed over years [1,2]. However, complex profile microoptics remains a difficult task for many fabrication methods [1].

3D structuring of polymers by nonlinear laser lithography becomes a prominent method for high precision rapid prototyping at micro and nano scale [3]. Various structures for micromechanics, microoptics and photonics are shown to be successfully formed by multiphoton polymerization [4].

We present several fairly novel structures for microoptics formed by Two-Photon Polymerization (TPP) technique and provide their basic characterization.

Micro-scale spiral phase plates. Spiral Phase Plate (SPP) is a transparent optical element with height proportional to the azimuthal angle. For a plane wave SPP imposes azimuth dependent retardation on the optical field generating an optical vortex [5]. Optical waves that possess helical phase distribution have been addressed in various studies for manipulation of small microscopic particles [6], spiral phase contrast imaging [7], optical vortex coronagraphy [5], etc.

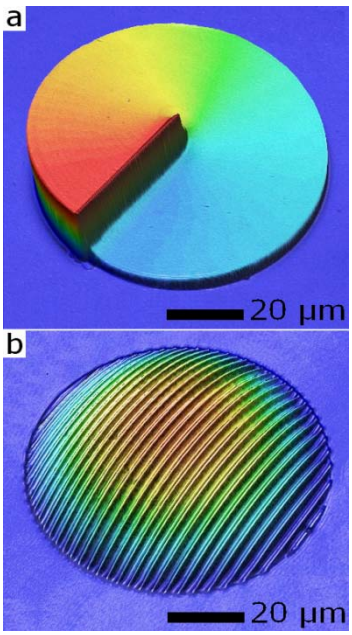

Fig 1. Topographic images by optical profilometer (PLµ2300) of microoptical elements formed by TPP technique: a - spiral phase

Microlenses with phase gratings. A spherical microlens profile was combined with a phase grating in one optical structure with surface characteristic details finer than optical wavelength. Hybrid refractive-diffractive elements formation brings the field of microoptics to exiting and much promising grounds.

1. J. Jahns, *Microoptics From Technology to Applications* (Springer press, USA, 1-26, 2004).
2. H. Ottevaere, R. Cox, H.P. Herzig, T. Miyashita.and H. Thienpont, Appl. Opt. **8** (7), 407-429 (2006).
3. S. Juodkazis, V. Mizeikis, H. Misawa, Adv. Polym. Sci. **213**, 157-206 (2008).
4. C. La Fratta, J. Fourkas, T. Baldacchini, Angew. Chem. Int. Ed. **46**, 6238-6258 (2007).
5. D.M. Palacios, G.A Swartzlander, D. Mawet, Proc. of Coronagraph Workshop, 148-156 (2006).
6. M.E.J. Friese, J. Enger, H.N.R. Heckenberg, Phys. Rev. A **54** (2), 1593-1596 (1996).
7. S. Furhapter, A. Jesacher, S. Bernet, M. Ritsch-Marte, Opt. Express **13** (3), 689-694 (2005).

PP61

LASER 3D MICRO/NANOFABRICATION OF POLYMERS FOR TISSUE ENGINEERING APPLICATIONS

P. Danilevičius and M. Malinauskas

Vilnius University, Faculty of Physics, Department of Quantum Electronics, Laser Research Center
Saulėtekio av. 10, LT-10223 Vilnius
paulius.danilevicius@ff.stud.vu.lt

Laser Three-Dimensional (3D) photostructuring of polymers allows production of various photonic and optical components, electromechanical systems and other objects in micro- and nanoscale. Currently, there are a range of techniques to obtain micro/nanoobjects, such as self-organization, electron beam lithography and nanoimprinting. However, optical fabrication employing ultrafast pulses provides unmatched flexibility and true 3D structuring [1].

In this work, Femtosecond Laser Two-Photon Polymerization (FLTPP) method was applied to produce 3D microstructures for tissue engineering applications. Ultrashort pulsed laser beam is tightly focused in the bulk of the photosensitive material, thus nonlinear light and mater interaction creates small region of photomodified volume in the vicinity of focus. This induces photopolymerization reaction and forms non-soluble polymers from initial monomers. By moving laser light focus we can directly write complex 3D structures in photopolymer directly from Computer Aided Design (CAD) model. Using this approach fabrication spatial resolution can reach few hundred nanometers [2].

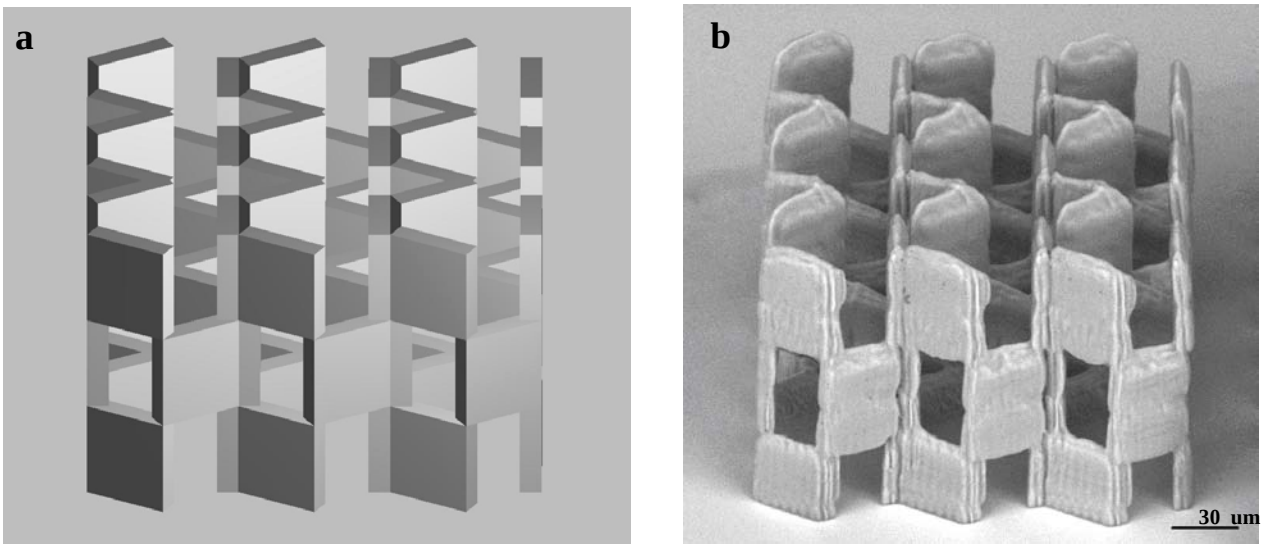

Fig. 1. CAD model of porous 3D honeycomb scaffold a) and the same microstructure out of Zr containing hybrid organic-inorganic biocompatible polymer SZ2080 [3] b).

FLTPP is attractive technology for tissue engineering applications. Nowadays, complex form polymeric matrices are designed for primary stem cell growth. It can serve as artificial scaffold for growing tissue. Therefore, the demand in technologies for 3D cell culture scaffolds is required. FLTPP provides unique possibility of 3D sculpting without geometrical restrains and it satisfies the resolution needed for artificial scaffolds. Also, depending on final application biocompatible or even biodegradable polymers can be used. However, much of efforts are still needed to be invested in order to improve fabrication throughput of technology and cell behavior studies at microscale in third dimension [4].

In this paper, we present the 3D scaffolds fabricated via FLTPP technique and their biocompatibility investigation using rabbit myogenic stem cells.

1. S. Juodkazis, V. Mizeikis and H. Misawa, Adv. Polym. Sci. **213**, 157-206 (2008).
2. M. Malinauskas, V. Purlys, A. Žukauskas, M. Rutkauskas, G. Bičkauskaitė, D. Paipulas, D. Baltriukienė, R. Širmenis, V. Bukelskienė, R. Gadonas, V. Sirvydis and A. Piskarskas, Femtosecond Laser Microstructuring of Biocompatible Polymers for Biomedical Application, XII International Conference on Laser Applications in Life Sciences, upcoming June 9-11 (2010).
3. A. Ovsianikov, J. Viertl, B. Chichkov, M. Oubaha, B. MacCraith, I. Sakellari, A. Giakoumaki, D. Gray, M. Vamvakaki, M. Farsari and C. Fotakis, ACS Nano **2**(11), 2257-2262, 2008.
4. M. Malinauskas, V. Purlys, A. Žukauskas, M. Rutkuskas, P. Danilevičius, D. Paipulas, G. Bičkauskaitė, L. Bukelskis, V. Chorosajev, D. Baltriukienė, V. Bukelskienė, R. Širmenis, R. Gadonas, V. Sirvydis and A. Piskarskas, Large Scale Laser Two-Photon Polymerization Structuring for Fabrication of Artificial Polymeric Scaffolds for Regenerative Medicine, Proc. of Ico-Photonics (Emerging Trends and Novel Materials in Photonics), to be printed (2010).

PP62

FABRICATION OF 3D PHOTONIC CRYSTALS BY MULTI-PHOTON FABRICATION

M. Rutkauskas[1], L. Maigytė[2], M. Malinauskas[1], M. Peckus[1] and K. Staliūnas[2]

[1] *Vilnius University, Physics Faculty, Department of Quantum Electronics, Laser Research Center, Saulėtekio ave. 10, LT-10223 Vilnius, Lithuania*

marius.rutkauskas@ff.vu.lt

[2] *ICREA, Departament de Fisica i Enginyeria Nuclear, Universitat Politecnica de Catalunya, Colom 11, E-08222 Terrassa, Barcelona, Spain*

Recently Photonic Crystals (PhC) have drawn high attention due to possibility to form photonic bandgaps, ranges of frequencies in which light cannot propagate through. These elements are attractive for controlling and manipulating the flow of light. PhC are the structures with periodical refractive index modulation, where periodicity is proportional to the wavelength of light. Under these conditions light propagation depends on it's the spatial distribution resulting to spatial filtering, Fig. 1 [1,2]. It is challenging to create 3D PhC, which could be used for visible light due to required high structuring resolution [3]. One of the possibilities to fabricate such photonic elements of woodpile geometry is Laser Two-Photon Polymerization (LTPP) [4].

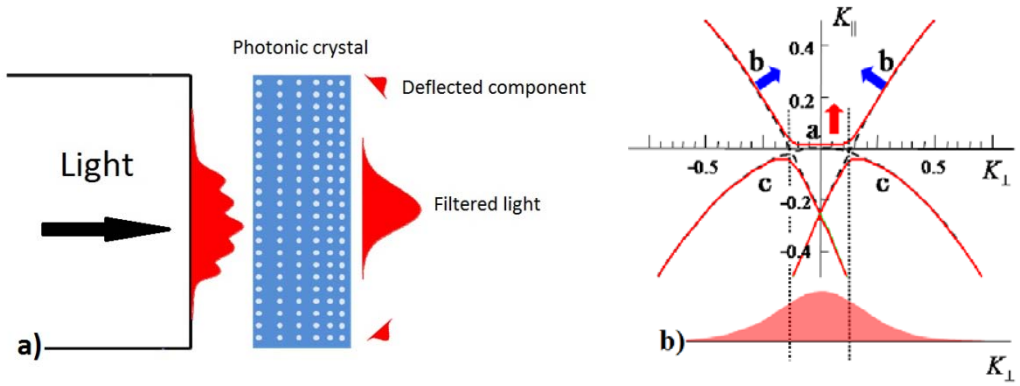

Fig. 1. a) Spatial filtering of light propogating through PhC. b) The part of the beam with wavevectors on the flat segment of the curve propagates diffractionless through PhC; the other part of the beam with wavevectors positioned at the slopes of the curve is strongly deflected, and thus filtered out [1,2].

LTPP is a direct laser writing technique based on ultra-localized polymerization reaction initiated by nonlinear absorption of short pulsed light in the tiny volume of the photosensitive material. By moving the sample relatively to the fixed focus spot it is possible to point by point modify the material along the scanning trace with subdiffractional resolution [5].

PhC and chirped PhC were theoretically designed and fabricated for red and green light. There are three essential parameters of the PhC to specify: the variance of refraction index, the longitudinal l_l and transverse l_t periods of the modulation index.

Rough specification is that the refractive index modulation wavenumbers in transverse direction q_t and the longitudinal q_l direction must fulfill the following condition:

$$q_t^2 + (k - q_l)^2 = \sigma^2 k^2 \qquad (1)$$

In Eq. (1) k is the wavenumber of the radiation in the material and σ is the parameter depending on the angular width of the filtering Δk. The spatial filtering efficiency depends on number of PhC layers [1-2].

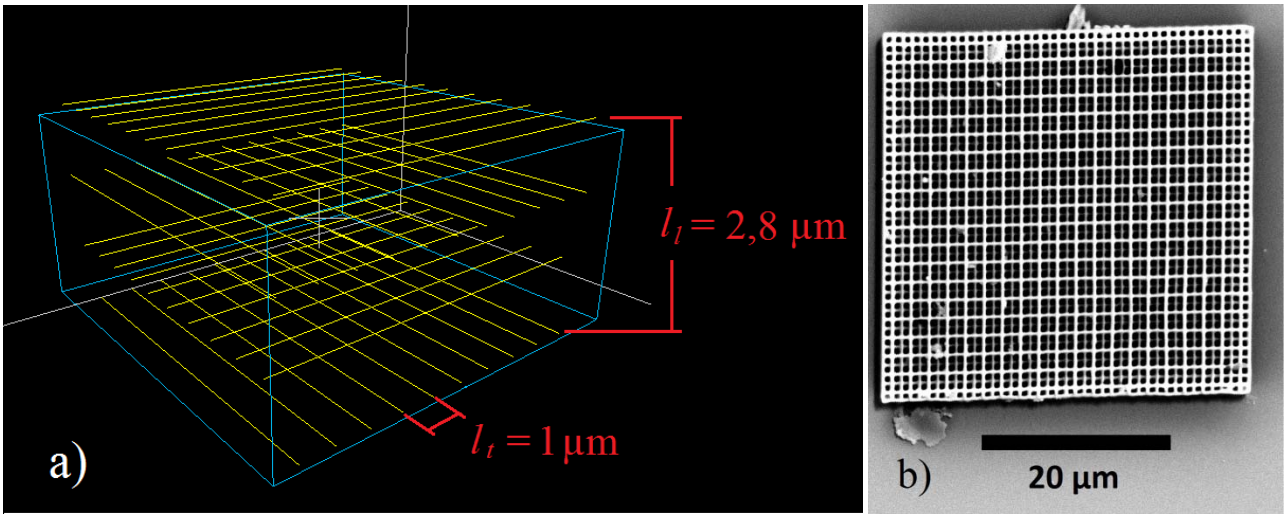

Fig. 2. a) Image of computer generated PhC. b) SEM image of PhC fabricated via LTTP technique.

The theoretically designed photonic crystals were manufactured out of Zr containing hybrid organic-inorganic SZ2080 (FORTH) photopolymer (n = 1,504) via LTPP technique. The quality of elements was investigated with Scanning Electron Microscope (SEM). Later, in order to tune the refractive index modulation, the 3D matrix was infiltrated with required refractive index monomer.

1. K. Staliunas, V.J. Sánchez-Morcillo, I.Pérez-Arjona, F. Redondo and V. Espinosa, Method and device for efficient filtering of spatial structure of light beams, Spanish patent (2007).
2. K. Staliunas and V. J. Sánchez-Morcillo, Phys. Rev. A **79**, 053807 (2009)
3. S. Juodkazis, V. Mizeikis and H. Misawa, Adv. Polym. Sci. **213**, 157-206 (2008).
4. J. Serbin, A. Ovsianikov and B. Chichkov, Opt. Express **12**, 5221-5228 (2004).
5. M. Malinauskas, H. Gilbergs, V. Purlys, A. Žukauskas, M. Rutkauskas and R. Gadonas, Proc. SPIE **7366**, 736622 (2009).

PP63

INTEGRATED MICRO-OPTICAL COMPONENTS FABRICATED BY LASER TRUE 3D LITHOGRAPHY TECHNIQUE

A. Žukauskas and M. Malinauskas

Vilnius University, Physics Faculty, Department of Quantum Electronics, Laser Research Center, Saulėtekio al. 10, LT-10223 Vilnius

mangirdas.malinauskas@ff.vu.lt

Femtosecond Laser Two-Photon Polymerization (FLTPP) fabrication is non-linear Direct Laser Writing (DLW) lithography technology [1] which explores new areas in micro/nanometer scale fabrication and high quality 3D structuring capabilities of microoptical components [2, 3]. Due to simultaneous Two-Photon Absorption (TPA) ultralocalized photochemical reaction is initiated in the bulk of the photopolymer. Complex geometry true Three Dimensional (3D) structures with the sub 100 nm spatial resolution [4] can be point-by-point directly written in the photopolymer from Computer Aided Design (CAD) models and thus the architecture of the structure can be changed flexibly. The integrity of the FLTPP technology opens possibilities to fabricate microstructures on various substrates such as glass, plastic or metal [5].

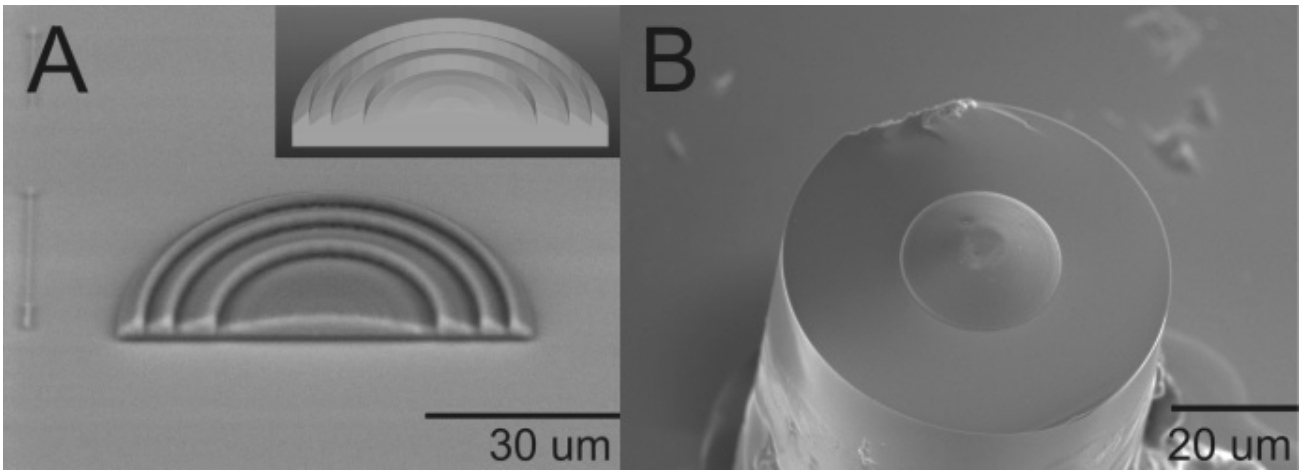

Fig. 1. SEM images of the Fresnel lens (radius 30 μm, height 6 μm) cross section (a) and aspherical lens (radius 25 μm, height 10 μm) fabricated on the top of the single-mode optical fiber (b). Inset depicts the respective CAD model.

In this report, we present micro-optical components fabricated on the top of the optical fiber out of commercially available hybrid zirconium-silicon containing photopolymer SZ2080 (FORTH,

Crete, Greece) [6]. The structural quality and surface roughness of the lenses were investigated by Scanning Electron Microscopy (SEM) and Atomic Force Microscopy (AFM). The optical focusing characteristics of the lenses fabricated on the glass substrate and on the top of the fiber were measured and compared with theoretical calculations. The principal setups of the FLTPP and methods of focal lengths' measurement have been described previously elsewhere [7]. The obtained results show possibility to integrate micro-optical components on the top of the fiber and use it for creation of 3D optical circuitries.

1. C.N. LaFratta, J.T. Fourkas, T. Baldacchini and R.A. Farrer, Angew. Chem. Int. Ed., **46**, 6238-6258 (2007).
2. R. Guo, S. Xiao, X. Zhai, J. Li, A. Xia and W. Hung, Opt. Exp. **14** (2), 810-816 (2006).
3. Q-D. Chen, D. Wu, L-G. Niu, J. Wang, X-F. Lin, H. Xia and H-B. Sun, Appl. Phys. Lett. **91,** 171105 (2007).
4. S. Juodkazis, V. Mizeikis, K. K. Seet, M. Miwa and H. Misawa, Nanotechnology **16**, 846-849 (2005).
5. M. Malinauskas, V. Purlys, A. Žukauskas, T. Gertus, G. Bičkauskaitė, M. Rutkauskas, D. Paipulas, P. Danilevičius, H. Gilbergs, D. Baltriukienė, A. Kraniauskas, R. Širmenis, V. Bukelskienė, R. Gadonas, V. Sirvydis and A. Piskarskas, Proc. SPIE (to be printed 2010).
6. A. Ovsianikov, A. Gaidukevičiūtė, B.N. Chichkov, M. Oubaha, B.D. MacCraith, I. Sakellari, A. Giakoumaki, D. Gray, M. Vamvakaki, M. Farsari and C. Fotakis, Laser Chem. 2008, 493059 (2008).
7. M. Malinauskas, H. Gilbergs, A. Žukauskas, V. Purlys, D. Paipulas and R. Gadonas, J. Opt. **12**, 1-8 (2010).

PP64

EFFICIENT ABLATION OF *EX VIVO* CORNEA USING THE FIFTH HARMONIC OF FEMTOSECOND YB:KGW LASER

E. Gabrytė[1, 2], M. Vengris[1], R. Danielius[2], O. Rukšėnas[3], A. Vaičeliūnaitė[3]

[1] *Laser Research Centre, Faculty of Physics, Vilnius University, Lithuania*

Egle.Gabryte@ff.vu.lt

[2] *Light Conversion Ltd, Lithuania*

[3] *Faculty of Natural Sciences, Vilnius University, Lithuania*

Corrective eye surgery is a rapidly developing and promising field of ophthalmology [1, 2]. Processes of corneal flap creation and shaping of cornea are currently performed using two different lasers (ArF excimer and femtosecond solid-state), or excimer laser in combination with microkeratome [3]. In this study, we aim to develop an universal solid-state femtosecond laser that can be used during both stages of the surgery.

Here we presented the system of all-solid-state femtosecond laser and a fifth harmonic generator and its applications to the ablation of transparent materials, including PMMA plastic, gelatine and *ex vivo* porcine corneas (Fig. 1). Spherical structures were produced in samples of these materials. Resulting surfaces possessed a fine optical quality. Corneal shaping to the 12 D refraction change lasts ca. 180 s using current system. The presented system has a great potential to be applied in different areas of ophthalmic laser surgery, because it produces high-intensity femtosecond laser pulses at 1027, 514 and 205 nm.

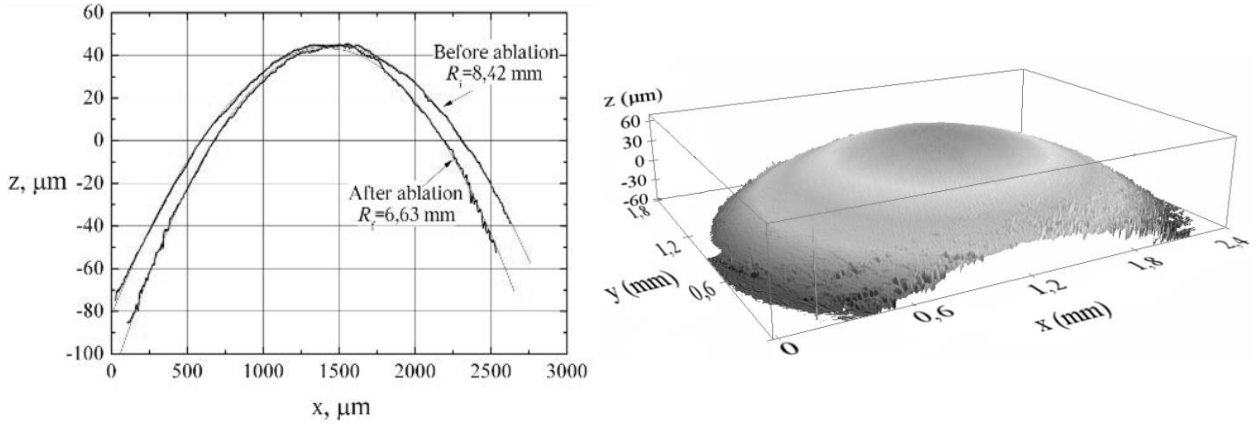

Fig. 1. Results of *ex vivo* porcine corneas shaping. (A) Surface topographic image after ablation; (B) cross-section of corneal surface before and after shaping, resulting a positive 10 D refraction change.

1. I. G. Pallikaris et al., Lasers in Surgery and Medicine, **10(5)**: 463-468 (1990).
2. S.L. Trokel, R. Srinivasan, and B.B. Braren, American Journal of Ophthalmology, **96**: 710-714 (1983).
3. R. Montes-Mico, A. Rodriguez-Galietero, and J.L. Alio, Ophthalmology, **114(1)**, 62-68 (2007).

PP65

TRANSPARENT AND CONDUCTIVE ITO AND IZO COATINGS ABSORPTION MEASUREMENT

G. Šumskis, A. Melninkaitis, V. Sirutkaitis

Laser Research Center, Saulėtekio av. 10, 10223 Vilnius, Lithuania

gediminas.sumskis@ff.stud.vu.lt

Indium oxide doped with tin oxide (ITO) is used to make transparent conductive coatings. Typical applications of such ITO-coated substrates include touch panel contacts, electrodes for LCD and electrochromic displays, energy conserving architectural windows, defogging aircraft and automobile windows. The deposited film layer must contain a high density of charge carriers for it to conduct. These carriers are free electron and oxygen vacancies, and an excessive population produces absorption. High conductivity is balanced against high transmission in the visible region. To obtain transmission near 90%, sheet resistance must be > 100 Ω/sq. Due to the fragility and lack of flexibility of ITO layers, and the costly layer deposition requiring vacuum, alternatives for ITO coatings are being sought. Indium-doped zync oxide (IZO) coatings are a prospective replacement. For particular technical demands it is important to know such parameters as transmission, reflectance and absorption of such coatings.

Transmission of ITO and IZO coatings deposited on 15×15×2 mm BK7 glass plates, and BK7 glass plate without any coating was measured by spectrophotometer in this experiment (Fig.1).

Absorption of the same samples was measured with laser calorimetric system. Absorption measurement was performed using NL220 nanosecond ND:YAG laser's second and third harmonics, 532 and 355 nm respectively. Pulse duration was ~10 ns, repetition rate – 1 kHz. Power of 532 and 355 nm radiation was 380 and 200 mW, respectively. Absorption results (Table 1) were analyzed by three methods, two of them (impulse and gradient methods) are standardized in ISO/DIS 11551 (International Organization for Standardization).

Results show that transmission of IZO and ITO coatings decreases when wavelength becomes shorter. Absorption of ITO and IZO coatings especially increases for 355 irradiance which could become a significant restrictive factor for many applications.

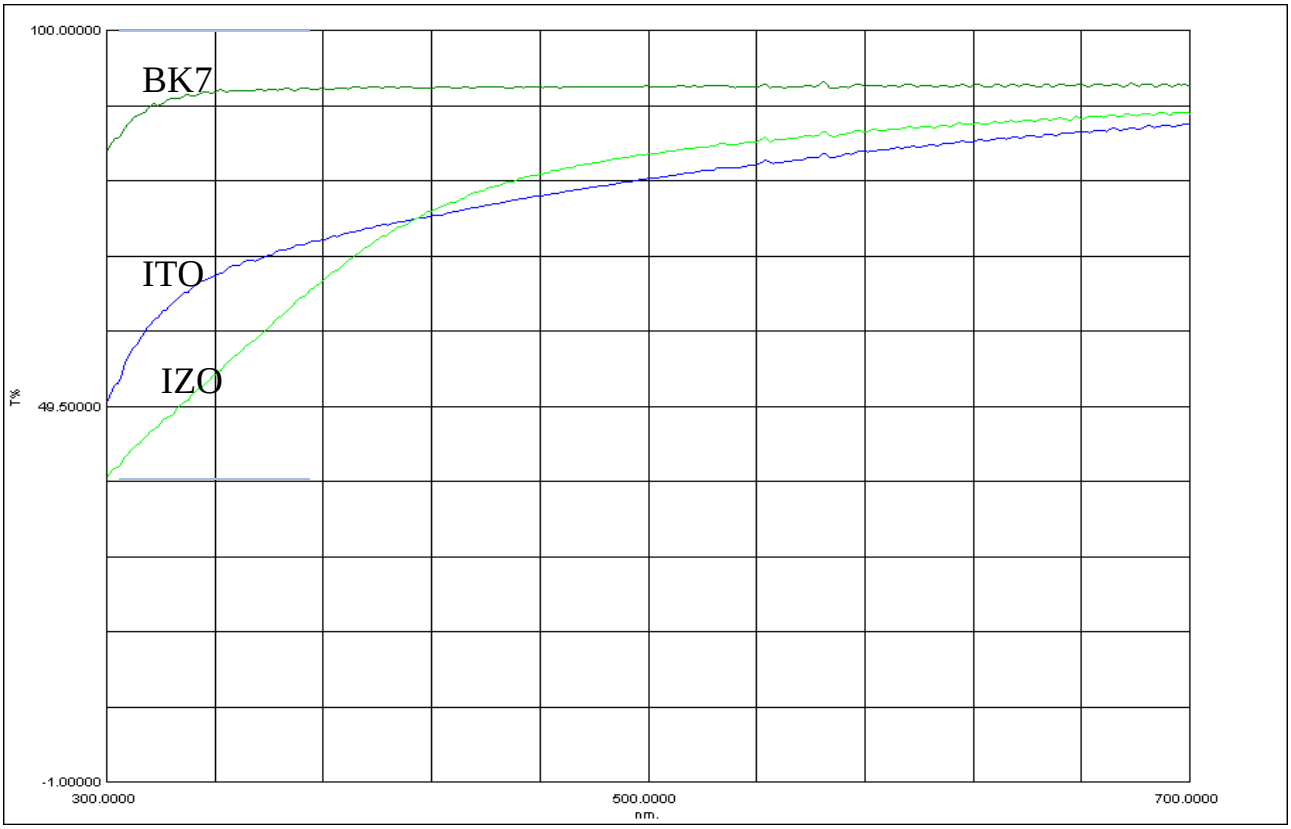

Fig. 1. Transmission of BK7 glass , ITO and IZO coatings.

Material	**Exponential method α, %**	**Gradient method α, %**	**Pulse method α, %**
BK7 (532nm)	0.0675	0.058	0.0713
BK7 (355nm)	0.186	1.15	1.6
ITO (532nm)	0.1933	0.201	0.268
ITO (355nm)	1.2	1.15	1.6
IZO (532nm)	0.147	0.163	0.208
IZO (355nm)	9.29	8.73	12.97

Table 1. ITO and IZO coatings and BK7 glass absorption for 532 and 355 radiation.

1. Chongmu Lee, R. P. Dwivedi, Wangwoo Lee, Chanseok Hong, Wan In Lee, Hyoun Woo Kim, J Mater Sci: Mater Electron **19**:981-985 (2008).
2. International Standard ISO 11551. Test method for absorptance of optical laser components. International Organization for Standardization, Geneva, Switzerland, 1997.

PP66

OBSERVATION OF SPONTANEOUS PARAMETRIC DOWN-CONVERSION EXCITED BY HIGH-BRIGHTNESS BLUE LED

G. Tamošauskas, J. Galinis, A. Dubietis, A. Piskarskas

Department of Quantum Electronics, Faculty of Physics, Vilnius University, Saulėtekio ave. 9-III, LT-10222 Vilnius, Lithuania

justinas.galinis@gmail.com

The spontaneous parametric down-conversion (parametric fluorescence) in crystals with χ^2 nonlinearity was observed experimentally in 1967 [1]. In this process, three optical fields with different frequencies, satisfying conservation of energy and momentum, are coupled through the second-order nonlinearity of the medium. Photon generation via parametric down-conversion, pumped by a laser source of high spatial and temporal coherence, is accessed in many different operating regimes, ranging from a single photon [2] to broadband [3] emission and in a variety of the nonlinear media using different interaction geometries [4]. In this contribution we report how the parametric fluorescence with appreciable power is generated in bulk $LiIO_3$, KDP and BBO crystals, using an incoherent high-brightness blue LED as a pump source [5].

Figure 1 shows examples of the angular distributions of the parametric fluorescence excited in type I phase matching $LiIO_3$, and KDP crystals, recorded with pump power of 0,53 mW, and in type II phase matching BBO crystal, recorded with pump power of 77 μW. The crystal offset Δθ is defined with respect to the scalar phase matching angle for degeneracy θ_s for central pump wavelength (457 nm). We also show how the coherence properties of the parametric fluorescence could be varied by varying spatial and temporal coherence properties of the LED radiation.

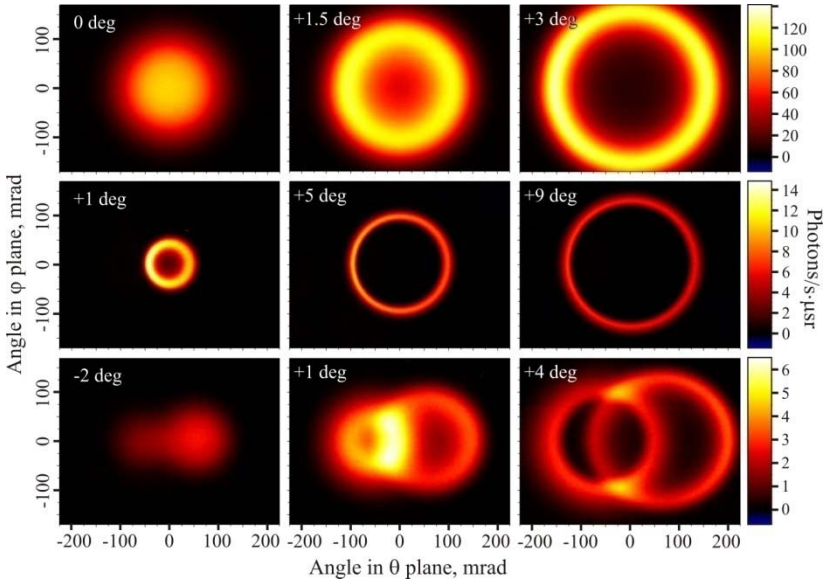

Figure 1. Angular distributions of the parametric fluorescence excited (a)–(c) in LiIO3, (d)–(f) in KDP, (g)–(i) in BBO crystals, recorded at different crystal offset Δθ from the scalar phase matching angle.

Present results suggest that high-brightness LEDs could be used as an attractive alternative to laser sources for excitation of well-detectable parametric fluorescence in bulk nonlinear crystals, so making LED a versatile source for many experiments in quantum optics, for instance, for studies of quantum-classical transitions and for testing of quantum communication networks, to mention a few.

1. S. E. Harris, M. K. Oshman, and R. L. Byer, Phys. Rev. Lett. **18**, 732–734 (1967).
3. S. A. Castelleto and R. E. Scholten, Eur. Phys. J. Appl. Phys. **41**, 181–194 (2008).
4. M. B. Nasr, S. Carrasco, B. E. A. Saleh, A. V. Sergienko, M. C. Teich, J. P. Torres, L. Torner, D. S. Hum, and M. M. Fejer, Phys. Rev. Lett. **100**, 183 -601 (2008).
5. J.Perina, Jr., M. Centini, C. Sibilia, and M. Bertolotti, Phys. Rev. **A 80**, 033844 (2009).
6. G. Tamošauskas, J. Galinis, A. Dubietis, A. Piskarskas, Opt. Express **18**, 4310-4315 (2010).

PP67

RADIOACTIVE RELEASES IN THE ENVIRONMENT

A. Kuzmanović

Department of Physics, Faculty of Natural sciences of University of Novi Sad, Serbia
ancica86@hotmail.com

Radionuclides occur naturally as trace elements in rocks and soils as the products of the radioactive decay of uranium-238 (U-238) and thorium-232 (Th-232). The half-lives of naturally occuring radionuclides are so long that they have not yet completely decayed. They release energy through emitting ionizing radiation, which may be alpha particles, beta particles, or gamma rays. They play an important role in many technologies that provide us with food, water and good health.

Nowadays one can choose an appropriate method for calculating the number of radionuclides in the environment and see how the results can be calculated.

One of the main principles used, is mathematical modeling of the dispersion of radionuclides in the environment, and concentrations of radionuclides in aquatic and terrestrial environments. This search operates with informational parameters based on the movements of radioactivity in aquatic and terrestrial systems.

1. John R. Cooper, Keith Randle, Ranjeet S. Sokhi, *Radioactive releases in the environment– impact and assessment (*John Wiley and Sons, 2003).

PP68

MERCURY CONCENTRATION MEASUREMENTS IN PEAT OF OMBROTROPHIC BOGS IN LATVIA

A. Svagere, M. Zinge

Institute of Atomic Physics and Spectroscopy, University of Latvia, Skunu street 4, LV – 1050 Riga, Latvia
anda.svagere@gmail.com

For a long time it is well known that mercury and its compounds are highly toxic to humans, ecosystems and wildlife. Mercury is not usually found free in nature and is primarily obtained from the mineral cinnabar; additional releases from anthropogenic sources have led to significant increase in environmental exposure and deposition. Due to mercury toxicity it is important to understand historical trends of its release.

Wetlands play an important role in the transport and cycling of Hg in nature. Ombrotrophic bogs are isolated from the influence of local ground water and surface water, and receive their inorganic content by atmospheric deposition only, therefore, the peat from such bogs can be used to study long-term historical trend of atmospheric metal deposition.

Mercury was analyzed in several peat samples from three ombrotrophic peat bogs located in Latvia (*Dizais Veikenieks*, *Taurene*, *Dzelve*). The mercury distribution profile in the upper layer with thickness up to 120 cm was analyzed using mercury analyzer RA-915+.

Method used for the mercury determination in peat is based on the atomization of mercury contained in the sample in an RP-91C attachment and subsequent mercury determination by flameless Atomic Absorption Spectroscopy (AAS) in a mercury analyzer RA-915+. Using mercury analyzer RA-915+ together with attachment RP-91C allows determination of mercury in soil and other similar samples without specific sample preparation and mercury accumulation on a sorbent.

Mercury content in the sample is determined from the integrated analytical signal with the account of the preset calibration coefficient. The sample is weighed and put into the injection spoon of the RP-91C attachment. Integration of the analytical signal is turned on and the injection spoon is placed into the attachment. The measurement time for a single sample is less than 2 minutes.

Measured mercury concentrations in peat bog *Dizais Veikenieks* range from 30 to 120 µg/kg. The lowest mercury concentration was determined at the surface (about 30 µg/kg), then it increases reaching 120 µg/kg, at the depth of 100 cm, followed by sharp decrease till 40 µg/kg (in the depth of 120 cm). However, in bogs, *Taurene* and *Dzelve*, concentrations are smaller – they are in range 15 µg/kg - 60 µg/kg and 17 µg/kg - 120 µg/kg, respectively. In peat bog *Taurene* mercury

concentration smoothly decreases with increasing depth, but in *Dzelve* we can observe a peak at 70-75 cm, reaching 120 µg/kg, rapidly decreasing afterwards and getting to the lowest value, 17 µg/kg, at 100 cm depth. At the surface Hg concentration was determined to be about 85 µg/kg.

Similar measurements have been performed all over the world, for example in Norway [1], Chile [2] and Switzerland [3], and determined mercury levels are of the same order-of-magnitude as measured in this work.

Acknowledgments: The work was partly supported by European Social Fund project Nr. 2009/0210/1DP/1.1.1.2.0/09/APIA/VIAA/100.

1. E. Steinnes, T.E. Sjobakk, Environmental Pollution **137**, 365-370 (2005).
2. H. Biester, R. Kilian, C. Franzen et al., Earth and Planetary Science Letters **201**, 609-620 (2002).
3. F. Roos-Barraclough et al., Earth and Planetary Science Letters **202**, 435-451 (2002).

PP69

HIGH AEROSOL CONCENTRATION IN LITHUANIA CAUSED BY LONG RANGE TRANSPORT: EPISODE ON MARCH 31 – APRIL 3, 2008

J. Kilpys, V. Ulevicius, S. Kecorius, J. Andriejauskiene, V. Remeikis, A. Garbaras

Institute of Physics, Savanoriu ave. 231, LT-02300 Vilnius, Lithuania

simolas2008@gmail.com

Particulate air pollution plays important role in the atmospheric radiation balance and can influence global and regional climate. Moreover, it can cause a variety of respiratory and cardiovascular system diseases. Such effects depend on the particle size, concentration and chemical composition. The main sources of fine particles are their secondary formation by gas-to-particle conversion process in the atmosphere and primary emissions. However, if local emissions are low, high aerosol particle concentration levels could be associated with long range transport of such particles [1, 2]. The goal of this study is to examine the unusual high aerosol particle concentration event caused by long range transport.

We analyzed data from Preila environmental pollution research station and Vilnius air quality stations. Preila station is located on the coast of Baltic Sea, on the Curonian Spit, and is far from substantial local sources airborne pollutants and thus can be characterized as a regionally representative background site. Continuous BC measurements were performed using the Aethalometer AE31 (Magee Scientific Company). The optical transmission of carbonaceous aerosol particles was measured sequentially at seven wavelengths (370, 450, 520, 590, 660, 880 and 950 nm). The concentration of black carbon corresponds to the 800 nm wavelength. The total aerosol concentration was measured by using Condensation Particle Counter (CPC) UF-02 (Institute of Physics), which can register 4.5 nm particles. The PM10 measurement data from two Vilnius air quality stations were analyzed. Zirmunai station represents a downtown area with very active transport system, and Lazdynai station is an urban background station. The air mass backward trajectories were calculated to find out the origin of air mass during this event. The series of three-day air mass backward trajectories were calculated for the entire period using the Hybrid Single – Particle Lagrangian Integrated Trajectories model Version 4 (HY-SPLIT) (NOAA) [3]. Fire maps were used to show burning of biomass, because the March 31 – April 3 event is characterized by high BC concentration. Fire maps were collected using FIRMS (Fire Information for Resources Management System). Data in FIRMS system are provided by Terra and Aqua satellites Moderate Resolution Imaging Spectrometer (MODIS).

Aerosol particle and BC concentration reached very high levels during the event on March 31 – April 3, 2008. The 1-hour average value of aerosol concentration reached 30 000 cm^{-3}, BC – 19 000 ng/m^3 (fig. 1); usually average particle concentration values vary in the range from 500 to 4000 cm^{-3}, BC – 300 to 1500 ng/m^3. BC measurements are performed at different wavelengths and during this high concentration event measurements at different wavelengths had significant differences (fig. 1b). This shows that there is high organic material content in aerosol. BC is a tracer of primary anthropogenic emissions, and its variability reflects changes in source strengths, long range transport and atmospheric mixing characteristics. Analysis of backward trajectories and fire maps from FIRMS confirmed that there were a lot fires in Ukraine and Russia at the end of March and beginning of April. These grass fires produced a high number of particles with significant BC content. Particles due to long range transport air masses were brought to the territory of Lithuania in 3 days and caused high peaks of aerosol particles and BC concentration (fig. 1).

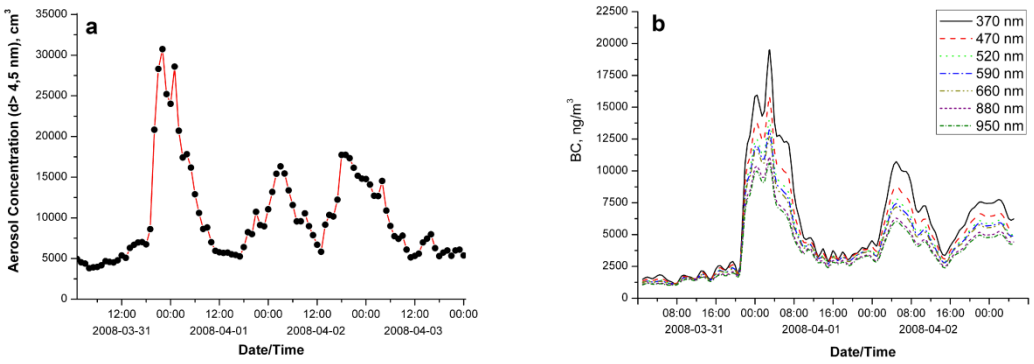

Fig. 2. High aerosol concentration at Preila station on March 31- April 3, 2008: a) aerosol particle hourly variation; b) BC hourly variation.

PM10 concentration exceeded the European PM10 limit value (50 $\mu g/m^3$) during the same event in urban territories of Lithuania. High PM10 concentrations were measured in different districts of Vilnius. At Zirmunai station the PM10 limit values was exceeded 2-3 times on researched event. At Preila station aerosol concentration values were 10 times higher than usual, BC values – 20 times higher.

Acknowledgment: This research described in this paper was supported partially by FP6 projects ACCENT and EUSAAR. The authors are grateful for this assistance.

1. Andriejauskiene J., Ulevicius V., Bizjak M., Spirkauskaite N., Byčenkienė S., Lithuanian Journal of Physics **48**, 183-194 (2008).
2. Wuzler S., Niemann K., Engel I., Garus G., Olschewski A., Friesel J., Pfeffer U., Hoogerbrugge R., Bruckmann P. European Aerosol Conference 2008, Thessaloniki, Abstract T06A1790.
3. Draxler, R. R., & Hess, G. D. (1997) NOAA Tech Memo ERL SRL-**224**, 24p.

PP70

DYNAMIC CLUSTER DEVELOPMENT FOR SIMULATION CLASS

G. Bašinskas, R. Jasinskas

Department of Theoretical Physics, Faculty of Physics, Vilnius University, Sauletekio ave. 9-III, LT-10222 Vilnius, Lithuania

drakagytis5@gmail.com

The computational science community is on the cusp of a new era in high-performance computing. Our objective was to create a place for students to work with multiprocessing and molecular simulations, which requires high computing resources. In addition, we wanted to use our university resources as efficiently as possible. We used a simple simulation class at university and design a dynamic cluster, as clusters have clear price/performance, user interface, and maintenance advantages over traditional supercomputers [1].

Cluster objectives:

a) to make sure students can use parallel processing and molecular simulations on the cluster and it will not affect ordinary usage of the computer class.

b) automatic maintenance and monitoring of this dynamic cluster.

c) cluster modifications for optimal performance.

d) ability to work from home.

1. G. Heber, D. Lifka, and P. Stodghill. Post-Cluster Computing and the Next Generation of Scientific Applications, Sixth World Multiconference on Systemics, Cybernetics and Informatics, June, 2002.

PP71

EFFECT OF QUANTUM DOT-PROTEIN INTERACTION ON STABILITY AND SPECTRAL PROPERTIES OF CdTe QUANTUM DOTS IN AQUEOUS MEDIA

M. Matulionytė[1], D. Motekaitis[1], V. Poderys[1,2], R. Rotomskis[1,2]

[1] *Laser Research Center, Department of Quantum Electronics, Faculty of Physics of Vilnius University, Saulėtekio ave. 10, LT-10223 Vilnius, Lithuania*

maria.matte@gmail.com

[2] *Laboratory of Biomedical Physics, Institute of Oncology, Vilnius University, Baublio 3b, LT-08406, Vilnius, Lithuania*

Fluorescent semiconductor nanoparticles – quantum dots – are very promising fluorescent markers due to their unique optical properties, however it is very little known about interaction of quantum dots with biomolecules. It is of great importance to know biological effects of quantum dots before using them in medicine. Stability and spectral properties of CdTe quantum dots in aqueous media and effect of quantum dot – protein interaction on these properties were investigated using steady state and time resolved spectroscopy and atomic force microscopy.

Quantum dots in aqueous solution without protein appeared to be not stable – after 144 hours photoluminescence intensity of quantum dots solution in saline started to decrease, photoluminescence band started getting narrower and shifted to longer wavelength region. Simultaneously absorption slightly decreased. This indicates aggregation of quantum dots. At 270th hour photoluminescence intensity was close to zero and after nine days precipitate was observed. Atomic force microscopy measurements confirmed quantum dots aggregation.

Addition of BSA changed dynamics of quantum dots spectral properties in aqueous solution. A sudden increase of photoluminescence intensity was observed after addition of BSA. Photoluminescence intensity further increased for 64 hours. After that photoluminescence intensity started decreasing but even after two months did not drop below half of the value of initial intensity, no precipitate was observed. This shows that bovine serum albumin stabilizes quantum dots and prevents them from aggregation. AFM image of a sample prepared from solution that was kept for two months also showed that bovine serum albumin stabilizes quantum dots and prevents from aggregation.

Time resolved spectroscopy studies showed that photoluminescence of quantum dots without protein decays faster, decay is described with four exponents (χ^2=1.018) while photoluminescence decay of quantum dots with BSA is tri-exponential (χ^2=1.063). Photoluminescence liftetime

analysis showed that in case of quantum dots with BSA fastest relaxation component (τ_1=3.4ns) disappeared. Fastest relaxation component should be related with defects of quantum dots. Elimination of the fastest non-radiative relaxation path increased photoluminescence quantum yield of quantum dots.

Our study revealed that BSA interacts with CdTe-TGA quantum dots, increases photoluminescence quantum yield, prevents from aggregation and makes them stable.

PP72

MODELING OF PROCESSES OF ORGANIC MOLECULES BY MOLECULAR DYNAMICS AND QUANTUM MOLECULAR DYNAMICS METHODS

R. Danilevičius, J. Šulskus

Department of Theoretical Physics, Faculty of Physics, Vilnius University, Sauletekio ave. 9-III, LT-10222 Vilnius, Lithuania

danilevicius.r@gmail.com

The aim of the study was to test classical molecular dynamics' and quantum molecular dynamics' computational methods and software from short picoseconds' to long – hundreds of nanoseconds' processes.

VASP [1] (*Vienna Ab Initio Simulation Package*) was installed in cluster and supercomputer in Department of Theoretical Physics. Package uses DFT (*Density Functional Theory*) and Car-Parrinello molecular dynamics calculation methods with ultra-soft and PAW (*Projector Augmented Waves*) pseudopotentials' basis. All calculations were processed using department cluster with 8 to 96 processors. GGA (*Generalized Gradient Approximation*) and Perdew-Wang (PW-91) [2] functional was used to approximate exchange-correlation energy.

As an example of short organic molecular process a double proton transfer in $DCOOH_2$ (*formic acid dimmer*) was chosen. DIIS (Direct Iteration in Subspace) and CG (Conjugate Gradient) optimization algorithms were used to optimize the ground state structure. Parameters of 20 ps molecular dynamics process were as in [3] calculation.

The results were similar to [3], however the time when the double proton transfer was calculated was 10 ps earlier than in [3]. The main reason of this difference is the structure's optimization caused changes in geometric parameters.

Simulation for indolobenzoaxizine [4] molecule was performed in order to evaluate the times necessary for relaxation from one local minimum in the ground electronic state to another. The times of evaluation are of the order of 100 ns. It is enormously long for VASP calculations. NAMD [5] classical molecular dynamics package did the calculation in a reasonable amount of time, but the methods were not sufficient for the process, as it has several local minimum states, although classical molecular dynamics' methods can not let the structure climb from the local minimum to another. Indolobenzoaxizine molecule changes it’s geometry after electronic excitation. In order to evaluate possible relaxation to different local structures of the ground electronic state excited states

energies for different potential energy surface points were evaluated by Gaussian 03 [6] quantum chemistry package.

1. Kresse G., Marsman M, Furthmuller J. *VASP the Guide* (Austria : Universitat Wien 163, 2009).
2. J.P. Perdew, J.A. Chevary, S.H. Vosko, K.A. Jackson, M.R. Pederson, D.J. Singh, and C. Fiolhais.. Phys. Rev. B, **46**:6671,(1992).
3. Shetty S., Pal S., Kanhere D. G., Goursot A. *A quantitative and a qualitative study of the resonance assited double proton transfer in formic acid dimer* 30**.**
4. Barkauskas M., Martynaitis V., A. Šačkus, Rotomskis R., Sirutkaitis V., Vengris M. Lithuanian J. Phys. 48, **11 (**2008).
5. James C. Phillips, Rosemary Braun, Wei Wang, James Gumbart, Emad Tajkhorshid, Elizabeth Villa, Christophe Chipot, Robert D. Skeel, Laxmikant Kale, and Klaus Schulten. Journal of Computational Chemistry, **26**:1781-1802,(2005).
6. Gaussian 03, Revision D.01, M. J. Frisch, et al., Gaussian, Inc., Wallingford CT, 2004.

PP73

RAMAN STUDY ON THE CONFORMATIONAL EQUILIBRIUM OF 1-DECYL-3METHYL IMIDAZOLIUM BROMIDE

T. Geryba, R. Cechanavičius, V. Aleksa

Department of General Physics and Spectroscopy, Faculty of Physics, Vilnius University, Sauletekio ave. 9-III, LT-10222 Vilnius, Lithuania

tomas.geryba@ff.stud.vu.lt

The interest in ionic liquids increased rapidly by a growing number of scientists and engineers as demonstrated by the increasing number of papers published in recent years. Study of ionic liquids based on imizadolium elucidate that up to four or even more conformations may exist [1].

Raman spectra of 1-decyl-3methyl imizadolium bromide were recorded at temperature range of –40°C ÷ 130°C. It is noticed that *anti* conformers superiority against *gauche* increases when temperature decreases from 130°C to 7°C. Especially it is noticible at crystal phase [2].

Aproximate description of vibrational frequencies and intensities of Raman bands was determined from *ab-initio* model calculations on 1-decyl-3methyl imizadolium bromide *anti* conformer.

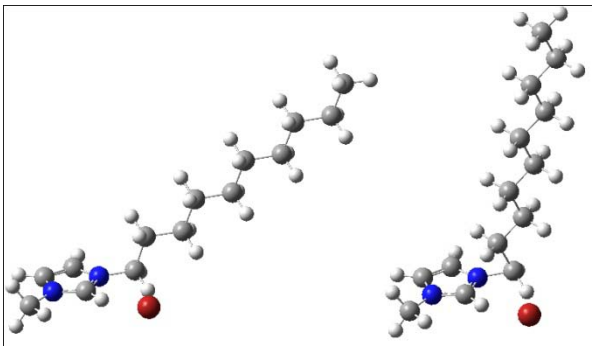

anti *gauche*

Fig 1. Conformers of 1-decyl-3-methyl imidazolium bromide

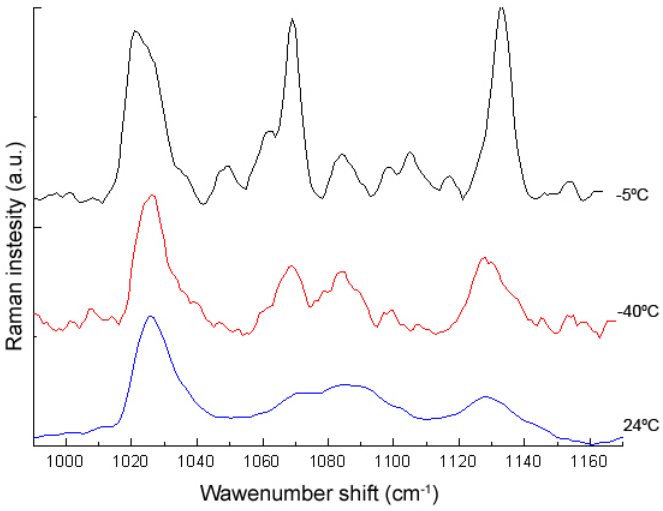

Fig. 2. Raman spectra of 1-decyl-3-methyl imidazolium bromide at different temperatures.

1. Rolf W. Berg, Raman Spectroscopy and Ab-Initio Model Calculation on ionic Liquids, Monatshefte für Chemie **138**, 1045–1075 (2007).
2. H. Hamaguchi, R. Ozawa, Structure of Ionic Liquids and Ionic Liquid Compounds: Are Ionic Liquids Genuine Liquids in the Conventional Sense?, Adv. in Chem. Ph. **131**, 85–102 (2005).

PP74

RAMAN SPECTROSCOPY STUDY ON WATER AGGREGATION IN 1-DECYL-3-METHYL IMIDAZOLIUM BROMIDE

J.Kausteklis, V.Aleksa

Department of General Physics and Spectroscopy, *Faculty of Physics, Vilnius University, Sauletekio ave. 9-III, LT-10222 Vilnius, Lithuania*

jonas.kausteklis@ff.stud.vu.lt

In many fields of application ionic liquids are involved as solvents. Important research direction is physical and chemical properties, their assurance of stability and variation identification. Water can significantly change the properties of ionic liquid. Electrical conductivity, solubility, viscosity, polarity can be changed by impurities, especially water [1]. Therefore the exact ionic liquid aqueous solution behavior must be carefully analyzed in order to further broaden the scope of the use of chemicals.

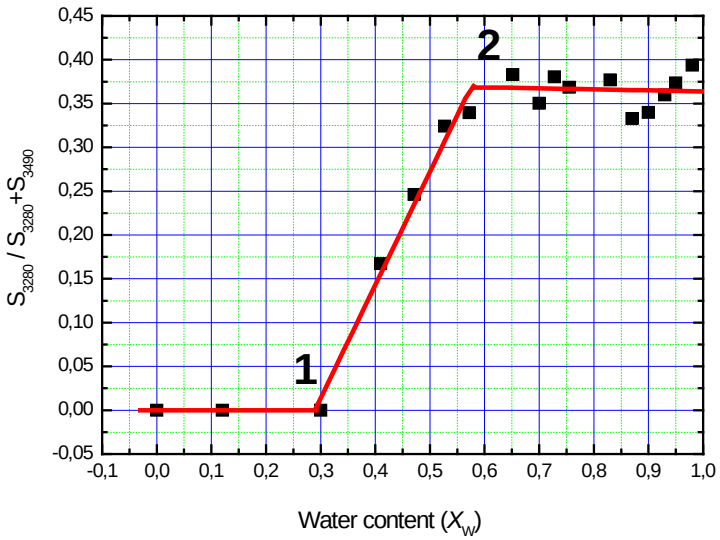

Fig. 1. Fraction of water molecules organized in network to the total self-aggregated water plotted vs X_M.

Raman spectroscopy has been used to investigate water role on the structural organization of 1-decyl-3-methylimidazolium bromide and H_2O mixtures over wide water concentration range (0 – 98 %) at room temperature. Two-dimensional correlation analysis let us look deeper in water molecules stretching spectral components. Indications of water molecules aggregation in network were obtained during the wide water concentration range (Fig 1). Break points (1,2) at water

concentrations 0,3 and 0,61 let us made a proposal how to explain water molecules organization in ionic liquid [2].

1. Y. Danten, M.I. Cabac, M. Besnard., Journal of Physical Chemistry **113,** 2873–2889, (2009).
2. B. Fazio, A. Triolo and G.Di Marco. Journal of Raman Spectroscopy **39**, 233–237 (2008).

PP75

APPLICATION OF LASER METHODS FOR DIAGNOSTICS AND TREATMENT OF THE INTERVERTEBRAL DISC DISEASES

D. Varanius[1], G. Terbetas[2], A. Vaitkuvienė[3]

[1, 3] *Vilnius University Institute of Applied Research, Saulėtekio av. 10, LT-10223 Vilnius, Lithuania*

Darius.Varanius@gf.stud.vu.lt

[2] *Vilnius University Clinics of Neurology and Neurosurgery, Šiltnamių 29, LT-04130 Vilnius, Lithuania*

The results indicate that auto fluorescence refers to different substances constituting intervertebral disc [1]. Spectral analysis can be used to determine biochemical changes in collagen types content of intervertebral disc matrix, and signs of disc degeneration can be identified indirectly. Spectroscopic investigation of degenerated disc according to the shape of spectra and spectroscopy may be a new very sensitive tool in determining changes in different anatomical parts of degenerating intervertebral disc.

The results allow to conclude that besides the classical open discectomy, new minimally invasive techniques of treating intervertebral disc emerges. Percutaneous Laser Disc Decompression (PLDD) has been recently accepted as effective surgical intervention on certain types of disc herniations [2]. Open discectomy and PLDD should not be compared as two different ways of treating the same patient because inclusion criteria for both methods differ due to morphology of disc herniation on MRI [3]. Intervertebral disc in laser surgery is assessed by needle under radiology control, no histological specimen is taken. Incorporation of spectral analysis in minimally invasive disc surgery is the challenge of nearest future. Spectroscopic investigation via fiber optics through the needle could give additional information of needle position, assuring the needle tip is directed into intervertebral disc material.

Spectroscopic analysis of intervertebral disc removed during open surgery, creates background for further investigation on degenerating intervertebral disc spectral features and biochemical changes.

1. T. Hoell, G. Huschak, A. Beier, G. Huttmann, Y. Minkus, H. J. Holzhausen, H. J. Meisel, Eur Spine J **15** (Suppl. 3):S345–S353 (2006)
2. Choy DSJ. *Percutaneous laser disc decompression: a practical guide.* (New York: Springer-Verlag, 2003).
3. John S. Thalgott, Todd J. Albert, Alexander R. Vaccaro, Charles N. Aprill, James M. Giuffre,John S. Drake, Jonathan P. Henke, The Spine Journal **2004**:167S–172S (2004);

PP76

APPLICATION OF FT-IR SPECTROSCOPY TO STUDY THE POLICHROMY OF EGYPTIAN SARCOPHAGUS

E. Rusinaite, T. Tichanavičius, V. Aleksa

Department of General Physics and Spectroscopy, Faculty of Physics, Vilnius University, Sauletekio ave. 9-III, LT-10222 Vilnius, Lithuania

egle.rusinaite@yahoo.com

Egyptian sarcophagus of the god‘s Amon singer (Thebes XI - IX century BC) represents the core of ancient Egyptian art in M. K. Čiurlionis Art Museum. This is the only such exhibition in Lithuania. The study of materials used by the artist is useful both for the knowledge of the artwork and for conservation and restoring interventions using Kremer pigments [1, 2].

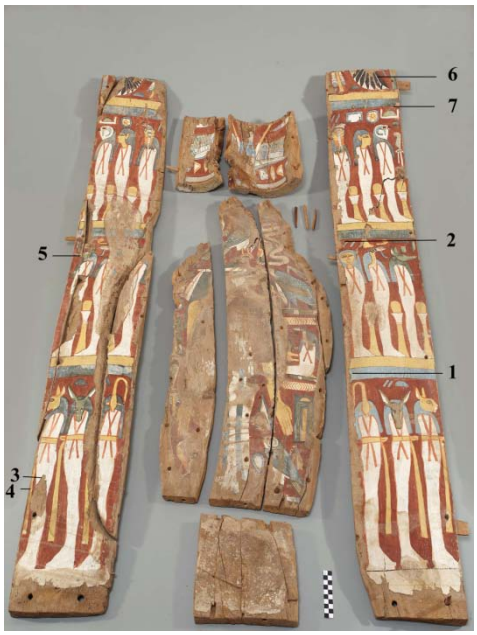

Fig. 1. Egyptian sarcophagus of the god’s Amon singer and sampling location (1-7).

Spectroscopic methods are widely used in analysis of art polychromy. Fourier transform - infrared spectroscopy (FT-IR) represents a powerful technique in diagnostic analysis of cultural heritage [1,3]. In this study the samples of sarcophagus were investigated by FT-IR absorption spectroscopyc, FT-IR microscopy and ATR methods.

Chalk, gypsum and animal glue were detected in all samples. The conclusion was made that sarcophagus soil consists of these materials. It was found that the green pigment is *emerald green* and azurite, white pigment is chalk and glue.

FT-IR absorption spectroscopy method is effective in the ground and soil spectral analysis, but for identification of pigments is insufficiently informative because of samples preparation method shortcomings. FT-IR microscopy and ATR techniques are suitable for sarcophagus surface spectra analysis.

A comparative analysis of the spectral methods (FT-IR, FT-IR microscopy, ATR and Raman) used in investigations of samples was performed.

1. E.L. Kendix, S. Prati, E. Joseph, G. Sciutto, R. Mazzeo, Anal Bioanal Chem. **394**, 1023-1032 (2009).
2. H. Brecoulaki, E. Fiorin, P.A. Vigato, Journal of Cultural Heritage **7**, 301-311 (2006).
3. J.R. Barnett, S. Miller, E. Pearce, Optics & Laser Technology **38**, 445-453 (2006).

PP77

RAMAN SPECTROSCOPIC STUDY OF ACETONITRILE CLUSTERS IN WATER AND IONIC LIQUIDS

D. Jankaitytė, L. Tamašauskas, V. Aleksa

Vilnius University, Faculty of Physics, Department of General Physic and Spectroscopy, Saulėtekio al. 9 – 3, LT – 10222 Vilnius, Lithuania

dovile.jankaityte@ff.stud.vu.lt

Acetonitrile (AN) is an important solvent and cosolvent, where C≡N vibration is of particular interest because of the specific shape of the band and unusual sensitivity of the band to the molecule‘s environmen. The molecules of AN in the liquid state may be in monomer (M) and aggregated (dimer (D), Fig.1.) states. Besides AN molecules easily form intermolecular bonds if they are in mixture with a solvent [1,3].

Raman scattering spectra of pure acetonitrile and mixture with water and ionic liquids in the C≡N stretching region were recorded in altering the temperature within 296 - 361 K. Experimental spectra of acetonitrile mode ν_2 (C≡N) were processed using two dimensional (2D) correlation method [2].

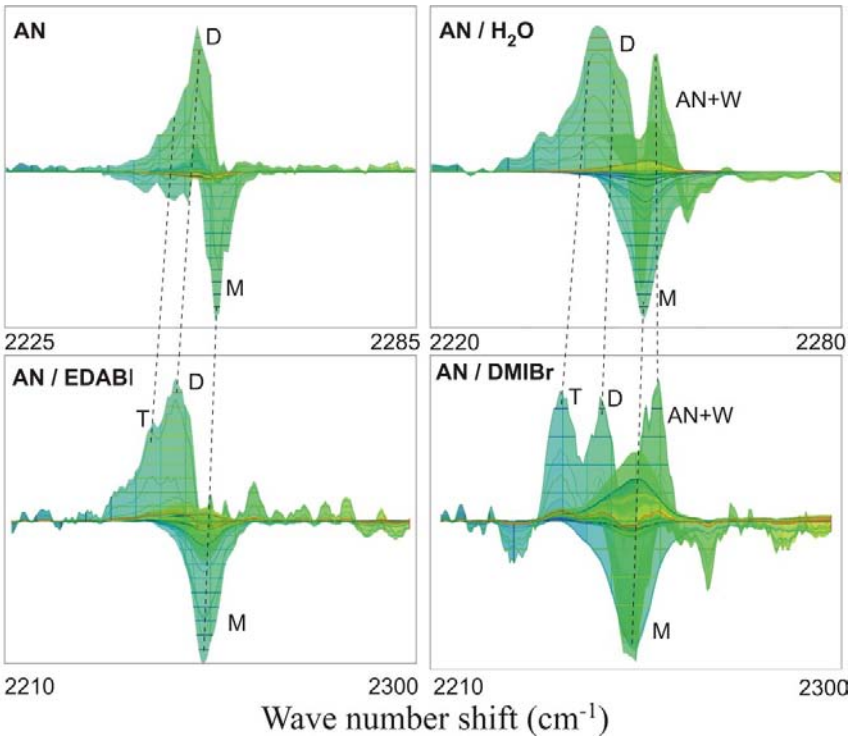

Fig. 1. Pseudo-three-dimensional representation of the asynchronous 2D Raman scattering correlation spectra in C≡N stretching region of pure AN and AN/ H_2O, AN / 1-decyl-3-methylimidazolium bromide (DMIBr) and AN / ethyl-dimethyl-propylammonium bis(trifluoromethylsulfonyl)imide (EDABI) solutions.

The structure of C≡N stretchi ng band which consist of several peaks is considered. Analysis of the different overlapping Lorentzians has shown possibility of formation of monomers, dimers, tetramers, complexes of acetonitrile/water and other structures.

1. F. H. Tukhvatullin, A. Jumabaev, G. Muradov, H. A. Hushvaktov and A. A. Absanov, Journal of Raman spectroscopy, **36**, 932-937 (2005).
2. I. Noda, Analytical sciences, **23**, 139 – 146 (2007).
3. Rolf W. Berg, Monatshefte für Chemie, **138**, 1045–1075 (2007).

PP78

CONFORMATIONAL CAPACITY OF QUERCETIN MOLECULE: AB INITIO STUDY

I.O. Protseko[1], L.A. Bulavin[1], D.M. Hovorun[2]

[1] *Molecular Physics Department, Faculty of Physics,Taras Shevchenko National University of Kyiv, Kyiv, Ukraine*

irene.protsenko@gmail.com

[2] *Institute of Molecular Biology and Genetics, National Academy of Sciences of Ukraine,Kyiv, Ukraine*

Quercetin – is a biologically active compound, which is found in many plants, such as a bow, garlic, carrot, whortleberries and other, also in red wine and green tea. It used widely in medicine and pharmaceutics. In particular it is used as a prophylaxis and treatment of oncologic diseases, especially it restrains growth of leukemia. Quercetin, as well as other bioflavonoid, protects the cardiovascular system from harmful influence of cholesterol.

That is why the further researching of this molecule is important. The purpose of this work was an ab initio quantum mechanics calculation of spatial molecular structure of quercetin. These researching of quercetin could explain its multifunctional characteristics, which could enable to estimate its structural factors of biological activity, in particular the presence of strong intramolecular hydrogen bonds (further will use as H-bonds) in all conformers. One of the tasks was to search all permissible conformers and to reveal the most beneficial energy conformers; and ways of their interconversions.

In this work were used Gaussian 03w and AIM2000 application programs that, to our opinion, most adequate to the decision of the put task. Using these packages, we can construct a computer experiment and then define the geometrical structure of, and calculate the intramolecular H-bonds.

Calculations of geometric structure of quercetin were transacted in full optimization conditions. We researched all possible conformers (Fig.1), which obtained from one another conformation by changing torsion angle for 180° round the single bond between phenyl and hetero-rings. Based on these two conformers was also found transition state using QST3 algorithm.

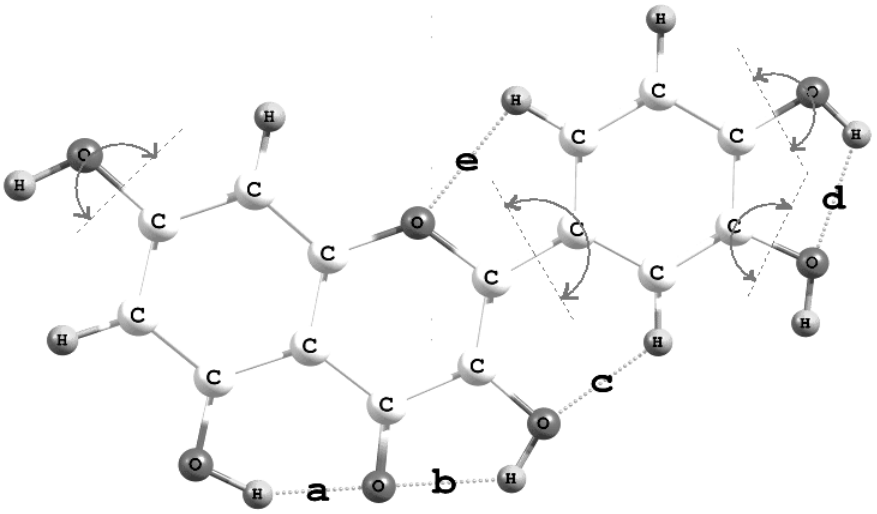

Fig.1. A schematic view of quercetin molecule (dot lines – H-bonds, circular arrows – show rotate groups, that change and create new conformation).

The calculable experiment showed, that the spatial structure of quercetin molecule has 12 mirror symmetrical pairs of conformers, which have a propeller orientation planes of planar hetero- and supple phenyl rings. It is discovered that a molecule of quercetin is a dipole unstable molecule and which geometry depends on a temperature.

The main result is that we found the most energy-efficient conformation, and available in each conformer H-bonds. In addition to the above we can say that almost all conformers have the same number of H-bonds, which energy differ just for 0,1-0,3 kcal/mole, even in transition state some intramolecular H-bonds didn't break. The hydrogen bond energy analysis [1] was performed.

It was found out that some hydrogen connections are not torn, even in the supple form of molecule, which testifies to their durability. Consequently, quercetin has flexible structure. Such plasticity is very comfortable for a liquid environment (namely for formation new molecules): as a molecule has considerable amplitude of oscillation. It means that at a supple form has greater probability of co-operating with other molecules.

1. Espinosa E., Molins E., Lecomte C., Chemical Physics Letters **285**, 170-173 (1998).

PP79

INVESTIGATION OF THE VARIATIONS IN THE ATMOSPHERIC RADIO REFRACTIVITY

E. Valma[1], M. Tamošiūnaitė[1], M. Svetikas[2]

[1] *Institute of Applied Research, Vilnius University*

egidijus.valma@ff.stud.vu.lt

[2] *Technology Faculty, Šiauliai University*

The value of the radio refractive index (the ratio of the radio wave propagation velocity in free space to the velocity in specified medium [1]) depends on the atmospheric pressure, temperature, and relative humidity. Even small changes in the meteorological parameters mentioned above may affect the radio wave propagation, because the signal can be refracted by many times over the entire track in the locality [2]. The electromagnetic wave path becomes curved because the wave encounters variations in the atmospheric radio refractive indices along its trajectory [1].

In Lithuania, the values of the temperature, relative humidity, and atmospheric pressure vary from place to place and in the time. Therefore it is important to analyze the changes in the radio refractive indices both in the localities of Lithuania and in time.

The value of radio refractive index is very close to the unit and the changes in this value are very small in time and space. With the aim of making them more visible, the term of refractivity N is used [1], [3]–[4]:

$$N = (n-1)\times 10^6, \tag{1}$$

According to [4]:

$$N = \frac{77.6}{T}\left(p + 4810\frac{e}{T}\right), \tag{2}$$

where T (K) is temperature; p (hPa) is the atmospheric pressure: e (hPa) is the partial water vapor pressure.

The relationship between e and the relative H (%) is [1], [3]:

$$e = \frac{He_s}{100}. \tag{3}$$

In the localities of Lithuania (Vilnius, Mažeikiai, Kaunas and Klaipėda), the values of the radio refractivity N have been determined by using Eqs. 1–3. The meteorological data (taken from http://www.rp5.ru/archive.php?wmo_id=) of the years 2008 and 2009 have been used. It was concluded that the time responses of N–values averaged over the month are near the same in Vilnius, Mažeikiai, and Kaunas (in Continental Part of Lithuania) and it is different from ones in

Klaipėda. Therefore, the data obtained in Vilnius and Klaipėda has been analyzed (see Fig. 1.) in more detail. The *N*–values were averaged over two years (2008 and 2009).

The data presented in Fig. 1 show that the highest values of *N* were in July in both localities mentioned above. The maximum *N*–value of *N* = 350.1 *N*–units was observed in July 2009 and the minimum one of *N* = 312.8 *N*–units was in Vilnius in October 2009.

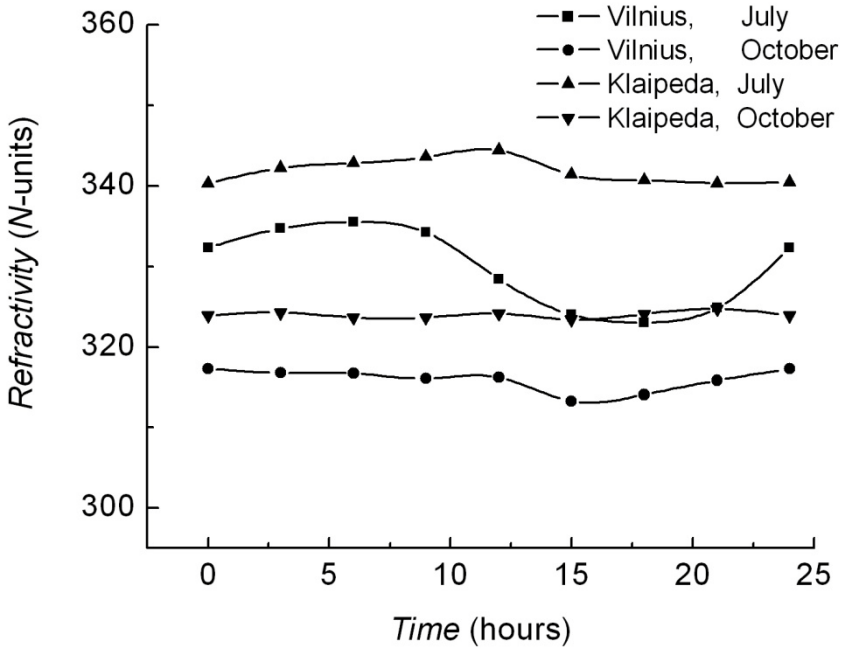

Fig. 1. The variations of averaged refractivity *N* depending on time of the day.

More noticeable variations in the radio refractivity values were observed in July in both localities: (ΔN =12.5 *N*–units in Vilnius and ΔN =4.1 *N*–units in Klaipėda). In October, ΔN =4.1 *N*–units in Vilnius and ΔN =12.5 *N*–units in Klaipėda. The minimum values of *N* were in the afternoon in Vilnius. The variations in the radio refractivity values are negligible in Seacoast (due to the influence of Baltic Sea) and more noticeable in Continental Part of Lithuania.

1. R. L. Freeman, Radio System Design for Telecommunications, Third Edition (WILEY–INTERSCIENCE, JOHN WILEYand SONS, INC., New York, 2007).
2. D.Serdega. and G. Ivanovs, Refraction seasonal variation and that influence on to GHz range microwaves availability, Electronics and Electrical Engineering, **6(**78) 39–42 (2007).
3. The radio refractive index: its formula and refractivity data, in: Recommmendation ITU–R P.453–9 (1970-1986-1990-1992-1994-1995-1997-1999-2001-2003).
4. E. Valma, M. Tamošiūnaitė, Radijo bangų lūžio rodiklio nustatymas, Laisvieji skaitymai 2009: 52nd, scientific conference for young students of physics and natural sciences. Vilnius, 3 April, 2009, p. 103–105.

PP80

LOW NOISE AMPLIFIER CONSTRUCTION TECHNIQUES

Mantvydas Jašinskas

[1] *Faculty of Physics, Vilnius University*

mantvisj@gmail.com

To amplify a very weak signal, we are inevitably confronted with a high-gain low noise amplifiers. It is known that the maximum amplifier noise is influenced by the first amplification stage[1]. Also it is known that then constructing low noise amplifiers, it is better to use field – effect transistors (FETs) rather than bipolar, because FETs have a lower noise factor [3][4].

Thus, it seems that it is enough to buy a low noise FET from a good manufacturer (Toshiba 2SK117GR) and as it is fitted into the circuit, we will have a high - performance low noise amplifier. Unfortunately it is not. Indeed, it is difficult to find the number of transistors with the best parameters. They are not the same. That's where the problem occurs.

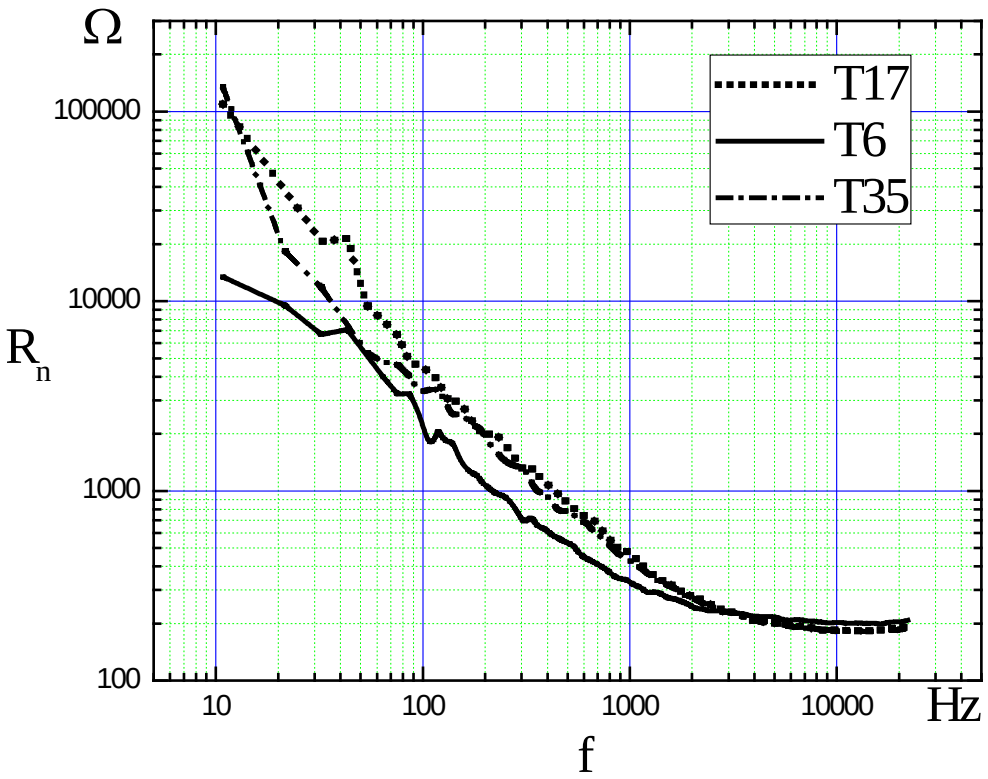

Fig. 1. Equivalent noise resistance (R_n) dependence on frequency (f) of three 2SK117GR transistors.

To show a solution, I made a low noise amplifier, which has the first stage, consisting of field - effect transistors, with the option to change them without soldering and the second stage – the AD797 operational amplifier. Transistor working point for all transistors was equal.

I researched thirty-five 2SK117GR field - effect transistors. To calculate equivalent noise resistance, for each transistor I measured the output signal spectrum, when amplifier input was connected to the ground, and when it was connected to the ground through the 4 KΩ resistor. Noise parameter difference between same marked transistors we see in Fig. 1.

So to make a really good low noise amplifier, it should buy at least a few tens of transistors, analyze them and select the best of them. Connect them into the circuit, then we will get a good quality low noise amplifier.

1. http://www.microwaves101.com/encyclopedia/noisefigure.cfm
2. http://www.datasheetcatalog.com/
3. M.J. Buckingham, *Noise in electronic devices and systems* (Ellis Horwood Ltd, England, 1983).
4. Aldert Van Der Ziel, *Noise in Measurements* (John Wiley & Sons Inc., U.S., 1976).
5. A. Lašas, B. Bartkevičius, *Pramoninė elektronika 1* (Mokslas, Vilnius, 1988).

PP81

SOFTWARE “ECGSIMPLE“ FOR ECG DATA ANALYSIS AND CLASSIFICATION

Martynas Plukys

Vilnius university, Physics faculty

martynas.plukys@yahoo.com

The main goal of this work is to create software that could be use for analysis of ECG data and enable to classify every single beat of ECG. This work is dedicated for scientists from Natural Sciences faculty (VU GMF) who works with ECG data, but also could be used for any scientific or educational purposes.

First main task was to gather a lot of scientific letters relative to ECG data analysis and try to realize at least few of them (the best ones). Second main task is to create user interface program with MatLab (GUI) which will meet scientist expectations. Third task is to write all MatLab code to JAVA for independent use of MatLab or operating system.

Analysis consists of: vanishing high low frequency noise, estimating ECG parameters and finally assign every single beat or spectrum to heart state. The scientist can choose wish methods to use. At this time there are five methods, but later will be added more. Different methods are used according ECG data, because of methods limitations. At the moment I have created demo user interface, but later it will change according scientific needs. Some example of ECG data analysis shown in 1 figure, user interface demo shown in 2 figure.

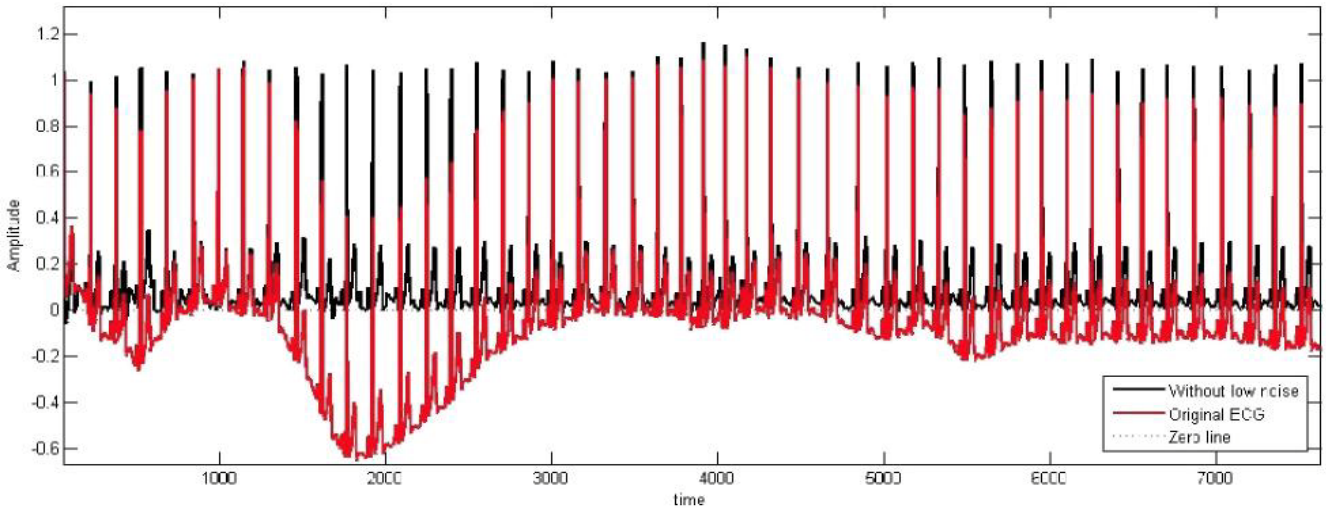

Fig. 1. ECG data analysis example. Red line – original ECG signal, black line – same signal without low noise frequency

Fig. 2. “ECG simple” user interface demo

1. K. Melcher, L.-M. Ng, E. Zhou et al., Nature **462**, 602-608 (1990).
2. Paul S Addison, Physiol. Meas. **26,** R155 – R199 (2005).
3. K. Daqrouq Asian Journal of Information Technology **4**(11): 989-995, (2005).
4. B. Mozaffary, M. A. Tinati, PWASET VOLUME **3,** ISSN 1307-6884 (2005).
5. N. Sivannarayana, D.C. Reddy, Medical Engineering and Physics **21,** 167–174 (1999).

PP82

NUMERICAL SIMULATIONS FOR ENVIRONMENTAL ENGINEERING

G. Liskiewicz

Technical University of Lodz

liskiewicz@gmail.com

Classic fluid physics faced an obstacle of limited applicability in real problems. This is because fluid motion is described by the Navier-Stokes equations, which are impossible to be solved with an exception of a few special cases. Moreover, every real situation cannot be reliably described without models of a wide range of complex phenomena such as viscosity, compressibility, boundary layer separation, turbulence, cavitation, fluid free surface, interaction with solid bodies etc. This caused a bottleneck in development of problems including fluid flows, which were examined empirically with the use of rather expensive wind tunnel experiments.

Recently, the growth of computing power available at affordable cost allowed the CFD (Computational Fluid Dynamics) simulations to cause an important breakthrough in fluid physics. Numerical methods provide both research and industry with cheap, fast and reliable information about demanded flow parameters. That led to a numerous successful applications including those regarding environmental protection [1-2].

Described work is devoted to presentation of a wide range of examples of use of CFD in different aspects of environmental protection. It will be shown that these methods provide substantial reductions in waste of energy and natural resources by optimizing flows in many different circumstances.

One of examples presented in the presentation regards turbomachines (turbines, compressors, pumps etc.) which are used in every energy system, such as power plant, jet engine, car engine [3]. Figure 1 presents static entropy distribution on a typical compressor obtained with the use of CFD. This parameter gives a quantitative measure of local energy dissipation. Therefore, it could be observed that main energy losses are attained at outer blades (so-called diffuser blades), which suggests some changes in their shape in order to improve the efficiency of the whole system. Consequently bigger energy production (for power plant)/smaller energy consumption (for engine) would be attained.

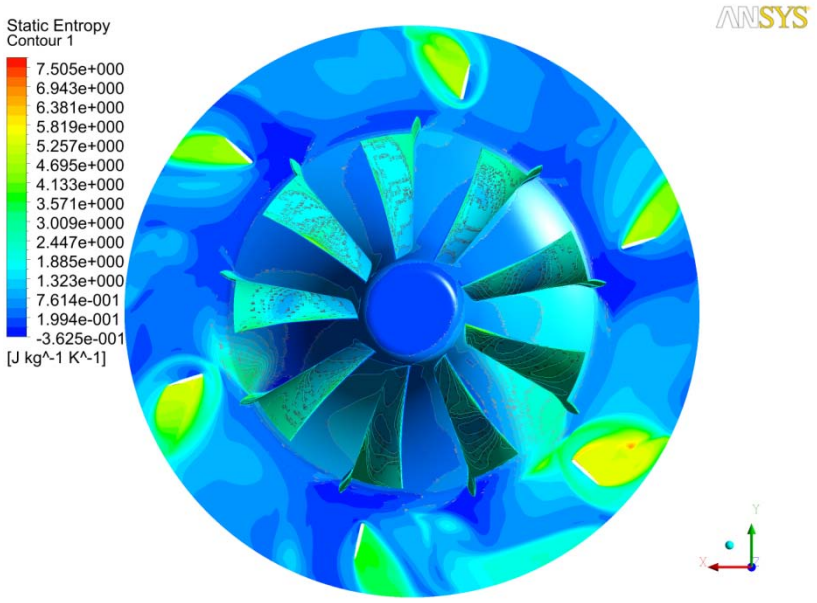

Fig. 1. Static entropy contour plot at radial compressor with diffuser.

1. C. Montavon, Assesing the wind power potential of a site, CFX Update Issue 23, Page 16 (2003).
2. Y. Shena, P. Diplas, Journal of Hydrology Volume 348, Issues 1-2, Pages 195-214 (2008).
3. P. Strohl, Designing for Quality, ANSYS Advantage Volume III, Issue 2, Pages 8-9 (2009).

PP83

ROTIFERS (ROTIFERA) DIVERSITY IN A KAUNAS BOTANICAL GARDEN PONDS AND IN THE RIVER NERIS

[1]Greta Lesivaitė, [2]Dr. Ingrida Šatkauskienė

[1] *Vytautas Magnus University, Natural Sciences faculty*

Bigbendas@yahoo.com

[2] *Vytautas Magnus University, Natural Sciences faculty*

Rotifers (Rotifera) are microscopic aquatic animals, generally smaller than 1 mm. They can be found in any water body, in mosesses, soil. Freshwater rotifers in the two ponds of Kaunas Botanical garden and in the river Neris were investigated from 2009 November until now. Altogether 8 rotifers families were found at investigated sites: *Philodinidae, Habrotrochidae, Collothecidae, Testudinellidae, Euchlanidae, Trichocercidae, Notommatidae, Collureidae*. *Keratella cochlearis* was the most abundant species in the stagnant water, meanwhile rotifers of genus *Habrotrocha* and *Philodina* dominated in the flowing water.

PP84

METHANOL FUEL CELLS, STATIC CHARACTERISTICS OF THE STUDY

E. Bagdonaitė, V. Šimaitis, doc. A. Lankauskas

ErnestaB@bamba.lt

The growth of global human population, and rising energy needs, global scale more and more countries are confronted with a lack of energy resources and energy dependence. Thus, the growth of energy demand and dwindling oil reserves makes finding alternative renewable energy sources. Especially when the European Commission is increasingly resorting to assert that Europe's energy resources are lacking. If no action is taken the EU bringing in fuel after 20 years at around 70%. Moreover, despite the Kyoto Protocol environmental pollution is increasing. Therefore, scientists around the world are constantly looking for new technological solutions to enhance existing energy convention systems.

The first fuel cell was discovered more than 170 years. Fundamental electrochemical principles underlying fuel cells work, 1839 Wales scientist has found William Grove. However, the actual materials and technologies suitable for practical application was developed in the second half of the twentieth century, fuel cells adapting aerospace industry.

Working at issue in the Methanol fuel cells, static characteristics of the study the aim: to investigate the methanol fuel cell and its static characteristics, and make recommendations for engineers who plan to use this type of fuel cells. The operation of fuel cells, fuel (CH_3OH) is continuously supplied to the anode and the oxidizer - the cathode. As oxidizing agent often used in the air. In this way the course of chemical reactions distinguished by electricity and heat. Direct effect of the methanol fuel cell performance is comparable to a proton exchange membrane fuel cells. Methanol Fuel Cell Prospects for recovery are very high and is now urgent to investigate them because the methanol fuel cell, its elements and thoroughly investigated only minimally, which is one of the newest energy source, taking into account the situation in Lithuania and the EU but it is the most promising energy storage and recovery element of its environmental impact.

PP85

SYSTEM OF WATER-SOLUBLE QUANTUM DOTS AND CHLORINE e_6: INTERACTION AND RESONANCE ENERGY TRANSFER

A.Skripka[1,2], J.Valančiūnaitė[1], R.Rotomskis[1,2]

[1] *Institute of Oncology, Vilnius university, Santariškių 1, LT-08660 Vilnius, Lithuania*

awefbeu@gmail.com

[2] *Faculty of Physics, Vilnius University, Sauletekio ave. 9-III, LT-10222 Vilnius, Lithuania*

Cancer is one of the biggest problems in nowadays medicine. Late diagnosis and inefficient treatment of cancer lead to large number of deaths every year. Nanotechnology could offer new opportunities in the fight against this disease. Semiconductor quantum dots (QDs) have received considerable interest in recent years as a result of their unique optical properties, leading to many applications in biology. Few years ago it was suggested that QDs also could be used in photodynamic therapy (PDT) to enhance the efficiency of conventional photosensitizers [1]. PDT is a treatment that uses a photosensitizing drug, usually porphyrin-type molecules, and the light to cure the malignant tumors and certain non-malignant pathologies. Once the light is applied, the excited molecules of photosensitizer generate cytotoxic reactive oxygen species, which in result damages cancer cells. It is believed that QD-PS system could perfect PDT in several ways [2]. The optical properties of QDs such as a high extinction coefficient and broad absorption spectrum make easier to excite photodrug (QD-PS). The excited QD at the same time can work as a fluorescent particle for imaging as well as a reactive singlet oxygen generator and energy donor for PS. The energy transmitted from QD to PS could further be used for generation of reactive oxygen species. It is believed that energy from QD to PS is transmitted by non-radiative Förster resonance energy transfer (FRET) mechanism [1].

In this work we present the spectral study on the interaction of CdSe/ZnS-PEG-amino (620 nm) quantum dots and second-generation photosensitizer, chlorine e6 (Ce_6), in different acidity buffers (PBS, pH=5.9 and pH=8).

Photophysical properties of Ce_6 are dependent on pH of solution. The absorption spectra of Ce_6 in alkaline and acid solutions differ, especially the region of Q bands. In acidic solution, the Soret band of Ce_6 becomes broader, while the region of Q bands contracts i.e. the red-side Q_x bands shift hypsochromically, while the blue-side Q_y bands shift bathochromically. Also, the molar extinction of Ce_6 in acidic solution is lower than in alkaline. The position and intensity of Ce_6 fluorescence band also vary with the acidity of solution. In alkaline solution, the fluorescence band

of Ce_6 is shifted bathachromicaly. All these spectral changes prove formation of Ce_6 aggregates in acidic medium [2].

In the presence of QD, we observed the significant changes in absorption and fluorescence spectra of Ce_6, which might be attributed to the formation of non-covalent QD-Ce_6 complex. Spectral changes of Ce_6 molecules bound to QD comprised of an enhancement in molar extinction coefficient and bathochromical shift of absorption and fluorescence bands. The absorption band of QD-Ce_6 complex appeared at 668 nm in both acidic and alkaline solutions. The molar extinction coefficient of alkaline QD-Ce_6 solution was higher than that of acidic solution. The fluorescence spectrum of QD-Ce_6 system displayed two fluorescence bands at 620 and 670 nm. The fluorescence band at 620 nm belongs to QDs, while the band at 670 nm could be assigned to bound Ce_6 molecules in QD-Ce_6 complex, since in the absence of QD, the fluorescence bands of Ce_6 is at 650 nm in acidic and at 662 nm in alkaline solution. In acidic solution, the fluorescence band of QD-Ce_6 complex (670 nm) dominated until the molar ratio of QD:Ce_6 increased from 1:0.01 to 1:10, while at higher ratios, the fluorescence of free Ce_6 became noticeable. In alkaline solution, the fluorescence of QD-Ce_6 complex dominated until the molar ratio of QD:Ce_6 was reached 1:2.

In the fluorescence spectrum of QD-Ce_6 solution, when the excitation at 465 nm was used, i.e. where only QDs can be excited, the same two fluorescence bands of QD and complex appeared. With an increase in QD:Ce_6 molar ratio, the spectrum of QD-Ce_6 showed the decrease in intensity of QD fluorescence band at 620, while the intensity of fluorescence band at 670 nm was increasing simultaneously. The fluorescence kinetic measurements of QD-Ce_6 solution displayed the shortening of QD's fluorescence lifetime at increasing Ce_6 concentration. As for chlorine, in the presence of QD, the fluorescence lifetime of bound Ce_6 molecules was longer in comparison with the lifetime of free Ce_6.

We conclude that photosensitizer Ce_6 forms non-covalent complex with CdSe/ZnS-PEG-amino quantum dot in acidic and alkaline solutions. In acidic solution, the aggregates of Ce_6 are disrupted upon binding to QD. In QD-Ce_6 complex, the FRET between QD and bound Ce_6 molecules occurs.

1. A. C. Samia, X. Chen, C. Burda, Journal of the American Chemical Society, **125**, 15736–15737 (2003).
2. E. Yaghini, A. M. Seifalian, A. J. MacRobert, Nanomedicine, **4**, 353-363 (2009).
3. B. Cunderlikova, L. Gangeskar, J. Moan, Journal of Photochemistry and Photobiology B-Biology, **53**, 81-90 (1999).

PP86

PARAMETERIZATION OF LONGWAVE RADIATION

M. Latinovic[1]

[1.] *Department of Physics, Faculty of Natural sciences of University of Novi Sad, Serbia*

milelatin27@gmail.com

Direct and diffuse sun rays of the atmosphere are falling at the Earth‘s surface, and together they represent the so-called „global radiation“.

One part of this „global radiation“ reflects back to the atmosphere, and second part absorbs, which leads to warming of the Earth‘s surface. Warm surface then radiate IR electro-magnetic waves back to the atmosphere and space. This radiation is known as atmospheric counter-radiation or longwave radiation.

Under longwave radiation is considered infrared radiation in the range of wavelengths from 0.3 μm up to several tens of microns while the maximum radiation occurs at the wavelength of about 10 μm.

In the field of climatology, atmospheric infrared radiation is monitored to detect trends in the energy exchange between the earth and the atmosphere. These trends provide information on long term changes in the Earth's climate. It is one of the primary parameters studied in research into global warming together with solar radiation.

Parameterization of radiation transport in the atmosphere is one of the most important moments in creating models for numerical weather forecasting of different proportions.

1. PhD M.Milosavljevic, *Meteorolgija* (Naucna knjiga, Beograd, 1975).
2. Zizic B, *Kurs opste fizike* (Beograd: Gradjevinska knjiga, 1989).

PP87

DESIGN AND TESTING OF FULLERENE PHOTOPROBES FOR ds-, ss-DNA MOLECULES

I. Sporysh[1] , O. Kysil[1], E. Buzaneva[1], T. Erb[2], G. Gobsch[2], U. Ritter[2] and P. Scharff[2]

[1] *Taras Shevchenko Kiev University, Volodymyrska str. 64, 01033 Kiev, Ukraine*

iryna.sporysh@gmail.com

[2] *Institute of Physics, TU of Ilmenau, Germany*

Designed photoprobes are nanofluids, which contain hydrated C_{60} aggregates or hydrated C_{60} derivative aggregates in aqueous suspensions [1,2]. Their photoresponse under UV-vis excitation depends from electronic features of biomolecular surrounding. These photoprobes, used for ds-,ss-DNA molecule detection by UV-vis absorption and photoluminescence spectroscopy of fluids, show features in absorption spectra at (275-380) and (235-290)nm ranges and in photoluminescence spectra at (490-635) and (525-635)nm ranges, caused by the absorption and photoluminescence at interface between C_{60} , C_{60} derivative core and ds-,ss-DNA molecules, respectively. The analysis of spectra is based on models of electrostatic and/or hydrophobic interactions of C_{60} and C_{60} derivatives with negatively charged phosphate groups and/or DNA bases of DNA molecules in aqueous fluids. These models result from our investigations of the role of electrostatic and hydrophobic interactions between fullerene core and DNA molecule in aqueous suspensions .

The authors, Olena Kysil and Iryna Sporysh gratefully acknowledge DAAD for the support of their research at TU Ilmenau. The authors are also grateful to Norbert Stein, Katrin Risch and Carmen Siegmund for technical support.

1. Y. Prilutski, S. Durov, L. Bulavin., Y. Astashkin, V. Yashchuk, T. Ogul'Chanski, E. Buzaneva, G. Andrievsky. Mol.Cryst.Liq.Cryst., **324,** 65-70, (1998).
2. P. Scharff, C. Siegmund, K. Risch, I. Lysko, O. Lysko, D. Zherebetskyy, A. Ivanisik, A. Gorchinskiy, E. Buzaneva. Fullerenes, Nanotubes and Carbon Nanostructures, **(13)** supplementary 1, 497-509, (2005).

PP88

ENZYMATIC CATALYSIS FOR CONVERSION OF SUSTAINABLE RESOURCES IS ENVIRONMENTAL-FRIENDLY WAY TO PRODUCE SUSTAINABLE PRODUCTS

V. Kiseliovas[1], R. Beliunas[1], B. Surinenaite[1]

[1]*Institute of Biotechnology, Vilnius, Lithuania*

vjuksas@yahoo.com

Conversion of fat-rich feedstock or simply synthesis of sustainable products from pure components of renewable resources is additional source of bioenergy and in general of environmental-friendly compounds [1]. Chemical catalysis remains the main way to produce components of biofuel and biolubricants at large scale while bioplasticizers only recently started to be attractive for production [2]. Certain disadvantages of chemical methods lead to interest for development of biocatalytic processes run by lipolytic enzymes to provide alternative and advanced biotechnological way to synthesize those materials [3]. Specificity of lipases can be expected to ensure synthesis of final products of desirable composition and at high yield [4-6]. Enzymatic catalysis however also meets certain problems as high cost of biocatalyst and various factors affecting the process, consequently optimization of lipase-catalyzed processes by screening of enzymes and of substrates is a tool to make biocatalytic process competitive with chemical process [7]. The subject of the present research was to test lipolytic enzymes for laboratory-scale conversion of oils and their components to biodegradable derivatives of a number of higher alcohols. Activity of lipases was analyzed by titrimetric and spectrophotometric methods, TLC and GC chromatography. The most efficient biocatalyst should be expected to be used for further analysis in pilot technological processes. Commercial enzymes (Resinase HT, Lipozyme TL-100L, Lipolase 100 LEX and Lipoprime 50T) were compared to the lipase from *Enterobacter aerogenes* as local source (JCS Biocentras).

Concerning synthesis of trimethylolpropane (TMP) oleates as components of bioplasticizers vacuum control was shown to have more or less effect on the product yield. Highest yield of TMP oleates (85% after 72 hours) was reached in *Enterobacter aerogenes* lipase-catalyzed transesterification of methyl oleate. Temperature of 60°C was essential factor for the reaction efficiency (close to melting point of TMP). Other enzymes were found to be less efficient in those reactions under similar conditions.

2-ethyl-1-hexyl oleates are components both of bioplasticizers and biolubricants. In the synthesis reactions of this product commercial lipase Lipolase 100 LEX was found to be the best biocatalyst allowing reach 72% of the product after 48 hours at 30°C temperature.

Few lipases were tested for biocatalysis of ethylene glycol fatty acid esters derived from natural oils and oil emulsions. Those compounds are included in compositions of biolubricants. The reaction was found not to be efficient as product yield did not exceed 50% although 4 oils and oil emulsions with 5 emulsifying agents were tested in the catalytic process. The reasons of the result should be inactivating effect of glycols and emulsifiers and strong substrate specificity of lipolytic enzymes as was previously shown in our experiments.

Starting substrates were found to affect efficiency of synthesis of 1-heptyl oleates and 2-octyl oleates. Product yield also depended on the source of lipolytic enzyme used. The highest yields were the following: 90% of 1-heptyl oleate after 48 hours at 30°C temperature in *Enterobacter aerogenes* lipase-catalyzed transesterification of methyl oleate; 89% of 2-octyl oleate from the same substrates under similar conditions in Lipolase 100 LEX lipase-catalyzed reaction.

Resinase HT soluble lipase and Lipoprime 50T immobilized lipase were shown not to be the most efficient biocatalysts when synthesizing long fatty acid esters of TMP, higher alcohols and glycols although those enzymes were found to catalyze high yield synthesis of biofuel components and other fatty acid esters.

In conclusion, *Enterobacter aerogenes* lipase from local source can be considered as one of most efficient biocatalysts to be further tested in pilot technological processes for synthesis of sustainable products from sustainable resources. Also optimization of directed processes evaluating water activity (aw) parameter with new equipment will be provided. Moreover, synthesis of adipic acid esters (also components of biodegradable compounds) catalyzed by lipases is planned to be tested as those compounds are of great industrial interest.

1. J. Rass-Hansen, H. Falsig, B. Jorgensen et al., J Chem Technol Biotechnol **82**, 329-333 (2007).
2. M.P. Dorado, E. Ballesteros, F.J. Lopez et al., Energy & Fuels **18**, 77-83 (2004).
3. E. Uosukainen, Y.-Y. Linko, M. Lamsa et al., J Am Oil Chem Soc**75**, 1557-1563 (1998).
4. V. Athawale, N. Manjrekar, M. Athawale, Biotechnol Prog **19**, 298-302 (2003).
5. N.N. Gandhi, K.D. Mukherjee, J Am Oil Chem Soc**78**, 965-968 (2001).
6. A.-Z. Sulaiman, J Chem Technol Biotechnol **81**, 299-305 (2006).
7. G. Hills, Eur J. Lipid Sci Technol **105,** 601-607 (2003).

Table of contents:

Oral presentations

Posters

Author Index